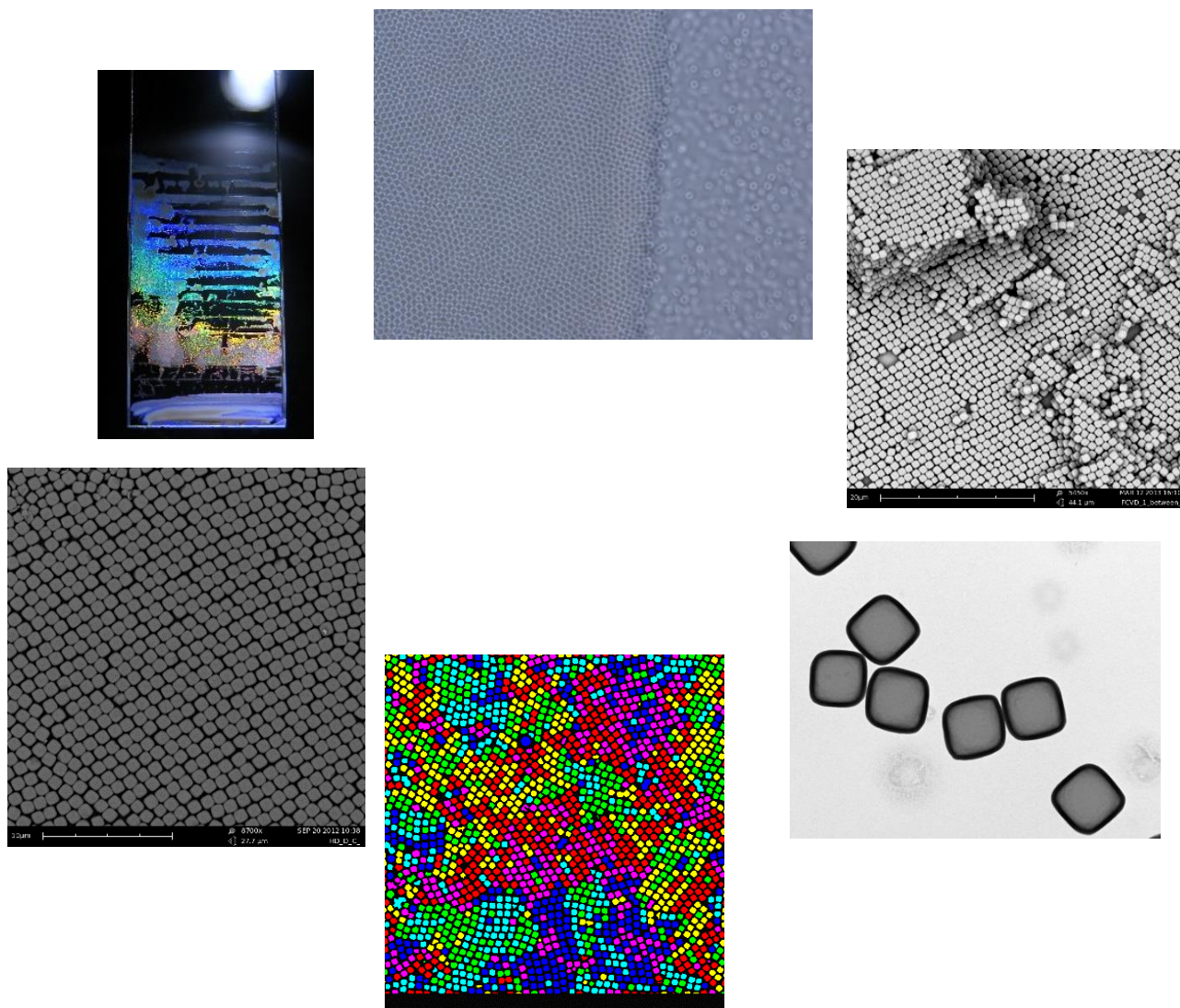


# Self-assembly of micron-sized hollow silica cubes using convective assembly methods



Masterthesis  
Vera Meester

Supervisors: J.M. Meijer, dr. A.V. Petukhov and prof. dr. A.P. Philipse

Performed at the Van 't Hoff Laboratory for Physical and Colloid Chemistry  
Utrecht University  
April 2014



# Abstract

Both simulations and experiments show interesting close-packed structures can be formed by superball-shaped particles. The arrangement of these particles depends on the roundness of the edges, which is defined by the deformation parameter  $m$ , where  $m = 2$  for a sphere and  $m = \infty$  for a perfect cube. Simulations predict that the highest packing density of superball/disk-shaped particles is obtained with two new Bravais lattices, called the  $\Lambda_0$  and  $\Lambda_1$  lattice. The maximum packing density (MPD) obtained with these lattices depends on the  $m$ -value of the particles. An experimental study with hollow silica cubes with  $m = 2.9$  shows that hexagonal-like and square-like arrangements similar to the  $\Lambda_0$  and  $\Lambda_1$  lattices can be formed. For superballs of  $m > 2.6$  the MPD of the  $\Lambda_1$  lattice is slightly higher compared to the  $\Lambda_0$  lattice and the difference increases with  $m$ . It is therefore expected that superballs with  $m$ -values  $\gg 2.6$  predominantly order on a  $\Lambda_1$  lattice.

In this experimental study dense structures of superballs with a high  $m$ -value are formed and analyzed. Therefore, micron-sized hollow silica cubes with  $m = 3.6$  are synthesized and used in convective assembly (CA) experiments to form dense ordered structures. CA experiments are performed using the drying droplet (DD), horizontal deposition (HD) and flow-controlled vertical deposition (FCVD) method. The thickness and shape of the cube deposits are observed to strongly depend on the method used. SEM images show that ordered mono- and multilayers are formed with all methods. The shape of the growth start is found to have a significant influence on the size and orientation of the ordered domains. With the DD and the HD method deposits with a curved growth start are obtained, whereas with the FCVD method a relatively straight growth start is induced. Structure analyses of SEM images of the cube deposits demonstrate that large ordered domains of similar orientation can be formed with the FCVD method, while small ordered domains of different orientation are observed when the DD and the HD methods are used.

Using the translational coordinates and orientation of the cubes Interactive Data Language (IDL) is used to analyze to what extent the cubes order on  $\Lambda_0$  and  $\Lambda_1$  lattices. It is found that with all three CA methods  $\Lambda_0$  and  $\Lambda_1$  order is observed in both mono- and multilayers. The analyses show that the  $\Lambda_1$  lattice is slightly preferred over the  $\Lambda_0$  lattice. This is in agreement with simulations of superballs, since the MPD of cubes with an  $m$ -value of 3.6 is higher on the  $\Lambda_1$  lattice compared to the  $\Lambda_0$  lattice.

Since the growth start has a significant influence on the structure formation, patterned substrates are used to influence and study the behaviour of cubes at the growth start. Substrates with straight polymer lines are used to induce a straight growth start. With all three CA methods cubes are observed to align at the polymer lines, therefore inducing a straight growth start. In monolayers the cubes are orientated with their face side parallel to the polymer line. The orientation of the aligned cubes influenced the orientation of the neighbouring cubes. Patterned substrates are therefore promising since the behaviour and therefore the structures formed by the cubes can be influenced and controlled.



# Contents

1. Introduction .....	7
2. Cube Synthesis .....	9
2.1. Theory & Background .....	9
2.1.1. Particle properties.....	9
2.1.2. Hollow silica cube synthesis.....	10
2.2. Experimental.....	13
2.2.1. Chemicals .....	13
2.2.2. Hematite cubes .....	14
2.2.3. Hollow silica cubes .....	15
2.2.4. Colloidal spheres.....	17
2.2.5. Characterization.....	17
2.3. Results & Discussion .....	18
2.3.1. Hematite cubes .....	18
2.3.2. Hollow silica cubes .....	20
2.4. Conclusions .....	21
3. Convective Assembly Methods.....	23
3.1. Theory & Background .....	23
3.1.1. Mechanism.....	23
3.1.2. Methods.....	28
3.1.3. Structures of colloidal superballs.....	30
3.2. Experimental.....	37
3.2.1. Sample preparation .....	37
3.2.2. Fabrication of templates.....	37
3.2.3. Setups.....	40
3.2.4. Characterization.....	42
3.3. Results & Discussion: Spheres.....	43
3.3.1. Drying droplet .....	43
3.3.2. Horizontal deposition.....	45
3.3.3. Flow-controlled vertical deposition .....	47
3.3.4. Conclusion.....	48
3.4. Results & Discussion: Cubes.....	49
3.4.1. Drying droplet .....	49

3.4.2.	Horizontal deposition.....	53
3.4.3.	Flow-controlled vertical deposition .....	59
3.5.	Results & Discussion: Fluorescent cubes .....	63
3.5.1.	Drying droplet .....	63
3.5.2.	Horizontal deposition.....	64
3.5.3.	Vertical deposition .....	65
3.6.	Results & Discussion: Controlling Crystal Growth .....	67
3.6.1	Straightener try-outs.....	67
3.6.2.	Polymer coated templates.....	68
4.	Crystal Structure Analyses .....	75
4.1.	Theory & Background .....	75
4.1.1.	Radial distribution function, $g(r)$ .....	75
4.1.2.	$\Lambda_0$ and $\Lambda_1$ Classification.....	75
4.2.	Experimental.....	76
4.2.1.	Particle tracking .....	76
4.2.2.	Structure analyses.....	77
4.3.	Results & Discussion .....	78
4.3.1.	Monolayers .....	78
4.3.2.	Multilayers .....	83
5.	Conclusions .....	87
6.	Outlook .....	89
	Acknowledgements.....	90
	Bibliography .....	91

# 1. Introduction

Colloids can be defined as particles with sizes ranging from 1 – 1000 nm that exhibit significant thermal motion, so-called Brownian motion.<sup>1</sup> Brownian motion and interactions between colloids can be studied by dispersing colloids in a medium, forming a colloidal dispersion.<sup>2</sup> Colloidal and atomic systems show similar phase behaviour, forming isotropic, crystal and glass phases.<sup>3 4</sup> The Brownian time, the typical time scale on which a colloid moves a distance comparable to its own diameter, and size of colloids are both much larger compared to atoms. Since the Brownian time of colloids is on the order of seconds, colloidal systems can be easily studied with optical microscopy. Therefore, these systems are often used as a model system to study atomic and molecular behaviour.<sup>5 6</sup>

Colloids are also of great interest since they can form colloidal crystals, which are ordered periodic structures of colloids. These crystals are used in applications such as optical information processing and storage, catalysis, coatings and other nanotechnologies.<sup>7 8</sup> Furthermore, their specific size makes it possible to form structures with a photonic bandgap.<sup>9 10 11 12</sup> The structure of a colloidal crystal is determined by the shape of the colloids and by interactions present in the system.<sup>2 7</sup> Interactions can be influenced by tuning particle properties as shape, size or surface functionalization or by tuning experimental conditions such as temperature, dispersion medium or pressure.<sup>13 14 15</sup> Depending on the experimental conditions used spherical colloids can form face centered cubic(FCC), hexagonal close packed(HCP), randomly stacked hexagonal close packed(RHCP) or body centered cubic(BCC) structures.<sup>16 17</sup> Non-spherical colloids can form other complex structures.<sup>18 19</sup> These particles are mainly of interest because they often show rich phase behaviour, including the formation of liquid crystal phases, as is shown for ellipsoids, rods and plates.<sup>20</sup>

A colloidal crystal can be obtained in various ways by influencing important parameters of the crystallization process such as particle properties or experimental conditions.<sup>15 21</sup> One of the simplest ways to form a colloidal crystal is by sedimentation. By using gravity as an external force a concentration gradient is obtained where the density in the sediment is large enough to form a crystal. However, control over the final structure and the orientation of the crystal planes in the sediment is limited. To gain more control over crystal growth other external forces as magnetic or electric fields can be used to form a colloidal crystal with preferred symmetry.<sup>14</sup> Another way to obtain dense colloidal crystals without the use of external fields is by convective assembly.<sup>22 23</sup> With convective assembly methods many experimental conditions can be controlled. Therefore, self-assembly mechanisms of colloids can be tuned and influenced resulting in a variety of possible structures.

With convective assembly a colloidal crystal can be formed on a substrate, which is placed in a colloidal dispersion. By slowly evaporating the solvent a flux of particles is induced toward the liquid-air interface. When the thickness of the evaporating liquid film at the meniscus becomes thinner than the particle diameter the particles are pinned on the substrate. Due to attractive capillary forces the particles are pushed together and self-assemble into a close packed structure.<sup>24 25 26 27</sup> Convective assembly methods are often preferred since crystals with a high packing fraction can be obtained in a controlled way.<sup>28 29</sup>

Colloidal crystals with high packing densities can be formed by colloidal cubes. Perfect cubes can form 100% spacefilling three-dimensional structures by arranging in a simple cubic lattice, in contrast to the maximum packing density of 74% for spheres, obtained in a HCP/FCC lattice.<sup>30</sup> Recently, Rossi *et al.* were able to synthesize a new system of colloidal cubes, hollow silica cubes.<sup>31</sup> These cubes are synthesized using hematite cubes as templates.<sup>32</sup> The hollow silica cubes are of interest because they

can form spacefilling structures. Another point of interest is the cavity inside the cubes and the high porosity of the edges, which can be used for catalytic purposes.<sup>33 34 35</sup>

The edges of the hollow silica cubes are slightly rounded, therefore their shape can be approached by that of a superball.<sup>36</sup> The roundness of the edges of superballs can be defined by a deformation parameter  $m$ , with  $m = 2$  for spheres and  $m \rightarrow \infty$  for perfect cubes.<sup>37</sup> For superball-shaped particles interesting structures and phase behaviour is predicted by simulations.<sup>38 39</sup> Simulations in 2D of rounded squares predicted the existence of two new Bravais lattices, the  $\Lambda_0$  and  $\Lambda_1$  lattice, with high packing densities. 3D simulations of superball-shaped particles predicted the densest packing can be obtained with the  $C_0$  and  $C_1$  arrangements analogue to the  $\Lambda_0$  and  $\Lambda_1$  lattices found in 2D.<sup>40 41</sup> Recently, the phase behaviour of superballs was studied as well, supporting the existence of  $C_0$  and  $C_1$  arrangements at high packing fraction.<sup>42 43</sup>

Experimentally, it has been found that a simple cubic arrangement of large hollow silica cubes could be obtained by the introduction of a small depletant.<sup>30 36</sup> In absence of depletant other arrangements and richer phase behaviour was observed by Meijer *et al.*<sup>44</sup> A particular convective assembly method, the vertical deposition method, was used in this study to form colloidal arrays of 774 nm hollow silica cubes with an  $m$ -value of 2.9. Mainly hexagonal-like structures were obtained, but square-like ordered domains were formed under specific conditions as well. Structures of superballs with a larger  $m$ -value are interesting as well since the roundness of the edges is predicted to have a large effect on the structure formed.

The goal of this study is the synthesis of hollow silica cubes with a large  $m$ -value, the fabrication of ordered structures of these cubes and the analyses of the structures formed. The results of this study will be compared to results obtained for smaller hollow silica cubes and simulations of superballs to obtain more insight in the role of particle size and shape in the crystallization process.<sup>38-44</sup> For hematite cubes it is known that the  $m$ -value increases with particle size.<sup>36</sup> By using large hematite cubes as templates hollow silica cubes with a large  $m$ -value can be synthesized. To fabricate dense ordered structures of large hollow silica cubes convective assembly methods can be used. Since sedimentation is a problem with these large cubes, the vertical deposition method used for the smaller cubes of Meijer *et al.* will not be sufficient. Other convective assembly methods have to be optimized to form ordered structures of large hollow silica cubes.

This thesis is divided in three components, including the syntheses, CA experiments and the analyses performed with hollow silica cubes. In chapter 2 the synthesis of micron-sized hollow silica cubes with an  $m$ -value of 3.6 is discussed. In the 3<sup>rd</sup> chapter the resulting cube structures formed in convective assembly experiments are discussed. Here, the results obtained with three different convective assembly methods are presented. We will show that with the drying droplet method information about dynamics, interparticle interactions and the growth process during convective assembly was obtained.<sup>27</sup> A horizontal deposition method was used to fabricate large monolayered structures.<sup>45</sup> With the flow-controlled vertical deposition method many experimental conditions were controlled, leading to large ordered multilayered structures.<sup>22 46</sup> In the 4<sup>th</sup> chapter electron microscopy images of the cube structures are qualitatively and quantitatively analyzed in iTEM and IDL. To analyze the range of the ordered domains the radial distribution function,  $g(r)$ . To determine whether the cubes arrange on the  $\Lambda_0$  and  $\Lambda_1$  lattice, which is predicted by simulations of superballs, a structure analysis was performed. The analyses show that the cubes arrange on both the  $\Lambda_0$  and  $\Lambda_1$  lattice in mono- and multilayers with a small preference for the  $\Lambda_1$  lattice. These results are in agreement with simulations of superballs with  $m = 3.6$ .<sup>39 40</sup>

## 2. Cube Synthesis

### 2.1. Theory & Background

Previous studies have shown that colloidal cubes of different sizes, shapes and materials can be synthesized.<sup>19 21 32 47</sup> In CA experiments properties as density, shape and surface functionality are determinant for the resulting structure. It will be shown that the hollow silica cubes suit these requirements best compared to the other materials that can be used to synthesize colloidal cubes. Finally the synthesis of hollow silica cubes will be described.

#### 2.1.1. Particle properties

One of the goals of this study is to form ordered arrays of colloidal cubes using convective assembly methods. For convective assembly experiments particle properties such as shape, polydispersity, density and interparticle interactions are of major importance.<sup>24 26</sup> The shape of colloidal particles is very important in crystallization experiments since it is determinative for the final structure of the crystal.<sup>15</sup> A recent study by Rossi *et al.* shows it is possible to synthesize colloidal hollow silica cubes.<sup>31</sup> They also showed simple cubic arrangements can be formed by micron-sized hollow silica cubes when a small depletant is introduced.<sup>36</sup> Since the edges of these cubes are rounded other spacefilling square-like and hexagonal-like structures can be formed as well, as was shown by Meijer *et al.*<sup>44</sup> The actual shape of these cubes can be approached by the shape of a superball, defined in equation 1, where the deformation parameter  $m$  determines the roundness of the edges.<sup>37</sup> The axis length of a cube is defined by  $x$ ,  $y$  and  $z$  and  $a$  is half of the cube face side.

$$\left|\frac{x}{a}\right|^m + \left|\frac{y}{a}\right|^m + \left|\frac{z}{a}\right|^m \leq 1 \quad [1]$$

Hollow silica cubes have an  $m$ -value of  $2 < m < \infty$ , with  $m = 2$  for a perfect sphere and  $m = \infty$  for a perfect cube. At  $m$ -values  $< 2$  superball shaped concave particles are found where the faces of the cube are rounded instead of the edges.<sup>39</sup> In this study only superball shaped particles with  $m > 2$  are considered. For superballs with  $m$ -values  $> 2$  the roundness of the edges decreases with increasing  $m$ -value, as illustrated in figure 1.<sup>41</sup> To synthesize hollow silica cubes hematite cubes are used as templates, as described in section 1.1.2. For hematite cubes it has been found that the  $m$ -value increases with particle size resulting in cubes with less rounded edges at larger sizes.<sup>48</sup> The shape and size of the hematite precursor cubes is determinative for the shape and size of the hollow silica cubes, therefore the  $m$ -value of these cubes increases with size as well.<sup>36</sup> Hollow silica cubes can be synthesized with a low polydispersity, typically less than 5%, which is preferable for convective assembly experiments since the amount of defects in a crystal increases with polydispersity, decreasing the range of order in crystalline domains.<sup>49</sup>

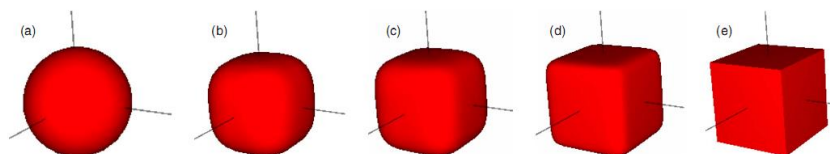


Figure 1: Superballs for different deformation parameter  $m$ -values. a)  $m = 2$ , b)  $m = 4$ , c)  $m = 6$ , d)  $m = 8$ , e)  $m = \infty$  [R. D. Batten *et al.* 2010]

Colloidal cubes of materials other than silica, such as sodium magnesium fluoride or hematite can be synthesized as well.<sup>50 51 52 53</sup> These cubes often have a relatively high density, 3.05 g/cm<sup>3</sup> and 5.26 g/cm<sup>3</sup> for sodium magnesium fluoride and hematite respectively, compared to silica, 2.2 g/cm<sup>3</sup>. In convective assembly experiments a low density is preferred since sedimentation can be a problem.<sup>54</sup> Another disadvantage of many other materials are the strong attractive interparticle interactions that are often present. Since in convective assembly experiments the flux of particles toward the meniscus and the capillary forces at this growth front should be the driving forces, other attractive interparticle interactions are unfavourable.<sup>29</sup> In conclusion, the particle properties of hollow silica cubes such as a well-defined cubic shape, a low polydispersity in both size and shape, a relatively low density and little interparticle interactions make hollow silica cubes an excellent system for convective assembly experiments. Note that hollow silica cubes are interesting for other reasons as well. Since silica is a well abundant biocompatible material, low in costs and easy to handle it is a very interesting material not only for academic reasons but for industrial applications as well.<sup>55</sup> Also, the cavity inside the porous silica cubes could be interesting for catalytic purposes.

The goal of this study is to fabricate and study structures of colloidal cubes with a high *m*-value formed using convective assembly methods, since cubes with less rounded edges are expected to form spacefilling structures with a high maximum packing density.<sup>39 40</sup> Therefore step 1 in this study is the synthesis of micron-sized hollow silica cubes with a higher *m*-value compared to the cubes used by Meijer *et al.*<sup>44</sup> The synthesized cubes will be analyzed using electron microscopy images.

## 2.1.2. Hollow silica cube synthesis

Hollow silica cubes are synthesized in three different steps.<sup>31</sup> In the first step precursor hematite cubes are synthesized according a method used by Sugimoto *et al.*<sup>1</sup> In the second step the hematite cubes are coated with a silica shell. To obtain hollow silica cubes the hematite cores are dissolved. In this section the details of these three steps are described.

### *Hematite cubes*

For the synthesis of hollow silica cubes hematite cubes are required as templates. These hematite cubes are synthesized according to a sol-gel method used by Sugimoto *et al.*<sup>32</sup> In this method an aqueous solution of iron(III)chloride,  $FeCl_3$ , is mixed with an aqueous solution of sodiumhydroxide,  $NaOH$ . By mixing these two salt solutions through stirring iron(III)hydroxide,  $Fe(OH)_3$ , is formed, as can be seen in step [1] and [2] of the reaction scheme shown in figure 2. The mixture is placed in the oven for eight days at 100 °C, where the iron(III)hydroxide is transformed into akaganeite needles,  $\beta$ - $FeO(OH)$ , which is step [3] of the process shown in figure 2. In the final step, step [4], the akaganeite needles assemble to form colloidal hematite particles,  $\alpha$ - $Fe_2O_3$ .



**Figure 2: Reaction scheme of the synthesis of cubic hematite particles according to the sol-gel method of Sugimoto *et al.*<sup>32</sup>**

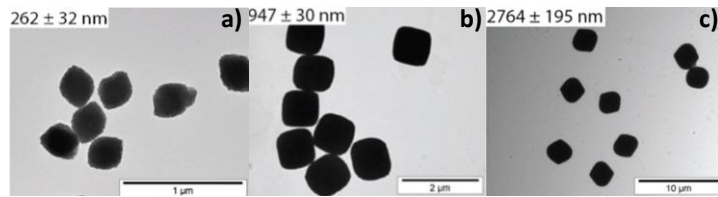


**Figure 3: Hematite particles synthesized under different conditions according to the sol-gel method of Sugimoto *et al.* a) Rugby-ball shaped particles b) Cube shaped particles c) Cube shaped particles with rounded faces<sup>57</sup>**

The final shape and size of the hematite particles is dependent on the ratio of  $\text{Fe}^{3+}$  and  $\text{OH}^-$  ions participating in the reaction.<sup>56</sup> The size of the particles increases with the molar excess amount of ferric ions,  $\text{Fe}_x^{3+}$ , used in the reaction. Cube shaped particles can be formed with an edge length of 500 – 1500 nm. To obtain cube shaped particles a  $\text{Fe}_x^{3+}$  amount of typically  $\sim 0.020$  mol is used.<sup>57</sup> A smaller amount of  $\text{Fe}_x^{3+}$  results in rugby-ball shaped particles with a size smaller than 500 nm. Particles larger than 1500 nm are formed when a large amount of  $\text{Fe}_x^{3+}$  is used resulting in cube shaped particles with curved faces. TEM images of these typical shapes are shown in figure 3.

The internal structure of hematite cubes was studied by Park *et al.* using high resolution electron microscopy and energy-dispersive x-ray spectroscopy.<sup>58</sup> The interior was found polycrystalline, with radially developed subcrystals from the middle of the cube in all directions. A TEM image of this polycrystalline interior is shown in figure 4. The full mechanism of the formation of these cubes is not yet understood, but the acid environment during the synthesis is thought to contribute to the polycrystallinity of the cubes.

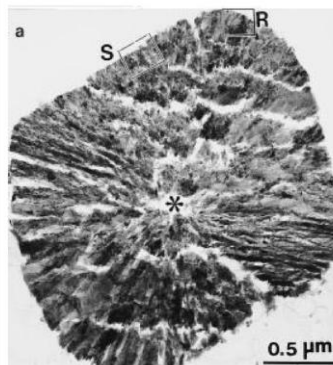


**Figure 4: Transmission electron micrograph of a thin section of a pseudo-cubic hematite particle [Park *et al.* 1996]**

## Silica coating

To stabilize the precursor cubes and to stimulate the adsorption of silica, the surface of the hematite cubes is functionalized with PVP-monomers prior to the silica coating. The silica coating is performed in a mixture of ethanol(100%, interchem), a small amount of water, tetramethylammoniumhydroxide (TMAH), functionalized hematite cubes and tetraethylorthosilicate (TEOS). A silica shell around the hematite cubes is formed by the hydrolyses of the silica precursor TEOS,  $nSi(OEt)_4 + 2nH_2O \rightarrow nSiO_2 + 4nEtOH$ .<sup>59</sup> The OH<sup>-</sup> ions in TMAH catalyze this reaction. TEOS is added drop wise to the reaction mixture and by varying the amount of TEOS the thickness of the silica shell can be tuned. A large amount of TEOS will result in a thick silica shell, while a small amount of TEOS will result in a thin shell. In most syntheses a silica shell with a thickness of 50 -150 nm is formed. A shell thinner than 50 nm is often unstable causing the silica cubes to collapse due to pressure on the walls. Thick silica shells of 150 nm and larger are also not preferred for this study, since the roundness of the edges increases with shell thickness resulting in cubes with a lower m-value. The silica shell can be made visible using electron microscopy. In figure 5a a TEM image of a silica coated hematite cube is shown. In this figure it can be seen that the hematite core and the silica shell can easily be distinguished by the difference in contrast. The thickness of the silica shell is determined by distracting the average size of hematite cubes from the average size of silica coated hematite cubes. The average size of cubes is determined using at least 100 TEM images of different individual cubes from the same batch.

## Removing hematite cores

To obtain hollow silica cubes the hematite cores are dissolved. To dissolve hematite concentrated hydrochloric acid(HCl) is required,  $Fe_2O_3 + 6H^+ + 6Cl^- \rightarrow 2Fe^{3+} + 3Cl^- + 3H_2O$ . The dissolution of hematite can be observed macroscopically by a colour change of the solution. A colour change from red, indicating the presence of hematite, to yellow, indicating dissolved iron(III)chloride, shows all hematite has been dissolved. After repeated washing with water a white sediment of hollow silica cubes should be obtained. If the sediment is slightly orange this can be an indication not all hematite has dissolved, which can be checked with electron microscopy. Figure 5b and 5c show a completely hollow silica cube and a silica cube containing hematite rattlers, respectively. In cases similar to figure 5c more HCL is required to dissolve all hematite to obtain hollow silica cubes. The resulting hollow silica cubes appear to be porous with a density difference of  $\sim 0.2 \text{ g/cm}^3$  compared to solid silica particles. A recent study shows that the porosity of the silica layer can be tuned by surface protective water etching.<sup>33</sup>

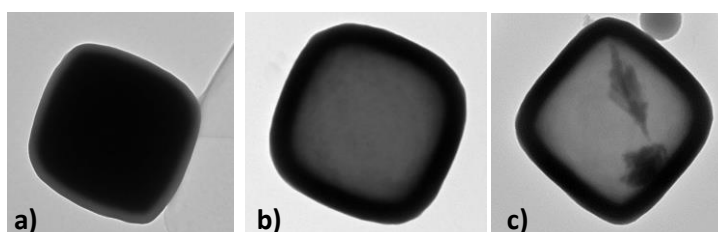


Figure 5: TEM images of micron-sized silica cubes a) hematite cube coated with silica b) Hollow silica cube c) Silica cube with a hematite 'rattle'

## 2.2. Experimental

All chemicals and procedures used to synthesize hematite cubes and hollow silica cubes are described in this section. Properties of colloidal spheres used for test experiments with CA methods are listed as well.

### 2.2.1. Chemicals

All chemicals used, listed in table 1, were used as received from the supplier. All water used was purified by a Millipore filter, unless stated otherwise.

**Table 1: Properties of all chemicals used for the synthesis of hollow silica cubes**

<b>Chemical name</b>	<b>Molecular formula</b>	<b>Supplier</b>
Ethanol, 100%	C <sub>2</sub> H <sub>5</sub> OH	Interchem
Ethanol, p.a.	C <sub>2</sub> H <sub>5</sub> OH	Merck
Sodiumhydroxide, p.a.	NaOH	Merck (Emsure)
Iron(III)chloride hexahydrate, 99%	FeCl <sub>3</sub> · 6H <sub>2</sub> O	Sigma-Aldrich
Hydrochloric acid, 37%wt	HCL (aq)	Emsure
Polyvinylpyrrolidone, 40000 kDa	C <sub>6</sub> H <sub>9</sub> NO	Sigma-Aldrich
Rhodamine B	C <sub>28</sub> H <sub>31</sub> N <sub>2</sub> O <sub>3</sub> Cl	Sigma-Aldrich
Tetraethylorthosilicate, ≥99.0%	Si(OC <sub>2</sub> H <sub>5</sub> ) <sub>4</sub>	Sigma-Aldrich
Tetramethylammoniumhydroxide, 25%wt	(CH <sub>3</sub> ) <sub>4</sub> NOH (aq)	Fluka
Rhodamine B isothiocyanate	C <sub>29</sub> H <sub>30</sub> ClN <sub>3</sub> O <sub>3</sub> S	Sigma-Aldrich
Aminopropyltriethoxy-silane	C <sub>9</sub> H <sub>23</sub> NO <sub>3</sub> Si	Sigma-Aldrich

## 2.2.2. Hematite cubes

An adjusted version of the sol-gel method used by Sugimoto *et al.* was used for the hematite cube syntheses in this study.<sup>57</sup> In total ten different syntheses were performed resulting in ten batches. The syntheses were performed in two series, S1 and S2, of five syntheses. Here, a typical synthesis is described. The correct quantities and conditions used for the individual syntheses are summarized in table 2 and 3. A typical synthesis started with the preparation of two salt solutions. A NaOH-solution was prepared by dissolving 20.14 g of NaOH pellets in 100 mL water under stirring. A solution of FeCl<sub>3</sub>, was prepared by dissolving 50.39 g FeCl<sub>3</sub>(s) in 100 mL water by shaking and ultrasonication in a 250 mL Pyrex bottle under nitrogen flow. Weighing of the FeCl<sub>3</sub>(s) was done quickly, since the salt is very hygroscopic. In ~20 s the NaOH solution was added to the FeCl<sub>3</sub> solution under stirring using a magnetic stir bar. During the addition the stirring rate was increased to 1100 rpm, because the viscosity of the mixture increased rapidly upon mixing. When the solution turned dark purple, indicating ironoxide compounds were formed, the solution was stirred for another ten minutes. The exact amount of NaOH-solution used in the reaction was determined by weighing.

The mixture was placed in a preheated oven at 100 °C for 8 days. This was followed by the removal of the yellow supernatant containing Fe<sup>3+</sup>, Na<sup>+</sup>, Cl<sup>-</sup> and OH<sup>-</sup> ions from the dark purple to brown sediment containing the hematite particles. The cubes were washed by repeated centrifugation and redispersed in water until the pH of the supernatant had increased to 4. For the batches of the S1 syntheses these washing steps were first performed in 250 mL polypropylene-copolymer bottles. However, from TEM images was observed that this volume was not satisfactory to remove the large excess of salt and small particles. Therefore, 1L propylene bottles were used to wash the S2 batches and to further purify batches 1\_S1 to 4\_S1. Since batch 5\_S2 contained very small particles with a high polydispersity in both size and shape, this batch was not further purified. The resulting hematite cubes were stored in water. Comparison of table 2 and 3 shows that the excess of Fe<sub>x</sub><sup>3+</sup> ions used in the syntheses, which determines the size of the cubes, is larger in the S2 serie. Therefore, it was expected that the cubes formed in the S1 syntheses were smaller in size compared to the cubes formed in the S2 syntheses. An eleventh batch of cubes was provided by R. de Groot. These hematite cubes HC\_R have a diameter of 996 nm with a polydispersity in size of 8%.

**Table 2: Amounts of reactants and conditions used for the syntheses of the S1 serie**

Batch	NaOH (g)	OH <sup>-</sup> reaction (mol)	FeCl <sub>3</sub> * 6H <sub>2</sub> O (g)	Fe <sup>3+</sup> reaction (mol)	Fe <sub>x</sub> <sup>3+</sup> (mol)	Mixing time (s)
1_S1	20.16	0.503	50.01	0.185	0.0175	22
2_S1	20.30	0.504	50.07	0.185	0.0173	23
3_S1	20.15	0.501	50.01	0.185	0.0181	21
4_S1	20.14	0.499	50.05	0.185	0.0189	20
5_S1	20.38	0.507	50.02	0.185	0.0162	24

**Table 3: Amounts of reactants and conditions used for the syntheses of the S2 serie**

Batch	NaOH (g)	OH <sup>-</sup> reaction (mol)	FeCl <sub>3</sub> * 6H <sub>2</sub> O (g)	Fe <sup>3+</sup> reaction (mol)	Fe <sub>x</sub> <sup>3+</sup> (mol)	Mixing time (s)
1_S2	20.14	0.498	50.39	0.186	0.0204	20
2_S2	20.15	0.499	51.26	0.190	0.0233	20
3_S2	20.15	0.502	50.55	0.187	0.0197	22
4_S2	20.23	0.502	50.96	0.189	0.0213	20
5_S2	20.18	0.500	50.53	0.187	0.0203	20

### 2.2.3. Hollow silica cubes

Three batches of hollow silica cubes, 4\_S2\_H, 5\_S2\_H and HC\_R\_fIH, were synthesized using hematite cubes from batch 4\_S2, 5\_S5 and HC\_R respectively as template. The synthesis procedure described here was used to synthesize fluorescent hollow silica cubes, HC\_R\_fIH. Apart from the addition of aminopropyltriethoxy-silane(APS) and Rhodamine B this procedure is similar to pure silica coatings. The quantities of reactants used in the three individual syntheses are listed in table 4 and 5.

The first step in the synthesis was the addition of a PVP-solution, 11.05 g PVP-40 in 100 mL water, to a 25 mL dispersion of HC\_R cubes, 12.8 %wt in water. The addition of PVP was necessary to stabilize the hematite cubes in ethanol and to improve the adsorption of silica on the surface of the hematite cubes. The mixture was stirred for three days to ensure the PVP-molecules had adsorbed at the surface of the cubes. The functionalized hematite cubes were washed with water in 250 mL polypropylene-copolymer bottles to remove the excess of PVP. Small hematite particles located at the water-air interface were removed as well together with the clear supernatant. The functionalized cubes were transferred to ethanol(100%, interchem) by repeated centrifugation and redispersed by shaking and ultrasonication. A dye solution was prepared by mixing 0.80 g APS dissolved in 5 mL ethanol(p.a. Merck) with 8.31 mg Rhodamine B isothiocyanate dissolved in 5 mL ethanol(p.a. Merck). The dye solution was shaken for three days and stored at 3 °C in the dark.

The silica coating of the hematite cubes was performed using a 2L two-necked round bottomed flask in a temperature controlled ultrasonic bath. Before the silica coating, 920 mL ethanol(100%, interchem), 42 mL (3.8 %wt) functionalized hematite cubes in ethanol(p.a. Merck), 62 mL water and a 10 mL solution of 1 %wt TMAH in water was added to the flask under mechanical stirring and ultrasonication. The fluorescent silica coating was performed in two steps. In the first step a solution containing 5 mL TEOS, 4 mL dye solution and 1 mL ethanol(p.a. Merck) was added to the reaction mixture in 30 minutes using a peristaltic pump. Immediately after this step the second coating step was performed, where a mixture of 5 mL TEOS and 5 mL ethanol(p.a. Merck) was added to the reaction mixture in 1 hour using a peristaltic pump. Note that for the non-fluorescent hollow silica cube syntheses only one coating step, the addition of TEOS in ethanol(p.a. Merck), was required. The reaction mixture was thoroughly stirred mechanically for three hours under ultrasonication to complete the fluorescent silica coating. Finally, a solution of 2.47 g PVP-40 in 100 mL water was added and the reaction mixture was stirred for 16 hours to stabilize the silica coated cubes and to prevent aggregation. The excess of reaction components was removed by washing with ethanol(100%, interchem) until the supernatant was clear and colourless. The cubes were stored in ethanol(p.a. Merck) to avoid silica etching by water. The final stock concentration was 3.8 %wt.

**Table 4: Amounts of hematite cubes and PVP-40 used for the functionalization of hematite cubes**

Batch	Hematite cubes (g)	PVP-40 (g)
HC_R_fIH	3.2	11.05
4_S2_H	3.3	10.00
5_S2_H	3.3	11.03

**Table 5: Amounts of reactants and conditions used during the silica coating of hematite cubes**

<b>Batch</b>	<b>Hematite cubes (g)</b>	<b>1%wtTMAH in water (mL)</b>	<b>Water (mL)</b>	<b>TEOS (mL)</b>	<b>Addition time TEOS (h)</b>	<b>PVP-40 (g)</b>	<b>Dye solution (mL)</b>
HC_R_fIH	1.6	10	62	15	1½	2.5	4
4_S2_H	1.9	10	65	10	1½	20	-
5_S2_H	2.9	15	122	20	2¾	20	-

To dissolve the hematite cores the silica coated hematite cubes were transferred and redispersed in water by repeated centrifugation. This was followed by the addition of 100 mL concentrated HCl to 140 mL of dispersion under stirring. After 24 hours the cubes were washed with water resulting in a dark pink pellet and an orange supernatant. The addition of HCl followed by the washing steps were repeated until a yellow supernatant and a pink pellet were obtained. In the case of non-fluorescent silica cubes the procedure was repeated until a yellow supernatant and a white pellet were obtained. The cubes were finally transferred to ethanol(100%, interchem) by repeated centrifugation in glass bottles and stored in ethanol(p.a. Merck) to prevent silica etching in water. Analysis of TEM images showed all hematite was removed from the cores and hollow silica cubes were obtained.

## 2.2.4. Colloidal spheres

To optimize the CA methods for colloidal cubes test experiments were performed with colloidal silica and polystyrene spheres. Silica spheres, DB-303, of 1052 nm in diameter and a polydispersity of 8.9 % were provided by the 'deeltjesbank'. In figure 7a a typical TEM image of these spheres is shown, where spherical particles as well as dumbbell-shaped particles can be seen. By analyzing TEM images the polydispersity in shape was determined to be 16 %. Linear polystyrene spheres, LPS4, with a diameter of 1234 nm and a polydispersity of 1.7 % were provided by F. Hagemans. These colloids were synthesized using the dispersion polymerization method and stored in water.<sup>60</sup> A typical TEM image of these spheres is shown in figure 7b. Since these particles have a low polydispersity in both size and shape, it is expected that these particles can form long range ordered structures in convective assembly experiments. Therefore, these spheres are used to test and optimize convective assembly methods before performing experiments with cubes.

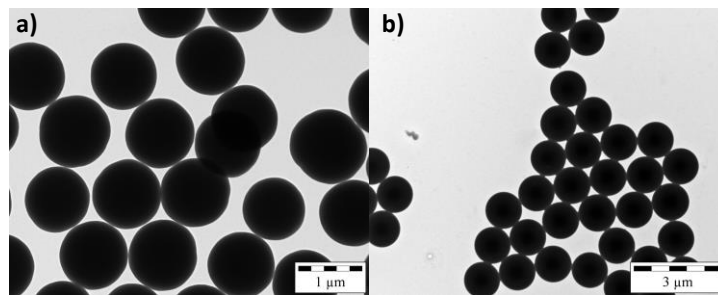


Figure 7: TEM image of a) Silica spheres, DB-303 b) Polystyrene spheres, LPS4<sup>60</sup>

## 2.2.5. Characterization

The colloidal particles were imaged using high resolution transmission electron microscopy (TEM). A Philips FEI Tecnai 10 operated at 100 kV with an analySIS MegaView II CCD camera and a Philips FEI Tecnai 12 operated at 120 kV with a analySIS MegaView II CCD (or Tietz CCD camera 1024x1024) camera was used to make TEM images. The images were analyzed using analySIS iTEM 5.0 to determine particle properties such as size, shape and shell thickness.

## 2.3. Results & Discussion

In this section the results of the various syntheses of hematite cubes and hollow silica cubes are shown and discussed.

### 2.3.1. Hematite cubes

#### *S1 serie*

The S1 syntheses of hematite cubes resulted in five batches with hematite particles of 280 - 810 nm in size. Table 6 lists the particle properties of the individual S1 batches. This table shows all batches have a polydispersity in size of ~10%. The average size of the particles in the batches 2\_S1 – 3\_S1 and 5\_S1 is < 500 nm. These particles have a rugby-ball like shape, which can be seen from the TEM images shown in figure 8b and 8c. The average size of the particles from batch 1\_S1 and 4\_S1 is > 500 nm and in figure 8a and 8d it can be seen that these particles have a cubic-like shape. In conclusion, the hematite particles of the S1 batches are smaller than 1  $\mu\text{m}$  with a high polydispersity and their shape is often non-cubic. Since the amount of  $\text{Fe}_x^{3+}$  used in the synthesis determines the size of the cubes, it is expected that the amount of  $\text{Fe}_x^{3+}$  used for the S1 syntheses was too low to result in micron-sized hematite cubes. For the synthesis of micron-sized hollow silica cubes, hematite cubes with a similar size and a low polydispersity are required, therefore the S1 batches are not suited for the synthesis of micron-sized hollow silica cubes.

Table 6: Properties of the hematite particles of the S1 batches

S1 Batch	Average size (nm)	Polydispersity (%)	Shape
1_S1	584	9.8	Cubic-like
2_S1	328	10.9	Cubic - Rugby ball
3_S1	465	10.7	Cubic - Rugby ball
4_S1	810	9.8	Cubic
5_S1	280 x 370	-	Rugby ball

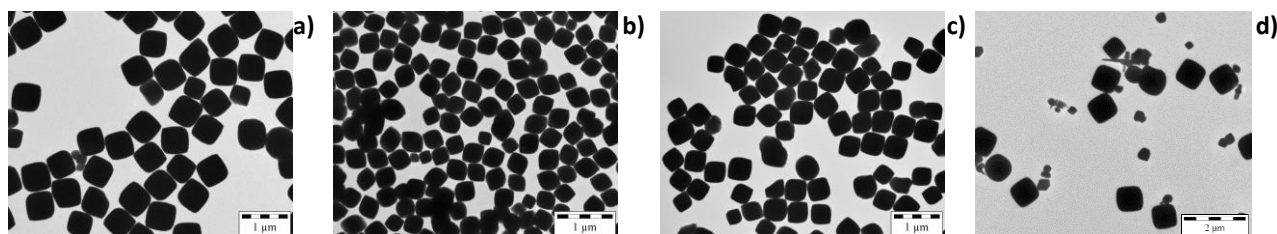


Figure 8: TEM images of hematite particles synthesized in the S1 serie a) 1\_S1 b) 2\_S1 c) 3\_S1 d) 4\_S1

## S2 serie

To obtain hematite cubes satisfying the requirements for the hollow silica cube syntheses five new syntheses were performed in the S2 serie. For these syntheses a larger amount of  $\text{Fe}_x^{3+}$  was used compared to the amounts used for the S1 syntheses and TEM images of the results are shown in figure 9. Properties of the individual S2 batches are listed in table 7. This table shows that the S2 syntheses resulted in five batches containing cubic shaped hematite particles in the size range of 922 - 1587 nm with a polydispersity < 6.5 % for all batches. Batch 2\_S2 contains the largest cubes, a typical TEM image shown in figure 9b, which is in agreement with the fact that the largest amount of  $\text{Fe}_x^{3+}$  was used for this synthesis. Figure 9b also shows akaganeite needles are sticking out at the surface of the cubes, indicating that the transformation of akaganeite needles to cubes was not finished yet. Typical TEM images of batches 1\_S2 and 3\_S2 – 5\_S2 are shown in figure 9a and 9c – 9e respectively, showing cubic shaped hematite particles were formed. Batches 4\_S2 and 5\_S2 were used for the syntheses of hollow silica cubes, since their size is close to 1  $\mu\text{m}$ , their polydispersity is low and their shape is cubic.

Table 7: Properties of the hematite cubes of the S2-batches

S2 Batch	Average size (nm)	Polydispersity (%)	Shape
1_S2	922	5.5	Cubic
2_S2	1587	5.4	Cubic + Needles
3_S2	1028	6.5	Cubic
4_S2	1180	3.7	Cubic
5_S2	932	5.5	Cubic

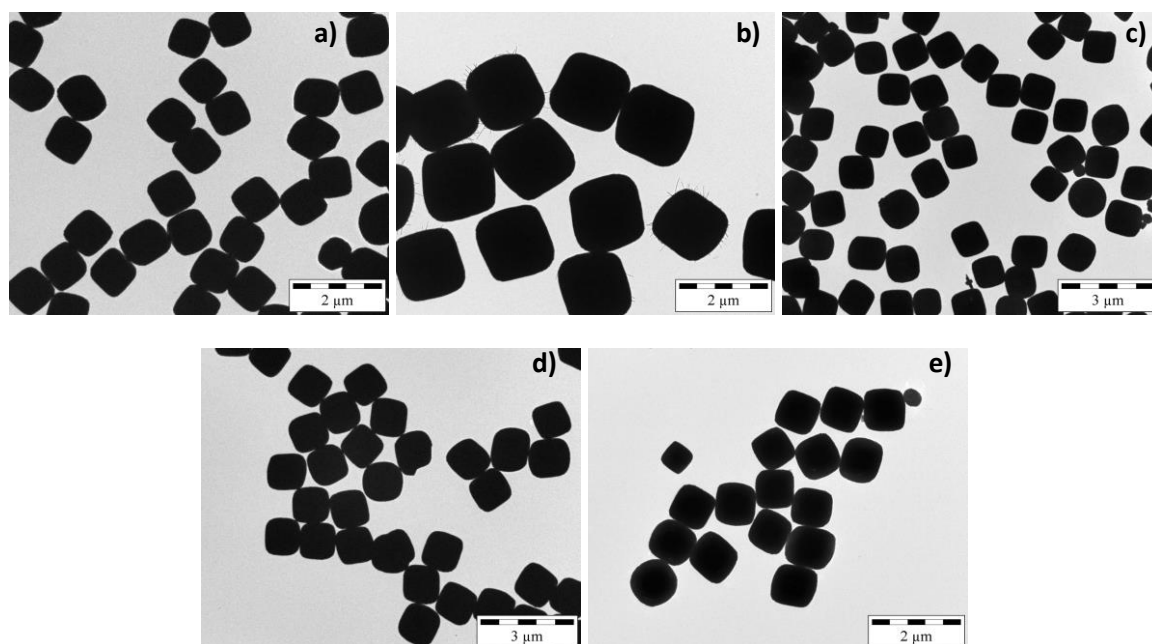


Figure 9: TEM images of hematite particles synthesized in the S2 serie a) 1\_S2 b) 2\_S2 c) 3\_S2 d) 4\_S2 e) 5\_S2

## 2.3.2. Hollow silica cubes

Three batches of hollow silica cubes, 4\_S2\_H, 5\_S2\_H and HC\_R\_fIH were synthesized using hematite cubes from batches 4\_S2, 5\_S2 and HC\_R respectively as precursor cubes. The first two batches were synthesized by a normal silica coating procedure, while the third batch was synthesized using a two-step coating including the addition of dye solution. Properties of the individual batches are summarized in table 8.

### *Silica coating*

The synthesis of 4\_S2\_H resulted in aggregates of hollow silica cubes, as can be seen in the typical TEM image of this batch shown in figure 10a. The size of the cubes was 1300 nm on average. Instead of single hollow silica cubes, most cubes were attached to other cubes with their sides forming large strings of particles. Many broken cubes were found as well, indicating that the shell thickness was too thin to be stable. Close inspection of figure 10a reveals that the thin silica layer between two cubes is too thin to originate from two single cubes. This unexpected result could be caused by several factors including not well dispersed hematite cubes due to a failure in the PVP coating or a failure of the ultrasonic bath during the synthesis. In conclusion, these cubes are not suitable for convective assembly experiments.

The synthesis of batch 5\_S2\_H resulted in micron-sized single cubes with a polydispersity in size of 3.5 %. Figure 10b shows a typical TEM image of this batch. To determine the roundness of the edges of these cubes the deformation parameter,  $m$ , was determined. The  $m$ -value was determined by analyzing 100 TEM images of single cubes using a fitting program written in Matlab. The  $m$ -value of the cubes is 3.55, which is much higher compared to the  $m$ -value of the smaller hollow silica cubes, 2.9, used by JM. Meijer *et al.*<sup>10</sup> The micron-sized cubes of this batch were therefore used in convective assembly experiments.

A fluorescent silica coating is performed using hematite cubes of batch HC\_R\_H. This resulted in micron-sized fluorescent hollow silica cubes with a polydispersity of 5.1%, batch HC\_R\_fIH. Figure 10c shows a typical TEM image of these single cubes. The size and low polydispersity of the cubes in this batch makes them suitable for convective assembly experiments. These cubes have fluorescent molecules incorporated, which makes them suitable for 3D studies with a confocal microscope.

**Table 8: Properties of the hollow silica cube batches**

Batch	Average size (nm)	Polydispersity (%)	Shell thickness (nm)
4_S2_H	~1300	-	-
5_S2_H	1028	3.5	48
HC_R_fIH	1186	5.1	95

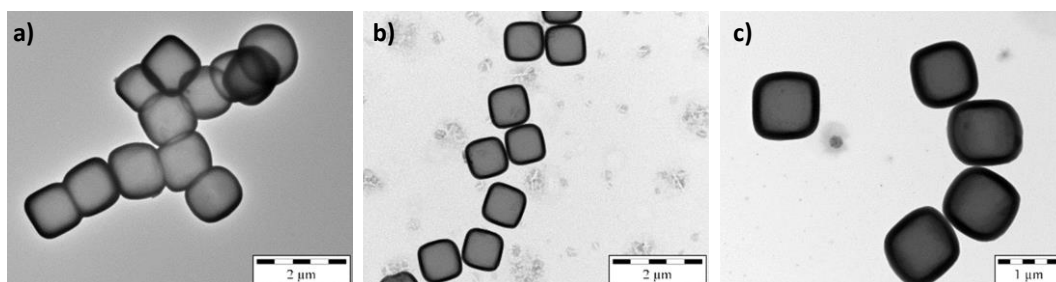


**Figure 10: Typical TEM image of hollow silica cubes of batch a) 4\_S2\_H b) 5\_S2\_H c) HC\_R\_fIH**

## 2.4. Conclusions

Ten different batches of hematite particles are synthesized in two series, S1 and S2. The batches of the S1 serie contain particles with an average size smaller than 1  $\mu\text{m}$  and a polydispersity of  $\sim 10\%$ . The shape of these particles is rugby ball-like to cubic-like. In the S2 serie a larger amount of  $\text{Fe}_x^{3+}$  was used in the syntheses resulting in large micron-sized cubes. These particles were cubic in shape with a low polydispersity. Therefore, the cubes of the S2 series are well suited for the syntheses of micron-sized hollow silica cubes. Two S2 batches, 4\_S2 and 5\_S2, were used to synthesize hollow silica cubes with one succesfull synthesis resulting in micron-sized hollow silica cubes, 5\_S2\_H. An eleventh batch of hematite cubes was used to synthesize fluorescent hollow silica cubes resulting in micron-sized hollow fluorescent silica cubes, HC\_R\_fIH. The fluorescent and non-fluorescent cubes of the batches 4\_S2\_H and HC\_R\_fIH are used in convective assembly experiments to fabricate ordered structures.



## 3. Convective Assembly Methods

### 3.1. Theory & Background

When heat is exchanged between a liquid and its surroundings a fluid or gas flux is induced in a certain direction. When the liquid contains particles, a particle flux in the same direction as the fluid or gas is induced, resulting in the assembly of particles at the position where the liquid evaporates. This process is called convective assembly(CA).<sup>24</sup> Since colloidal particles can self-assemble into ordered dense structures CA can be used to form colloidal crystals.<sup>61</sup> CA experiments with colloids have shown that the final structure of the array is mainly dependent on the properties of the colloidal system and the experimental conditions used.<sup>62</sup> Therefore, a good understanding of CA is required to perform successful CA experiments with colloidal systems, e.g. the formation of ordered structures.

In this chapter the theory of CA of colloids is described. This is followed by a description of the three CA methods used in this study; the drying droplet(DD) method, a horizontal deposition(HD) method and the flow-controlled vertical deposition(FCVD) method.

#### 3.1.1. Mechanism

##### *Convective transport of particles*

A well-known phenomenon illustrating the effect of convective assembly is the ‘coffee stain effect’. By drying a coffee droplet rings of colloidal particles are obtained. In this paragraph the mechanism behind the drying dispersion droplet, in a slightly different setup compared to the normal drying droplet, is used to describe convective transport of particles. When the solvent of a dispersion droplet is evaporated, solvent molecules will be moved from the bulk to the edges of the droplet to compensate for the evaporated molecules. This solvent flux induces a particle flux to the edges of the droplet. At the substrate-solvent-air meniscus colloids are pinned on the substrate forming the core for crystal growth. Other particles arriving at the edges of the droplet are pinned on the substrate as well and due to immersion capillary forces the particles are pushed together forming a colloidal array. The process is illustrated in figure 11.

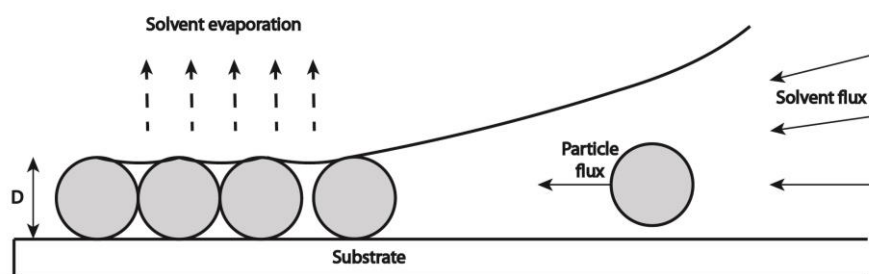


Figure 11: Convective assembly: Solvent evaporation induces convective transport of particles to the meniscus. At the meniscus an array of particles is formed due to immersion capillary forces.

## Fluid flow

Inside a liquid droplet a current of solvent molecules is induced, a fluid flow. Since the system is striving for a gas-liquid equilibrium solvent molecules evaporate at the liquid-gas interface.<sup>24 61</sup> Majumder *et al.* found that the direction of the fluid flow depends on the solvent used.<sup>63</sup> In case inorganic solvents were used, a solvent flux was induced from the bulk to the edges of the droplet, as illustrated in figure 12a. The solvent flux induced a particle flux in the same direction as the fluid flow. The particles were found to deposit in ring-like structures, similar to the well-known coffee stains, at the edges of the droplet.<sup>25 63 64</sup> When organic solvents were used the fluid was circulated within the droplet by a Marangoni flow, as is illustrated in figure 12b. Therefore, the particles were circulated within the droplet as well, resulting in a uniform deposit when all solvent had evaporated.<sup>65</sup>

For most applications large ordered colloidal arrays are required.<sup>28 66</sup> Unfortunately, many colloids are dispersed in inorganic solvents, resulting in ring-like deposits. Therefore, many studies have been performed to influence the fluid flow and thus the shape of the deposit obtained in CA experiments with the DD method.<sup>67 68</sup> A study by Deegan *et al.* showed that a Marangoni flow could be induced in inorganic solvents by changing the environment of the droplet. They covered an inorganic dispersion droplet with a chamber leaving only a small air-hole above the center of the drop. Therefore, heat transfer of the droplet with its surroundings could only occur through this air-hole. Consequently, the fluid flow was circulated in the same way as for organic solvents, by a Marangoni flow, and an uniform deposit was obtained. The fluid flow was also influenced by changing the gas surrounding the droplet. By exposing the droplet to air saturated with ethanol vapour a surface tension gradient was formed at the liquid-air interface.<sup>69</sup> Since the surface tension at the edges of the droplet was lower compared to the top of the droplet a Marangoni flow was induced resulting in the formation of a uniform deposit. Other studies showed that instead of changing the surroundings of the droplet, the fluid flow could also be influenced by changing the composition of the droplet.<sup>70</sup> Still *et al.* showed for instance that by the addition of a small amount of surfactant the surface tension of the droplet was locally changed.<sup>71</sup> This induced a Marangoni flow as well.

These studies show that the fluid flow and therefore the shape of the deposit can be influenced by changing the environment of the droplet or by changing the composition of the droplet. Therefore, large deposits can be obtained, which is interesting for applications such as the fabrication of photonic crystals.<sup>8</sup>

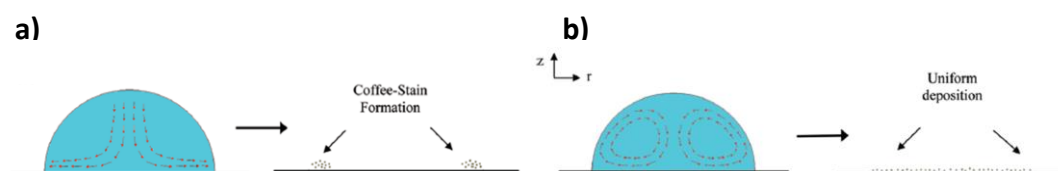


**Figure 12: Fluid flow inside a drying dispersion droplet using a) an inorganic solvent, resulting in a ring-like deposit of particles b) an organic solvent, resulting in a uniform deposit of particles[Majumder *et al.* 2012]**

## Meniscus pinning and capillary forces

How colloids deposit on a solid surface in CA experiments was studied by Deegan *et al.*, whom performed CA experiments using inorganic droplets with and without colloids.<sup>72</sup> They observed that the meniscus of a dispersion droplet was pinned, which was not observed in the absence of colloids. While the volume of the droplet decreased due to solvent evaporation, the contact line stayed in place, resulting in a decrease of the contact angle at the meniscus. By studying two-dimensional arrays of latex spheres, they observed that nuclei of colloids were formed at the contact line. From this nuclei larger structures were formed by attractive capillary forces.

Two kind of attractive capillary forces, flotation and capillary forces, were observed to contribute to the total capillary interaction energy,  $\Delta W$ . Flotation capillary forces are present when particles are floating at a liquid-air interface. When the gravitational force acting on the particles is large enough, the particles will deform the interface. Since this is energetically unfavourable particles are pushed together by flotation forces to account for this deformation, which is illustrated in figure 13a. Here is also illustrated that flotation capillary forces are only present when the interface is deformed. Immersion capillary forces are present when particles are immersed in a liquid on a solid surface. When the height of the solvent layer between two colloids is smaller than the size of the particles the liquid-air interface starts to deform. To correct for this deformation particles are pushed together by so-called immersion capillary forces, as illustrated in figure 13b.1 – 13b.4.

Denkov *et al.* determined that the contribution of flotation and immersion capillary forces to the total capillary interaction energy,  $\Delta W$ , depends on the size of the colloids, as can be seen in figure 14.<sup>24</sup> For small colloids the gravitational force acting on the particles is often too weak to cause a significant deformation of the interface. Figure 14 shows that for particles  $< 20 \mu\text{m}$   $\Delta W$  was only determined by immersion forces, therefore flotation forces could be neglected. Since in this study micron-sized colloids are used it is expected that only immersion forces will contribute to the formation of colloidal structures in CA experiments.

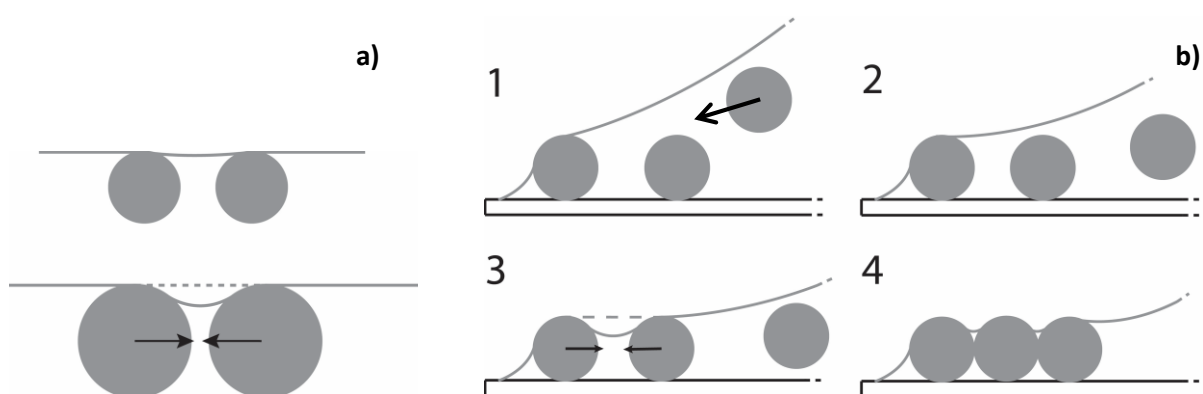


**Figure 13: Illustration of attractive capillary forces a) Top, floating particles without flotation forces. Bottom, floating particles pushed together by flotation capillary forces b) The role of immersion capillary forces in CA experiments 1) Convective transport of particles to the contact line of the meniscus with the substrate 2) A particle is pinned on the substrate and the contact angle is decreased due to solvent evaporation 3) Particles are pushed together by immersion forces since the height of the solvent layer between two pinned particles is smaller than particle size 4) A nucleus of particles is formed.**

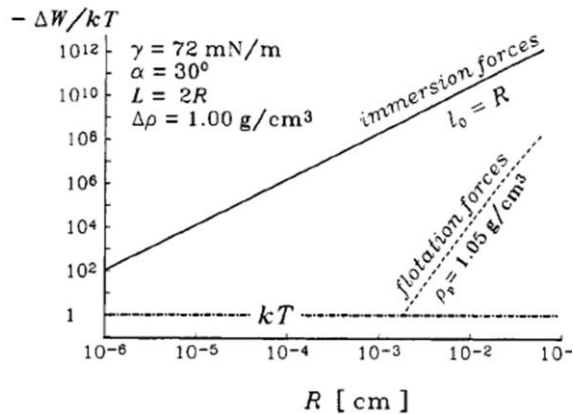


Figure 14: Plot of the total capillary interaction energy,  $\Delta W$  vs the radius of latex spheres showing the contribution of immersion capillary forces and flotation capillary forces to [Denkov *et al.* 1992]

## Structure formation

The formation of a structure of micron-sized silica spheres formed in CA experiments was studied in detail by Meng *et al.*<sup>29</sup> This CA process was studied in real-time with optical microscopy and the obtained deposits were studied with electron microscopy and confocal microscopy. They observed multilayered structures were formed with hexagonal order in the layers. Interestingly, other arrangements were found at transition regions from  $n$  to  $n+1$  layers, as can be seen in the SEM image shown in figure 15a. In figure 15b part of the transition region from bi- to trilayer is shown and a simulation of the order is shown as well. A change in order from hexagonal to rectangular to square was observed at the transition regions. The square order was finally developed to hexagonal order in the trilayer. This specific stacking occurs because the growth kinetics is affected not only by the physical constraint of the meniscus, but also the constant feedback between the deposited structure and the incoming particles. For structures with more than 4 layers the transition mechanism seems to be more complex. In crystallization experiments particle shape is known to be determinant for the order in the final structure.<sup>73</sup> It is therefore interesting to study the arrangements formed by non-spherical colloids and whether the order in the transition regions is different from the order in the layers as well.

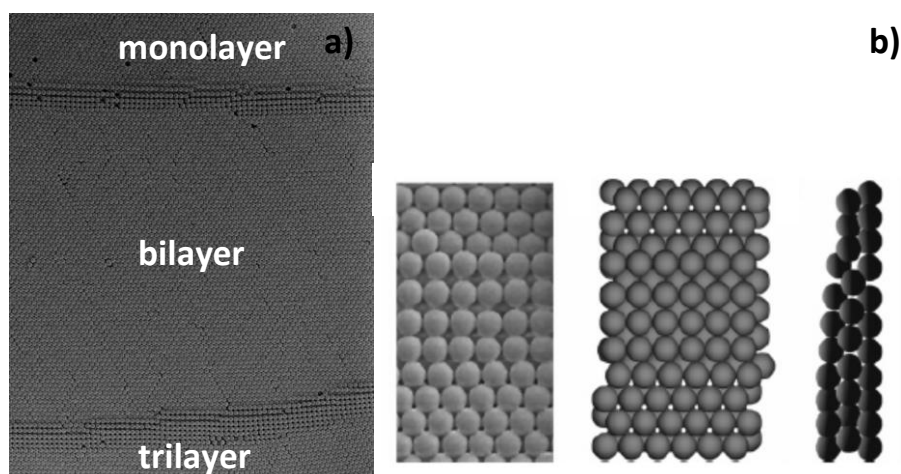


Figure 15: Structures of micron-sized silica spheres formed in a CA experiment in water a) SEM image of a monolayered structure. At the top of the image a monolayer can be seen. During growth (downward) the thickness of the crystal increases in monolayer steps. At the transition regions, two, shown in the images square packing is observed b) left, SEM image of a transition region from bilayer (top) to trilayer (bottom). Right, a simulation of the top and side view of a transition region [Meng *et al.* 2006]

## *Experimental parameters*

The formation of the structure is dependent on particle properties and the experimental conditions used. Conditions such as temperature, concentration, solvent and substrate are shown to be determinant for the orientation and size of the crystal domains, as well as the thickness of the structure.<sup>74</sup> Therefore, these experimental parameters are briefly discussed.

### Temperature

Temperature is important since it influences the evaporation rate of the solvent and therefore the timescale at which the structure is build.<sup>75 76</sup> At high temperatures the solvent is evaporated in a short time. Therefore, particles are transported to the growth front at the meniscus in a short time as well. Since many particles arrive as this growth front at the same time a multilayered structure is often formed. When a disordered structure is formed, the colloids did not have enough time to self-assemble in a dense ordered structure, indicating the temperature was too high. At low temperature the solvent is evaporated slowly and particles are transported to the meniscus on a long timescale. Monolayered structures can be obtained in this way, but for most CA methods a low temperature is unfavourable since colloids have often sedimented before reaching the growth front.

### Concentration

The concentration of the dispersion is important in CA experiments since the thickness of the structure can be tuned. A high concentration results in the convective transport of many particles to the growth front, resulting in a multilayered structure. A low concentration can be used to obtain monolayers. When the concentration is too low small areas of particles will be obtained instead of one single array, since only a few particles are pinned at the meniscus forming small nuclei for crystal growth.

### Solvent

The solvent choice is important since it determines the fluid flow inside the dispersion and therefore the shape of the deposit. Secondly, the density difference between the solvent and the particles can be tuned which is important since in this way sedimentation can be opposed.

### Substrate

The substrate is important because the shape of the meniscus and the contact line can be tuned. When water is used as a solvent a high contact angle will be obtained with a hydrophobic substrate, resulting in a multilayered structure formed at the growth start. A low contact angle can be obtained with a hydrophilic substrate, resulting in the formation of monolayers. To influence and control crystal growth patterned substrates can be used as well.

The parameters described are only a few of the parameters involved in CA experiments. The difficulty with CA experiments is that many parameters are interconnected. A raise in temperature for instance induces an increase in the solvent evaporation rate and concentration. Therefore, it is difficult but necessary to control the conditions during convective assembly experiments.

### 3.1.2. Methods

There are many methods that can be used to form a colloidal array using CA. In general important parameters such as temperature, concentration, solvent and substrate are tuned in each method. How these parameters are tuned is different for each method as well as the setup used. Therefore, it depends entirely on the system of interest and the preferred final structure which method is most suited. Since in this study large hollow silica cubes will be used, the main challenge will be to oppose sedimentation. Therefore, three different CA methods, the drying droplet(DD) method, a horizontal deposition(HD) method and a flow-controlled vertical deposition(FCVD) method will be used in this study. In this section the setup, experimental conditions, benefits and disadvantages of these methods will be discussed in detail.

#### *Drying droplet*

In the DD method a droplet of colloidal dispersion( $\sim 25 \mu\text{L}$ ) is placed on a substrate forming a setup as illustrated in figure 16a. The solvent is evaporated in less than one hour, resulting in a ring-like or uniform deposit depending on the solvent used. With this method the CA process can be studied in real-time using inverted microscopy. Therefore, dynamics and interactions present during CA can be studied.

This method is often used since the mechanism is well-studied, the setup is relatively easy to build, a small amount of material is required and the timescale of an experiment is short. Besides these benefits, there are disadvantages as well. Important experimental conditions such as temperature, fluid flow, droplet shape and the contact angle are difficult to control. Therefore, the reproducibility of DD experiments is low. Since colloids are often dispersed in inorganic solvents, ring-like deposits are obtained. To obtain larger ordered structures other CA methods are required.

#### *Horizontal deposition*

The HD method was first introduced by Prevo *et al.* in 2004.<sup>46</sup> With this method two microscope slides are positioned to make an angle of  $20 - 30^\circ$ , as illustrated in figure 16b. The sample,  $10 - 100 \mu\text{L}$  of dispersion, is placed in the corner made by the two slides. Due to CA a deposit of particles is formed on the horizontal slide in  $\sim 8$  hours. This deposit is formed from the growth front at the meniscus into the corner. Under ideal conditions a deposit of ordered mono- and/or multilayered structures covering a large area of the substrate, up to  $1 \text{ cm}^2$ , can be obtained.

With the HD method important parameters such as temperature, contact angle and slide angle, can be controlled. This method is also often used since a small amount of material is required, the setup is relatively easy to build and the duration of one experiment is relatively short. Another advantage of this method is that it can easily be adapted to the colloidal system of interest. Prevo *et al.* have shown for instance that the thickness of the deposit can be controlled by withdrawing the upper slide. Large thin films were obtained using this adapted version of the HD method.<sup>77</sup> Others have adapted the HD to oppose sedimentation, by tilting the setup of by using elevated temperatures.<sup>44 54</sup>

Although ordered structures can be formed with the HD method, the results are difficult to reproduce. This is mainly caused by the contact line at the growth start, which has a different shape in every experiment. Also, the setup is designed such that the sample is exposed to its surroundings at all sides. This makes it difficult to gain control over the fluid flow and it also causes that the growth start on the substrate is always curved which is thought to influence the orientation of the particles.

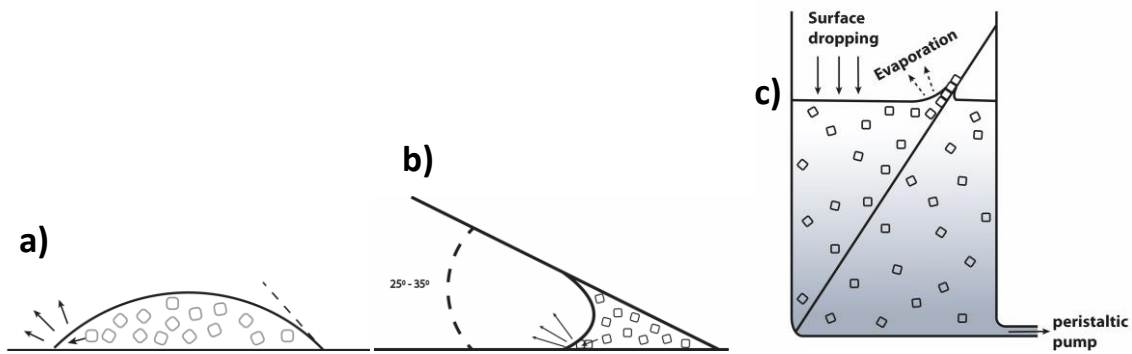


Figure 16: Illustrations of the side view of setups used in CA experiments with a) the DD method b) the HD method c) the FCVD method

### *Flow-controlled vertical deposition*

The FCVD method is an adjusted version of the normal vertical deposition (VD) method. In many studies the normal VD method was successfully used to form ordered colloidal arrays.<sup>78</sup> However, some colloidal systems require some adjustments. In CA experiments with micron-sized colloids sedimentation is known to be a problem.<sup>79-80</sup> The FCVD method was first used by Zhou and Zhao to form photonic crystals of polystyrene particles with sizes ranging from 0.5 – 1.5  $\mu\text{m}$ .<sup>22</sup> With the normal VD method a substrate is placed vertically or under a small angle in a sample cell containing the dispersion. By CA an array of particles is formed on the substrate. With the FCVD method the sample cell is connected to a peristaltic pump, regulating the surface dropping velocity. An illustration of a FCVD setup is shown in figure 16c. During the experiment the sample is heated, increasing the evaporation rate of the solvent and therefore the convective transport rate of particles toward the meniscus. The increased temperature increases the thermal energy of the particles as well, opposing sedimentation. The surface dropping velocity can be tuned such that a thick or thin deposit is obtained. In 20 – 40 hours a large deposit can be obtained. Under ideal conditions the deposit contains large ordered structures. Since the contact line is a relatively straight line it is expected that ordered domains with similar orientation can be formed. Since many experimental parameters can be controlled with the FCVD method the reproducibility of results is high. On the other hand, the method has some disadvantages as well, such as the large amount of material required, 10 – 20 mL dispersion, per experiment. The setup is relatively difficult to build and the experiments are time consuming. Experiments by Meijer *et al.* with 774 nm hollow silica cubes showed that the normal VD method was not suited to obtain ordered arrays of these cubes, since sedimentation was a problem.<sup>44</sup> To account for this problem they performed VD experiments at elevated temperatures resulting in ordered mono- and multilayers. Since in this study even larger cubes are used the method used by Meijer *et al.* will not account to the same extent for sedimentation. Therefore, the FCVD method will be used.

### 3.1.3. Structures of colloidal superballs

In this study hollow silica cubes with rounded edges are used. Although with CA experiments structures with a high packing density can be obtained, structures of lower density can be obtained as well, since polydispersity, drying effects and experimental errors can influence the structure formation. Therefore, experiments and simulations of 2D and 3D structures of superdisk and superball-shaped particles can be a useful tool in the analysis of experimental data. Simulations of cubes with rounded edges have been performed to study the phase behaviour and to determine the arrangement with the maximum packing density.

Cubes with rounded edges are approached by the superball-shape, where the roundness of the edges is quantified by a deformation parameter  $m$ , as described in section 2.1.1. Different definitions and characters can be used to define this deformation parameter. Table 9 lists some definitions used for the deformation parameter in different studies. In studies with superballs(3D),  $m$ ,  $p$  or  $q$  was used, where all characters are interconnected. The deformation parameter used for superdisks(2D) can be defined as  $p$  or  $L^*$ , where different descriptions are used.

The definitions and properties of the deformation parameters used in this study are listed in table 10. For clarity reasons the deformation parameter for superballs will be defined as  $m$  in this study. Therefore, results obtained in other studies of 3D structures will be presented here using the deformation parameter  $m$ . Since,  $p$  and  $L^*$  used in 2D studies are defined in a different way both characters will be used in this study.

**Table 9: Definitions of the superdisk/ball deformation parameter used in different studies**

Reference	Definition superball	# Dimensions	Deformation parameter
J.M. Meijer <i>et al.</i> 2012	$\left \frac{x}{a}\right ^m + \left \frac{y}{a}\right ^m + \left \frac{z}{a}\right ^m \leq 1$	3	$m$
R. Ni <i>et al.</i> 2012	$ x ^{2q} +  y ^{2q} +  z ^{2q} \leq 1$	3	$2q (= m)$
Y. Jiao <i>et al.</i> 2008, 2009	$ x_1 ^{2p} +  x_2 ^{2p} + \dots +  x_d ^{2p} \leq 1$	2, 3	$2p (= m)$
C. Avendano <i>et al.</i> 2012	$L^* = \frac{L}{\sigma}$ 	2	$L^*$

**Table 10: Definitions and characters of the deformation parameter for superdisks/balls used in this study**

Deformation parameter	Superball/ superdisk	Sphere/ Circle	Cube/ square
$m$	$2 < m < \infty$	$m = 2$	$m = \infty$
$p$	$1 < p < \infty$	$p = 1$	$p = \infty$
$L^*$	$0 < L^* < \infty$	$L^* = 0$	$L^* = \infty$

## 2D Phase behaviour

Simulations of hard squares were first performed by Wojciechowski and Frenkel in 2004.<sup>81</sup> The phase behaviour was studied by compressing and expanding a system of square-like molecules. An isotropic phase was observed at low pressure and a crystalline simple square phase at high pressure. Between these two extremes a tetratic phase was found, characterized by short range translational order and quasi long range orientational order.

An experimental study of the 2D phase behaviour of squares was performed by Zhao *et al.* in 2011.<sup>82</sup> Here, squares of SU-8 polymer were used with an edge length of  $2.4 \pm 0.1 \mu\text{m}$  and a thickness of  $2.0 \pm 0.1 \mu\text{m}$ . The corners of the squares were slightly rounded with an average radius of curvature of  $0.30 \pm 0.05 \mu\text{m}$ . A monolayer was formed by sedimentation and by using roughness-controlled depletion the squares were forced to lie flat at the bottom of the cell. The density in the monolayer was increased by tilting the cell. Phase behaviour was studied by increasing the particle area fraction,  $\phi_A$ , in the monolayer.

At  $\phi_A \leq 0.60$  an isotropic(I) phase was found, where the orientation of the squares was random (figure 17a). At  $0.61 \leq \phi_A \leq 0.63$  an hexagonal rotator (RX) phase was found, shown in figure 17b. In this phase the squares can still fully rotate, but as the Fourier transform shows, hexagonal translational order is present. For  $0.64 \leq \phi_A \leq 0.66$  a coexistence region (CE) containing both RX and rhombic (RB) crystallites was found. A typical optical microscopy image of this CE phase is shown in figure 17c. Here, the RX crystallites are encircled by a blue line and the RB crystallites are stroked with red. The Fourier transform clearly shows the six peaks of the RX phase and two peaks of the RB phase. A pure RB phase is found for  $\phi_A > 0.66$ , where strong orientational order is obtained as well (figure 17d).

These experimental results are not in agreement with the hard square simulations of Wojciechowski and Frenkel. The main difference of these studies is that Wojciechowki and Frenkel used perfect squares, whereas Zhao *et al.* used squares with rounded edges.

On the occasion of these findings, Monte Carlo simulations of squares with rounded edges were performed by Avendano and Escobedo in 2012.<sup>38</sup> The roundness of the edges was determined by the deformation parameter  $L^*$ . Simulations were performed at different  $L^*$ -values and different area fraction,  $\eta_A$ . The phase diagram shown in figure 18 shows five different phases were found. It was

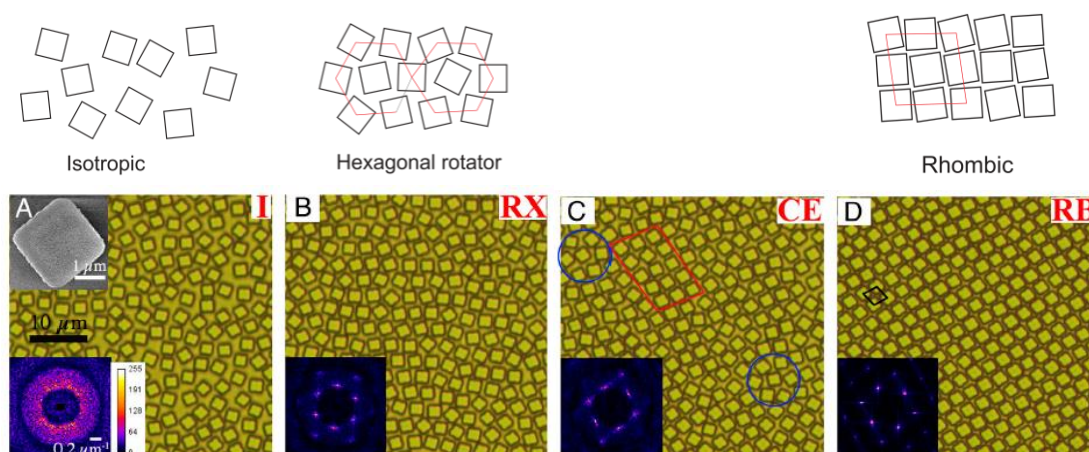


**Figure 17: Transmission optical micrographs showing different order in a monolayer of Brownian squares at different particle area fractions  $\phi_A$  a)  $\phi_A = 0.52$ , Isotropic(I) phase b)  $\phi_A = 0.62$ , hexagonal rotator crystal (RH) phase c)  $\phi_A = 0.65$ , coexistence region of RX and RB d)  $\phi_A = 0.74$ , rhombic (RB) crystal. The inset in the upper left corner shows a SEM image of a Brownian square. The insets in the lower left corners show FT intensities calculated from monochrome real-space images supporting the presence of the different phases [Zhao *et al.* 2011]**

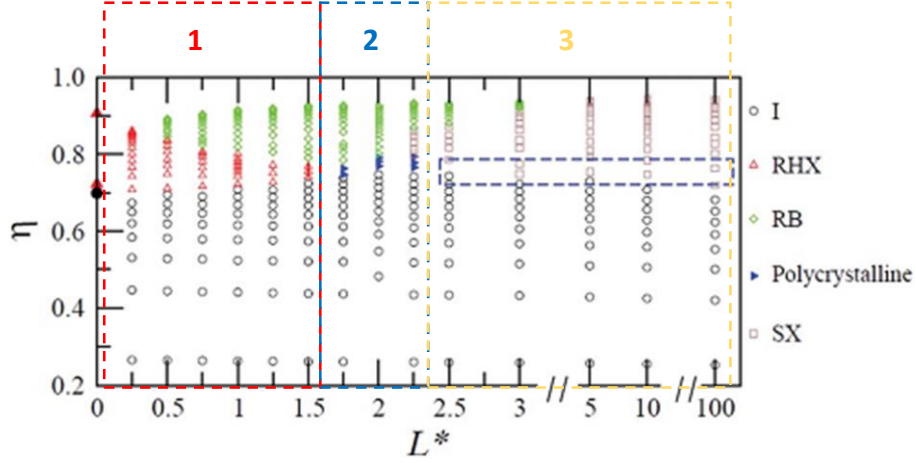


Figure 18: Phase diagram of rounded squares [Avendano *et al.* 2012]

observed that the maximum packing density (MPD) increased with  $L^*$  and in general an I phase was found at low  $\eta_A$ . At higher  $\eta_A$  the phase diagram can be divided in three regions,  $L^* < 1.5$ ,  $1.5 < L^* < 2.5$  and  $L^* > 2.5$ , where different phase behaviour was observed. In the first region,  $L^* < 1.5$ , the I phase proceeded in a RHX (RX) phase at  $\eta_A \sim 0.7$ . For  $0.5 < L^* \leq 1.5$  the MPD was obtained in the RB phase. In the second region,  $1.5 < L^* < 2.5$ , the I phase changed to a polycrystalline phase at  $\eta_A \sim 0.75$ , which is absent for squares with  $L^* < 1.5$  and  $L^* > 2.5$ . The MPD was obtained in the RB phase, which is similar to region 1. In the third region,  $L^* > 2.5$ , the I phase immediately evolves to a simple square (SX) phase at  $\eta_A \sim 0.75$ . For  $L^* \leq 3$  the MPD was still obtained with the RB phase but for  $L^* > 3$  the SX phase is preferred.

These simulations are in agreement with the experimental results of Zhao *et al.* In figure 18, the I phase evolves to a RX and a RB phase at  $0.5 \leq L^* \leq 1.5$ , which is also the case for the squares used in the experiments of Zhao *et al.* Both in experiment and simulation three phases, I, RX and RB, were found when the density was increased.

These studies emphasize the importance of particle shape on phase behaviour. A significant influence on the phase behaviour was observed when the roundness of the edges of squares was changed. The phase behaviour of squares with rounded edges was found to be much richer and more complex compared to perfect squares. It is therefore important to quantify the roundness of the edges and to mind the large influence of the rounded edges on the structures formed with CA.

## 2D Maximum packing density

An extended study was performed by Jiao *et al.* simulating the maximum packing density (MPD) of superdisks.<sup>39</sup> They determined the MPD of superdisks using an event-driven molecular dynamics packing algorithm.<sup>83</sup> Simulations were performed for convex,  $p \geq 0.5$ , and concave,  $0 < p < 0.5$ , particles. For superdisks  $p > 1$ , therefore only these results will be discussed here.

The MPD of superdisks is obtained when they arrange on a  $\Lambda_0$  and  $\Lambda_1$  lattice. The lattice vectors or these two new Bravais lattices are given by

$$\mathbf{e}_1 = 2\mathbf{i}, \mathbf{e}_2 = \mathbf{i} + (2^{2p} - 1)^{1/2p} \mathbf{j} \quad \text{and} \quad \mathbf{e}_1 = 2^{(1-1/2p)} \mathbf{i} + 2^{(1-1/2p)} \mathbf{j}, \mathbf{e}_2 = (2^{-1/2p} - 2^{1/2s}) \mathbf{i} + (2^{-1/2p} - 2^{1/2s}) \mathbf{j},$$

for  $\Lambda_0$  and  $\Lambda_1$  respectively, where  $\mathbf{i}$  and  $\mathbf{j}$  are unit vectors along  $x_1$ - and  $x_2$ -directions and  $s$  is the smallest positive value for  $|2^{-(1+1/2p)} - 2^{-1/2s}|^{2p} + |2^{-(1+1/2p)} + 2^{-1/2s}|^{2p} = 1$

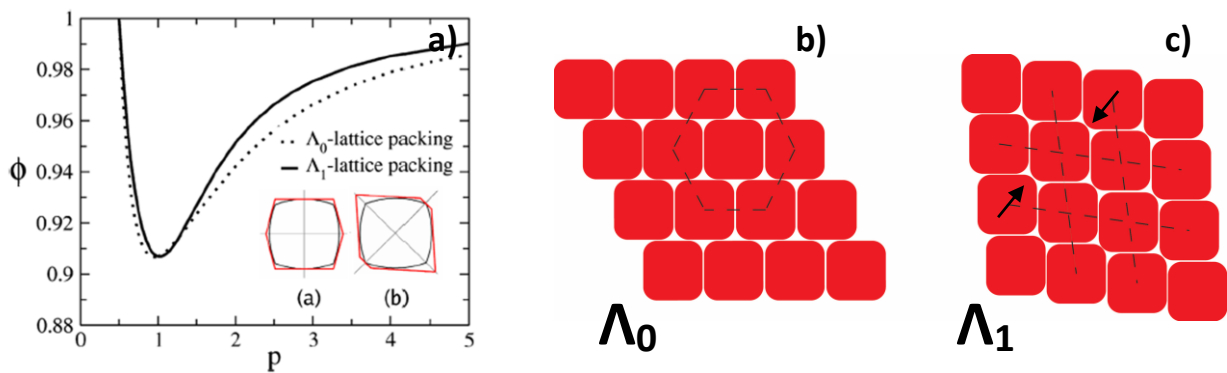


Figure 19: a) Maximum packing density plot of superdisks, represented as density vs deformation parameter  $p$ . MPD is obtained with the  $\Lambda_0$  and  $\Lambda_1$  lattice. At  $p_c = 1.282$  the packing density of the lattices is equal. At  $p > 1.282$  the packing density obtained with the  $\Lambda_1$  lattice is slightly higher compared to the density obtained with the  $\Lambda_0$  lattice[Jiao *et al.* 2008] b) An illustration of superdisks in a  $\Lambda_0$  arrangement c) An illustration of superdisks in a  $\Lambda_1$  arrangement

The MPD plot in figure 19a shows that the MPD increases with  $p$ , where a MPD of 100% is obtained for perfect squares, e.g. at  $p = \infty$ . At low  $p$ -values the superdisks are close to spherical and arrangements close to hexagonal are formed. At  $p = 1.286$  the MPD obtained with the  $\Lambda_0$  and  $\Lambda_1$  lattice is equal. The difference between the lattices becomes significant at higher  $p$ -values. On the  $\Lambda_0$  lattice the arrangement is still close to hexagonal, since the sides of the disks are aligned. On the  $\Lambda_1$ -lattice the edges of the disks are pushed together, resulting in more spacefilling structures at higher  $p$ -values, since the lattice evolves to a simple square lattice at  $p = \infty$ .

In an experimental study performed by Meijer *et al.* monolayers formed by superball-shaped particles were studied.<sup>44</sup> These monolayers were formed in CA experiments by hollow silica cubes of 774 nm with a polydispersity of 4.5% and a  $m$ -value of 2.9. The VD method was used at elevated temperatures. With an oven-setup, illustrated in figure 20a, large ordered crystalline films were obtained and with the  $\Delta T$ -setup, illustrated in figure 20b, ordered multilayered structures were formed. A SEM image of a monolayer of cubes obtained with the oven-setup is shown in figure 21a. In the encircled areas square-like and hexagonal-like arrangements can be observed, which are enlarged displayed in figure 21b and 21c. These findings were supported by small angle X-ray scattering experiments, as can be seen by the SAXS patterns shown below figure 21b and 21c. Mainly hexagonal-like structures with long-range order were found in this study. Comparison of these hexagonal-like structures to the  $\Lambda_0$  lattice of Jiao *et al.* for superdisks indicate these arrangements are similar.

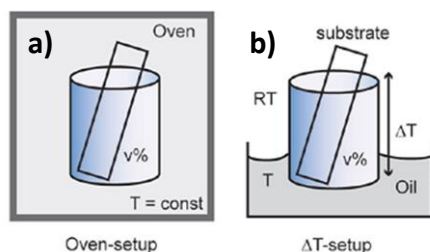
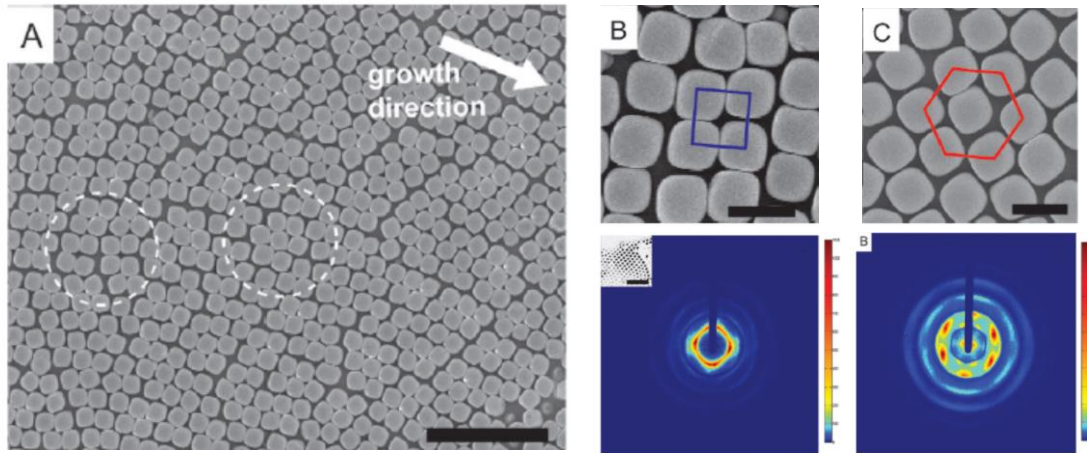


Figure 20: Schematic representation of two adapted VD setups a) An oven-setup, where the VD experiment is performed in the oven at an elevated temperature b) A  $\Delta T$ -setup, where the VD experiment is performed in an oil-bath creating a temperature gradient in the dispersion[Meijer *et al.* 2012]



**Figure 21: SEM images and SAXS patterns of a monolayer of hollow silica cubes obtained in VD experiment with the oven-setup a) SEM image of an ordered monolayer with square-like and hexagonal-like arrangements encircled by the white dashed lines b) Cubes in a square-like arrangement with below a SAXS pattern confirming square arrangements were formed by the cubes c) Cubes in a hexagonal-like arrangement with below a SAXS pattern showing hexagonal-like domains with long-range order were formed[Meijer *et al.* 2012]**

In figure 19a can be seen that at  $p = 1.45$  ( $m = 2.9$  in 3D) the MPD of the  $\Lambda_0$  and  $\Lambda_1$  lattice are almost equal. At larger  $m$ -values the difference in packing density between the  $\Lambda_0$  and  $\Lambda_1$  lattice increases. Therefore, it is very interesting to investigate which structures are formed by hollow silica cubes with a larger  $m$ -value and therefore a more cubic shape. Can we really differentiate between the two different lattices? And if so, is there a preference for one of the two lattices? In this study micron-sized hollow silica cubes are used to study the effect of the roundness of the edges on the formed structures.

### *3D Phase behaviour and maximum packing density*

Cubic colloids can form colloidal crystals which occupy 100% of space by adapting a simple cubic arrangement. Although it is experimentally shown that superball-shaped colloids can be driven in a simple cubic arrangement by the addition of a small depletant, simulations show the MPD for superballs is obtained with other arrangements.<sup>31,44</sup>

The phase behaviour in 3D was studied by Ni *et al.* whom calculated the free energy of superballs in both the fluid and crystal phases.<sup>42</sup> In the phase diagram shown in figure 22 can be seen that for superballs,  $q > 1$ , four different phases were found. Depending on the packing fraction ( $\phi$ ) and the roundness of the edges a fluid phase, a plastic face-centered cubic (fcc) crystal or a deformed  $C_0$  or  $C_1$  phase was obtained. Cartoons of the different phases are shown in the phase diagram as well. Similar to simulations of superdisks the maximum packing fraction, indicated by the bold black line increases with increasing deformation parameter. The MPD of spheres ( $m = 2$ ) is 0.74 and the MPD for perfect cubes is 1.0. In general a fluid phase is formed below  $\phi \sim 0.5$ . The fluid phase evolves in a plastic fcc crystal for low  $m$ -values, where hexagonal translational order is present, but the particles are still free to rotate. At higher  $\phi$  a deformed  $C_1$  lattice is found. At  $m$ -values close to 2, the fcc crystal phase develops to a deformed  $C_0$  lattice. At larger  $m$ -values the fcc crystal phase or the fluid phase evolves to the deformed  $C_1$  lattice.

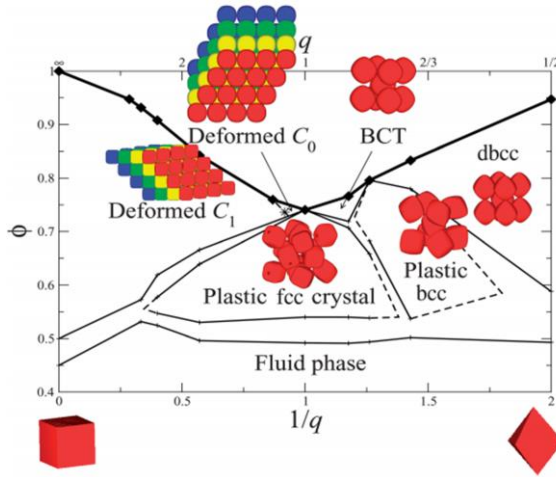


Figure 22: Phase diagram of hard superballs in the  $\phi$  versus  $1/q$  or  $q$  representation where  $q$  is the deformation parameter and  $2q = m$ . For superballs ( $q > 1$ ) four different phases are observed, a fluid phase, a plastic fcc crystal and the deformed  $C_0$  and  $C_1$  phases [Ni *et al.* 2012]

The  $C_0$  and  $C_1$  lattices were introduced in 2009 by Jiao *et al.* whom found that with these lattices the highest packing density of superballs was obtained.<sup>40</sup> A schematic view of the  $C_0$  and  $C_1$  lattices is shown in figure 23b and 23c. Both lattices are obtained by the deformation of a fcc crystal and each superball has 12 contacting neighbours. By increasing the  $m$ -value the continuous rotational symmetry of a sphere is broken but a threefold symmetry of the superball remains. The lattice vectors for a  $C_0$  lattice of superballs with a certain  $p$ -value are given by

$$\mathbf{e}_1 = 2^{1-1/m}\mathbf{i} + 2^{1-1/m}\mathbf{j}, \mathbf{e}_2 = 2\mathbf{k} \text{ and } \mathbf{e}_3 = -2s\mathbf{i} + 2(s + 2^{-1/m})\mathbf{j} + \mathbf{k}$$

where  $\mathbf{i}$ ,  $\mathbf{j}$  and  $\mathbf{k}$  are the unit vectors along the coordinate axis and  $s$  is the smallest positive root in  $(s + 2^{-1/m})^m + s^m + 2^{-m} - 1 = 0$

The lattice vectors for a  $C_1$  lattice are given by

$$\mathbf{e}_1 = 2^{1-1/m}\mathbf{i} + 2^{1-1/m}\mathbf{j}, \mathbf{e}_2 = 2^{1-1/m}\mathbf{i} + 2^{1-1/m}\mathbf{k}, \mathbf{e}_3 = 2(s + 2^{-1/m})\mathbf{i} - 2s\mathbf{j} - 2s\mathbf{k},$$

where  $s$  is the smallest positive root in  $(s + 2^{-1/m})^m + 2s^m - 1 = 0$

The plot in figure 23a shows the packing density of the  $C_0$  and  $C_1$  lattices vs the deformation parameter  $p$ . The lowest packing density of 0.74 is achieved for  $p = 1$ , representing spheres in a fcc lattice. From  $1 < m/2 < 1.1509$  slightly higher packing densities are obtained for  $C_0$  lattices compared to  $C_1$ . Similar to superdisks there is a critical value of  $m$ ,  $m_c$ , where the packing density of  $C_0$  and  $C_1$  are equal. For  $m/2 > 1.1509$  a higher packing density is obtained with the  $C_1$  lattice, since this lattice can deform from an fcc arrangement to approach the simple cubic lattice. This explains why in the phase diagram of Ni *et al.* (fig 22) the  $C_1$  lattice is preferred over the  $C_0$  lattice for most values of  $m$ .

The lattices found for superballs have some similarities with the arrangements found for superdisks, namely that in both cases two possible lattice arrangements are found with similar MPD and which both originate from hexagonal arrangements. It is shown that structures formed by superballs in 3D are similar to the  $\Lambda_0$  and  $\Lambda_1$  lattice for superdisks in 2D. This is confirmed when the lattice vectors are considered, showing the  $C_0$  and  $C_1$  lattices are the 3D analogue of  $\Lambda_0$  and  $\Lambda_1$  lattices. In CA experiments ordered structures are formed using a planar surface as substrate. While the  $C_0$  and  $C_1$  lattice cannot be build up from a planar surface, it could be difficult to study these lattices in this study.

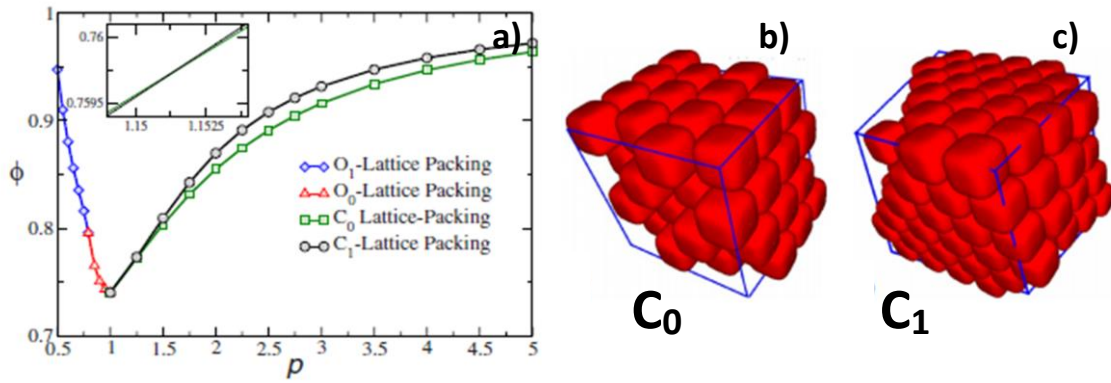


Figure 23: a) Maximum packing density plot of superballs, represented as density vs deformation parameter  $p$ . MPD is obtained with the  $C_0$  and  $C_1$  lattice. At  $p_c = 1.1509$  the packing density of the lattices is equal. At  $p > 1.1509$  the packing density obtained with the  $C_1$  lattice is slightly higher compared to the density obtained with the  $C_0$  lattice [Jiao *et al.* 2009] b) An illustration of superballs with  $p = 1.8$  in a  $C_0$  arrangement c) An illustration of superballs with  $p = 2.0$  in a  $C_1$  arrangement

## 3.2. Experimental

CA experiments with hollow silica cubes were performed using three different CA methods. In this section the setups and conditions used for experiments with the DD method, the HD method and the FCVD method are described. In these experiments plain glass substrates as well as patterned substrates were used to grow colloidal crystals. The pretreatment of these substrates as well as the fabrication of the patterns is describes here as well.

### 3.2.1. Sample preparation

#### *Colloidal dispersion*

The silica cubes were stored in ethanol to prevent etching of the cubes by water. To perform CA experiments in water, the cubes were transferred to water 1-5 days before the experiment was performed. The cubes were transferred to water by washing them at least three times using a microcentrifuge. The final concentration of the cubes was determined by measuring the ratio of the height of the sedimented cubes compared to the total volume in a 0.2 x 4.0 mm capillary. Assuming a packing density of 76% the volume concentration was determined.

#### *Substrates*

In CA experiments colloidal crystals were grown on plain glass substrates. These substrates were made from glass microscope slides(Menzel-Glaser) of 24 x 50 mm in dimensions. For the different CA methods substrates of different dimensions were required. Therefore, the original glass slides were cut to the preferred size with a diament pen. Before use the slides were pretreated by etching in a potassium-hydroxide(KOH) solution, consisting of 50 g KOH pellets(Merck) in a mixture of 100 mL water and 900 mL ethanol(100%, interchem). The slides were etched in this solution for 1-5 days, whereafter the slides were thoroughly washed with water and ethanol(100%, interchem) to remove remaining impurities.

The preparation of patterned substrates for CA experiments was slight different. First, these substrates were thouroughly cleaned with ethanol(100%, interchem) and water. Then, they were discharged using a Glow Discharger to make the polymer template lines more hydrophilic, thereby decreasing the contact angle of the meniscus. The glow discharge treatment was performed for 6, 15 or 30 s after which the substrates were used in CA experiments within 30 minutes.

### 3.2.2. Fabrication of templates

To regulate crystal growth in our CA experiments and to study the behaviour of the colloidal cubes during CA, templates were used. Experiments by Ng *et al.* showed that the meniscus can be pinned using substrates patterned with a hydrophic polymer, SU8.<sup>84</sup> Therefore, substrates with different patterns were fabricated to study whether different arrangements could be induced by influencing the orientation of the cubes at the growth start.

Patterned substrates were fabricated in a clean room at the MESA+ Nanolab facility with optical lithography. Square borosilicate wafers of 101.6 x 101.6 mm, with a thickness of 175  $\mu\text{m}$  were used as substrates. These wafers were provided with patterns of the epoxy-based negative photoresist SU8, which is a hydrophobic polymer with a molecular structure as shown in figure 24a.

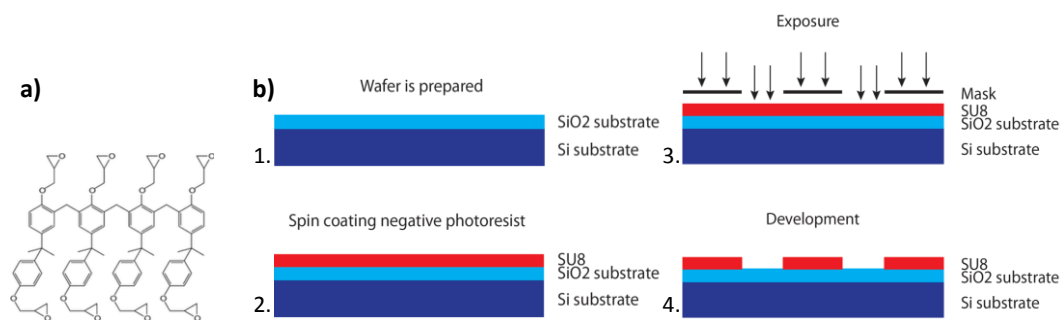


**Figure 24: Fabrication of patterned substrates a) Molecular structure of the SU-8 polymer b) Illustration of the different steps in the fabrication process**

Before the wafers were coated with SU8, they were thoroughly cleaned and prebaked. The SU8 was then spincoated on the wafer, whereafter the wafer was baked again. To provide the wafer with the preferred patterns a mask was used. The wafer with the mask was exposed to UV light of 365 nm, whereby the SU8 exposed to the light was removed by a reaction with the UV light. An illustration of this fabrication procedure is shown in figure 24b. In total four wafers were provided with patterns. The height of the polymer was measured at five different positions on the wafer, and ranged from 394 – 593 nm. The difference in height is a result of the spin coating procedure.

The mask divided each wafer into smaller individual slides, as shown in figure 25b. After fabrication the wafers were serrated into these slides and the exact dimensions of these slides are shown in table 11. Figure 25a illustrates that each slide contained several polymer lines with an interspacing of 900  $\mu\text{m}$ . Different kind of lines were fabricated including straight lines, arches, saw or tooth patterns. Graphical representations of the patterns are given in figure 25c.

The 10 x 10 mm slides were used in DD experiments and could be imaged with EM without the need of cutting. For HD experiments the 10 x 18.5 mm and 10 x 20 mm slides were used. The largest slides of 10 x 37 mm were used in FCVD experiments. Substrates with straight lines of  $10^4 \times 100 \times 0.5 \mu\text{m}$  were used to study whether a straight growth start could be induced in CA experiments by pinning the meniscus at the hydrophobic lines. The distance between two lines is 900  $\mu\text{m}$ , leaving enough space for the cubes to form ordered structures in between. The saw and tooth patterns were used to study whether cubes could be manipulated into a  $\Lambda_1$  and  $\Lambda_0$  arrangement respectively. The size of the saw and tooth ranges from 0.8 – 2.2  $\mu\text{m}$ , therefore the patterned substrates can be used for cubes of different sizes. Slides with arches contained arches of radii ranging from 10 – 200  $\mu\text{m}$ . This pattern was not used in this study but can be used to study the effect of a bend meniscus on the orientation of the cubes.

**Table 11: Dimensions and amounts of the individual slides per fabricated wafer**

Slides Wafer	1	2	3	4
# 1 x 1 cm	20	0	0	0
# 1 x 1.85 cm	20	20	20	20
# 1 x 2 cm	0	10	10	10
# 1 x 3.7 cm	10	10	10	10

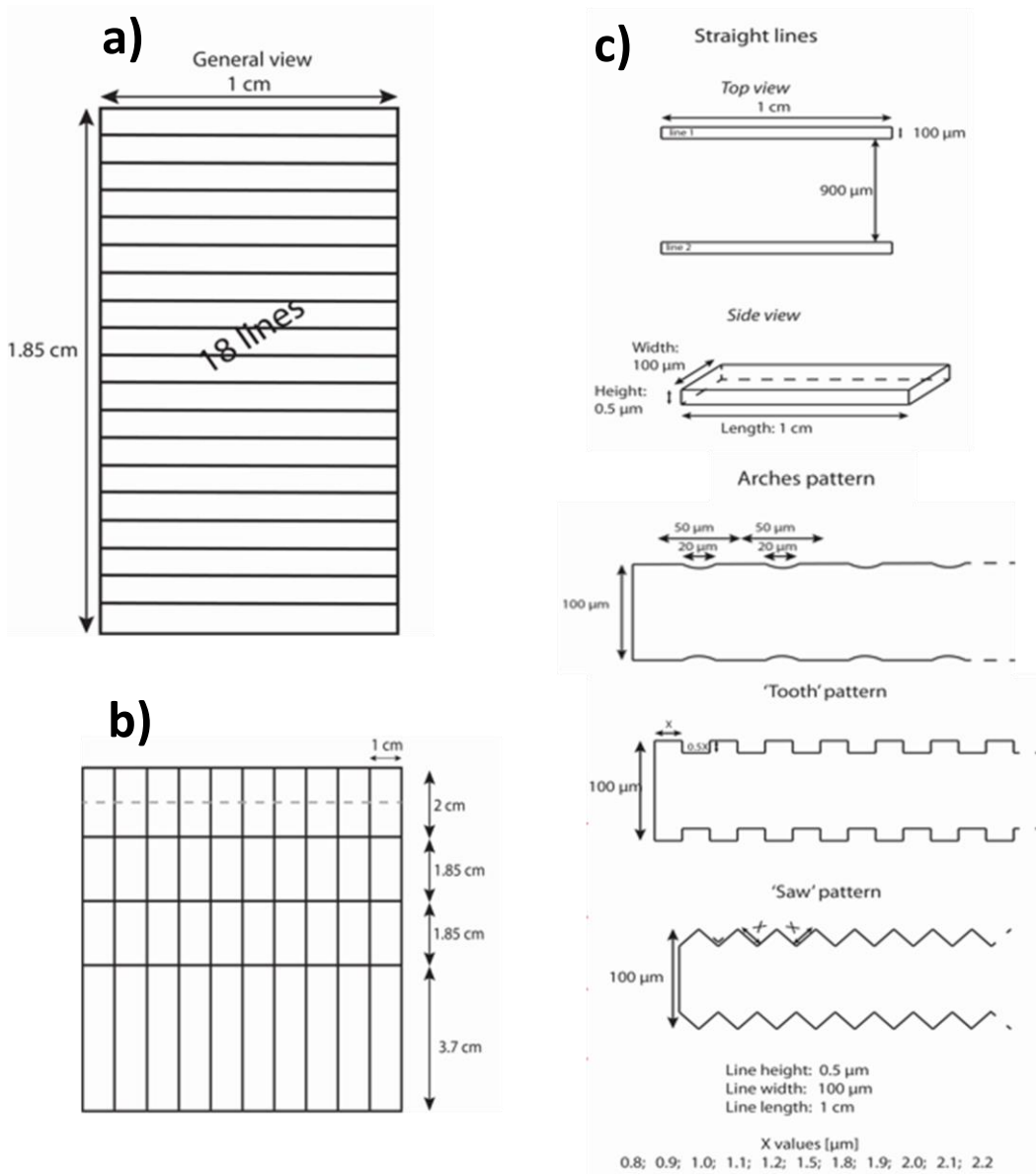
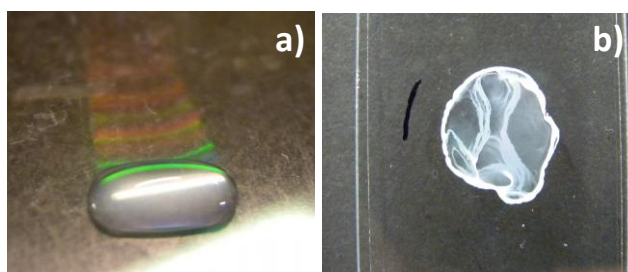


Figure 25: a) Mapping of the line structure on a single slide b) Dimensions of the individual slides prepared in one wafer c) Characteristic line patterns fabricated with their specific dimensions. From top to bottom; straight lines, tooth pattern, arches, saw pattern.

### 3.2.3. Setups

#### *Drying droplet method*

In DD experiments a dispersion droplet with a concentration ranging from 0.4 – 1 %V was placed on a substrate. When a plain glass substrate(24 x 50 mm) was used a 25  $\mu$ L droplet was dropped from  $\sim$ 3 cm height on the substrate. Therefore, the droplet was spread out and a low contact angle was obtained at the edges of the droplet. To further decrease the contact angle  $\sim$ 12  $\mu$ L of the volume was removed after  $\sim$ 30 s, when the meniscus was assumed to be pinned at the edges of the droplet. When a patterned substrate( $\sim$ 10 x 10 mm) was used a droplet of  $\sim$ 12  $\mu$ L was dropped on the substrate from  $\sim$ 3 cm height. Since the polymer pattern was slightly hydrophobic a high contact angle was obtained at the edges of the droplet. Therefore, the meniscus was not pinned easily and the contact angle could not be decreased by reducing the droplets volume. A picture of a droplet on a patterned substrate is shown in figure 26a. Here, it can be seen that light was reflected by the polymer lines on the substrate. After preparation the setup was moved by hand to an inverted optical microscope stage. Using this microscope in the transmission mode dynamics in the droplet were studied in real-time. During evaporation of the solvent interparticle interactions, interactions of particles with the substrate and growth of the colloidal array at the edge of the droplet was followed. The experiments were performed at constant temperature(293 K) in a low dust environment. Microscopy images were taken and real-time movies were constructed to study the behaviour of the colloids during CA in more detail. A ring-like deposit, such as shown in figure 26b was obtained in one hour and the deposits were imaged with SEM. Before SEM imaging the plain glass substrates were cut with a diamante pen to fit on the SEM-stud. The patterned substrates were in most cases small enough to fit on the stud, so no cutting was required.



**Figure 26: DD experiments with a dispersion of 0.4 %V hollow silica cubes(5\_S2\_H) in water a) a 12  $\mu$ L droplet on a patterned substrate with straight polymer lines b) A typical deposit of cubes on a plain glass substrate**



**Figure 27: Setup used in a HD experiment with 1 %V fluorescent hollow silica cubes(HC\_R\_fIH) in water, showing a deposit was formed at the bottom slide**

### *Horizontal deposition method*

For the HD method used in this study two plain glass substrates(10 x 50 mm) were placed under an angle of 25 - 35° using an optical table as subsurface, as can be seen in figure 27. 100 µL of dispersion with a concentration ranging from 0.1 – 1.2 %V was inserted in the corner made by the two substrates. Therefore, a droplet with a bend meniscus was formed in this corner. The setup was covered by a crystallizing dish to avoid irregular air flow. The solvent was evaporated in ~8 hours at roomtemperature and a deposit of particles was formed on the bottom substrate, as can be seen in figure 27. For the bottom substrate a patterned substrate(18 x 10 mm) was used as well, using the same procedure as for the plain glass substrates. The cube structures in the deposits were imaged in great detail with SEM. The plain glass substrates were cut with a diamante pen to fit on the stud, while for the patterned substrates this was unnecessary.

### *Flow-controlled vertical deposition method*

For the setup used in FCVD experiments a specially designed glass flask of ~50 mm in height and 20 mm in diameter, shown in figure 28a, was used. This flask has an outlet at the bottom that can be connected to a peristaltic pump to control the fluid flow and therefore the surface dropping velocity. In experiments, a peristaltic pump(Miniplus 3, Gilson silicon hose) was connected to this outlet, shown in figure 28b, resulting in a surface dropping velocity of ~1 mm/h. A sample with a concentration ranging from 0.5 – 2%V with a volume 8 – 20 mL of colloidal dispersion was inserted in the flask. The sample was heated to 45 °C using a thermostatic waterbath(Julaba ME) and a plain glass substrate(10 x 50 mm or 20 x 50 mm) or a patterned substrate (10 x 37 mm) was placed vertically at an angle of max 10° in the dispersion. Due to evaporation of the solvent particles were transported to the solvent-air meniscus and pinned on the substrate. An overview of the complete setup is shown in figure 28c. The total duration of an experiment was 24 – 40 hours. The dispersion residue collected with the peristaltic pump contained broken and collapsed silica cubes.

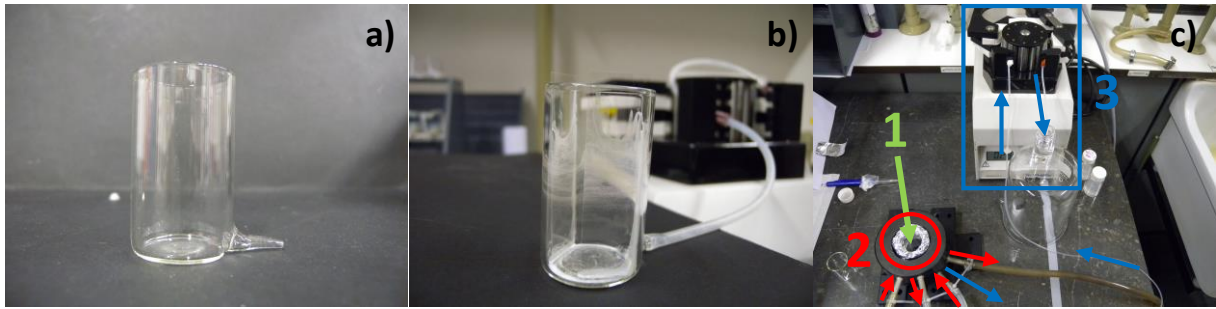


Figure 28: FCVD setup a) Specially designed glass flask used for FCVD experiments b) Flask after a FCVD experiment connected to a peristaltic pump, showing particles sedimented on the edges of the flask c) Complete setup of a FCVD experiment with 1. The sample 2. The construction of the thermostatic waterbath 3. The peristaltic pump

### 3.2.4. Characterization

#### *Optical microscopy*

To study dynamics of colloidal particles in a drying droplet a Nikon Inverted Microscope Nikon ECLIPSE Ti-U with TI-PS100W/A Power Supply, a TI-DH Dia Pillar Illuminator 100W and a TI-SR Rectangular Mechanical Stage was used. A Nikon Plan Aiko VC Oil immersion objective was used with a magnification of 100x.

To image structures formed in convective assembly experiments an optical Zeiss Axioplan Pol Universal Microscope was used with reflected light. Objectives with a magnification of 5x, 20x, 40x and 60x were used.

#### *Imaging*

A Nikon Coolpix P6000 digital camera was used to photograph the deposit of colloids formed in convective assembly experiments. White light was used to show the presence of Bragg reflections.

#### *Scanning electron microscopy*

A Phenom high-resolution scanning electron microscope with an optical camera was used to image deposits obtained from convective assembly experiments. A magnification ranging from 24x – 24.000x was used with a dimension imaging module of 286 x 566 x 495 mm. The samples were prepared for SEM imaging by attaching the sample to a SEM specimen stub with carbon tape. For electron conduction the samples were coated with a 6 – 8 nm layer of platina using a sputter coater. By analyzing these image order parameters could be determined using analySIS iTEM 5.0 and IDL.

### 3.3. Results & Discussion: Spheres

Colloidal spheres are used in CA experiments with the DD, HD and FCVD method to find the optimal conditions to form ordered structures of spheres. Since in this study micron-sized colloidal cubes are used, micron-sized silica spheres of 1052 nm with 8.9 % polydispersity(PD) in size, 16 %PD in shape and a density difference,  $\Delta\rho$ , with water of  $\sim 1 \text{ g/cm}^3$  are used to mimic the behaviour of the cubes. However, in CA experiments PD and sedimentation are known to induce the formation of defects in an ordered structure, which decreases the size of the ordered domains. Therefore, an 'ideal' colloidal system of 1234 nm polystyrene spheres with 1.7 %PD and a  $\Delta\rho$  with water of  $\sim 0.04 \text{ g/cm}^3$  is used to study whether long-range ordered domains of colloids can be formed with the DD, HD and FCVD method. Test experiments are performed using different solvents, concentration, setup properties and substrate pretreatment procedures. The conditions found best for spheres were later used in CA experiments with micron-sized hollow silica cubes.

#### 3.3.1. Drying droplet

With the DD method dynamics in the dispersion and the growth process of the structure at the edges of the droplet are studied. In DD experiments it is important that a particle flux toward the edges of the droplet is induced, since here a dense structure of colloids will be formed. Therefore, sedimentation, attractive inter-particle forces and attraction of particles with the substrate are unfavoured, since these can prevent particles from reaching the growth front at the edges. In this study attractive forces between the substrate and the particles are decreased by etching the substrate in a KOH-solution for 1-5 days. This treatment makes the substrate slightly negatively charged and since silica colloids are negatively charged as well the particles will not be attracted by the substrate. This resulted in a larger flux of particles toward the edges, which was observed with inverted microscopy(IM). By etching with KOH the substrate becomes more hydrophilic as well, therefore decreasing the contact angle with water. A lower contact angle at the meniscus results in the formation of monolayers of colloids at the growth start. Test HD experiments performed with different solvents showed the importance of the particle flux and the contact angle as well. When ethanol or ethanol/water mixtures were used the droplet was spread out over the substrate, as can be seen in figure 29a. A thin droplet with a very low contact angle at the meniscus was formed. Due to this shape and the high evaporation rate of ethanol the solvent was evaporated within minutes. On this time-

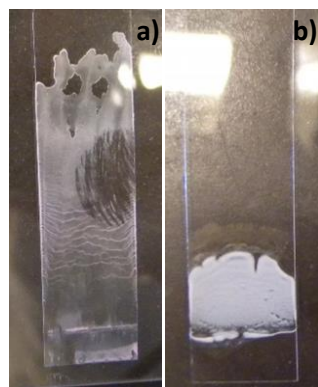
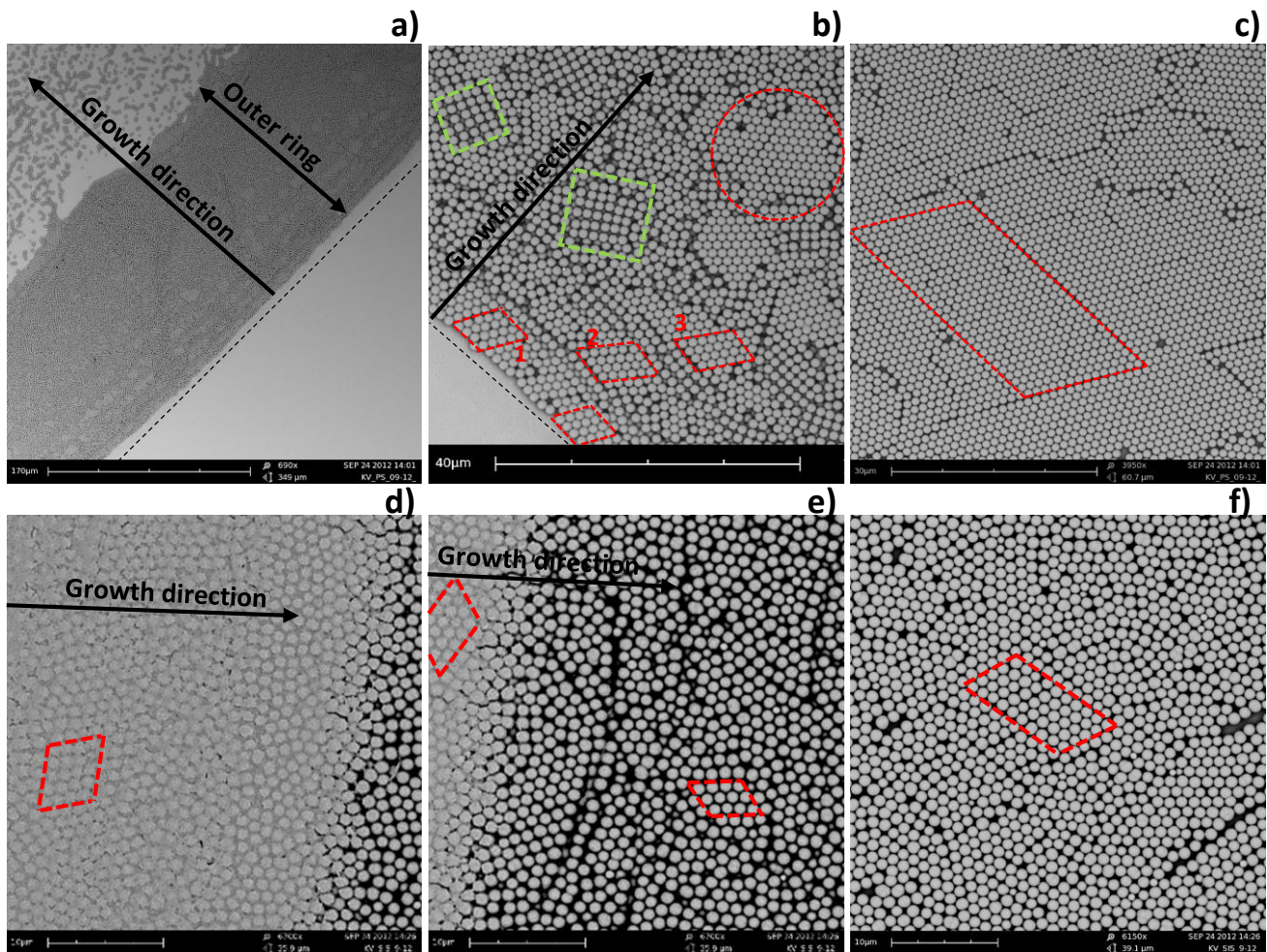


Figure 29: Deposits of silica spheres obtained from HD experiments performed in a) Water b) Ethanol

scale it was observed that only a few particles were transported to the edges of the droplet. When water was used, the solvent was evaporated in  $\sim 45$  minutes resulting in a ring-like deposit (fig 29b). In figure 30a a SEM image of the outer ring of a ring-like deposit of polystyrene cubes obtained from a DD experiment at 0.4 %V is shown. Note that with IM it was observed that at concentrations  $\ll 0.4$  %V often no ring-like deposits were formed since too little particles were transported to the edges and at concentrations  $\gg 0.4$  %V a thick ring-like deposit was formed where disordered structures. The structure in the outer ring in figure 30a is formed over a distance of  $\sim 400 \mu\text{m}$ . In figure 30b the edge of the outer ring is imaged in detail. Here, it can be seen that a monolayer is formed at the growth start and ordered domains are observed in the areas enclosed by the red lines. A monolayer was formed at the growth start since a low contact angle at the meniscus was induced by a special preparation procedure of the setup. Here, a dispersion droplet of  $25 \mu\text{L}$  was dropped from 3 cm height on the substrate. After 30 seconds the meniscus was assumed to be pinned by colloids at the edges of the droplet and  $12 \mu\text{L}$  of the droplet was removed from the center of the droplet.



**Figure 30:** SEM images of structures of colloidal spheres (a-c polystyrene spheres, d-f silica spheres) observed in ring-like deposits obtained from DD experiments at 0.4 %V in water a) Part of the outer ring of the deposit where a structure of spheres is formed over an area of  $\sim 400 \mu\text{m}$  b) A monolayer of spheres formed at the growth start, followed by the formation of a second layer after  $\sim 6 \mu\text{m}$  and a third layer after  $\sim 12 \mu\text{m}$ . Small domains with hexagonal or square order are designated by the red and green lines respectively c) A monolayer formed in an inner ring where long-range ordered domains are observed, indicated by the red lines d) An ordered monolayer at the growth start with on the left the infiltration of silica e) Layer transitions at the growth start where only short-range ordered domains can be observed f) A monolayer formed in an inner ring where very short-range ordered domains can be observed, indicated by the red dashed lines

This decreased the contact angle at the meniscus, resulting in the formation of a monolayer at the growth start. In figure 30b it is observed that at a distance of  $\sim 6 \mu\text{m}$  from the growth start a second layer is formed on top of the monolayer and a third layer is formed  $\sim 12 \mu\text{m}$  from the growth start. In this multilayered structure hexagonal and square ordered domains are observed, indicated by the red and green lines, respectively. In the inner rings of the deposit mostly monolayered films are formed as can be seen in figure 30c. These results show that ordered domains of polystyrene spheres are formed with the DD method.

DD experiments were performed with silica spheres at 0.4 %V in water as well. In figure 30d a SEM image of the growth start at the outer ring of a deposit is shown. In the light grey area on the left of the image a monolayer of spheres covered with precipitated silica is observed. The presence of precipitated silica was only found at the growth start and is assumed to be caused by the fact that the colloidal silica spheres dissolve in water. It is not clear whether the infiltration of silica in the structure occurred before or after formation of the structure. In figure 30e the transition of a monolayer with infiltrated silica(left) to a multilayered structure without infiltrated silica(right) can be seen. Here, small very short-ranged ordered domains are observed. In the inner rings of the deposit monolayers were formed and in figure 30f it can be seen that the silica spheres clearly deviate in size and shape. Therefore, defects are introduced decreasing the size of the ordered domains.

Since the polydispersity of the polystyrene spheres was much lower compared to that of the silica spheres, smaller ordered domains were expected to form with silica spheres. Comparison of figure 30c and 30f indicates that the ordered domains in monolayers formed by polystyrene spheres are of longer range, typically  $10 \times 25$  particle size(PS), compared to the domains formed by silica spheres, typically  $5 \times 10$  PS. This confirms that PD plays a large role in the CA process since it influences the size of ordered domains. Comparison of figure 30b and 30e shows ordered domains of  $4 \times 6$  PS and  $3 \times 4$  PS for polystyrene and silica spheres, respectively, are found in multilayered structures. From this it can be concluded that the ordered domains formed in monolayers are of longer range compared to the domains found in upper layers.

### 3.3.2. Horizontal deposition

In test experiments with the HD method the solvent, angle between the two slides(slide angle), sample volume and concentration were varied to determine which conditions are required to obtain deposits of ordered structures covering a large area of the substrate. All structures were formed on plain glass substrates, which were etched in a KOH-solution for 1-5 days to avoid attraction of the particles with the substrate. The time-scale on which all solvent had evaporated was approximately 8 hours. To cover a large area of the substrate a sample volume of  $100 \mu\text{L}$  was used. When larger sample volumes were used the solvent was evaporated on a longer time-scale. This resulted in the sedimentation of the particles before all solvent had evaporated when silica spheres were used. Also, larger volumes often resulted in leakage of the sample at the contact point of the two slides.

A deposit of polystyrene spheres obtained from a HD experiment in water with a slide angle of  $25 - 35^\circ$  is shown in figure 31a. The deposit covers a large area of the substrate,  $\sim 0.8 \text{ cm}^2$ , and strong Bragg reflections are observed under white light illumination, indicating ordered domains were formed. Note that at lower concentrations or when a slide angle  $< 25^\circ$  was used the deposit covered a smaller area of the substrate. When the spheres were dispersed in ethanol or ethanol/water mixtures similar behaviour as with the DD method was observed, e.g. spreading of the droplet, whereas when water

was used the sample was trapped in the corner between the two slides and a clear meniscus was formed, which is crucial to form dense ordered structures in CA experiments.

In figure 31b a SEM image of the structure of polystyrene spheres in the deposit is shown. At the top of the image the formation of a monolayer is observed at the growth start. By scanning the image downwards it is observed that a multilayered structure with up to 8 layers is formed. The order of the spheres can be recognized in figure 31c. Here, it can be seen that hexagonal order is dominant, but square-like order is observed in the transition region  $n$  to  $n + 1$  layers. This square-like order was also observed by Meng *et al.* whom studied the order found in transition regions in detail. Ordered domains of  $10 \times 20$  PS is size are observed, indicated by the dashed red lines.

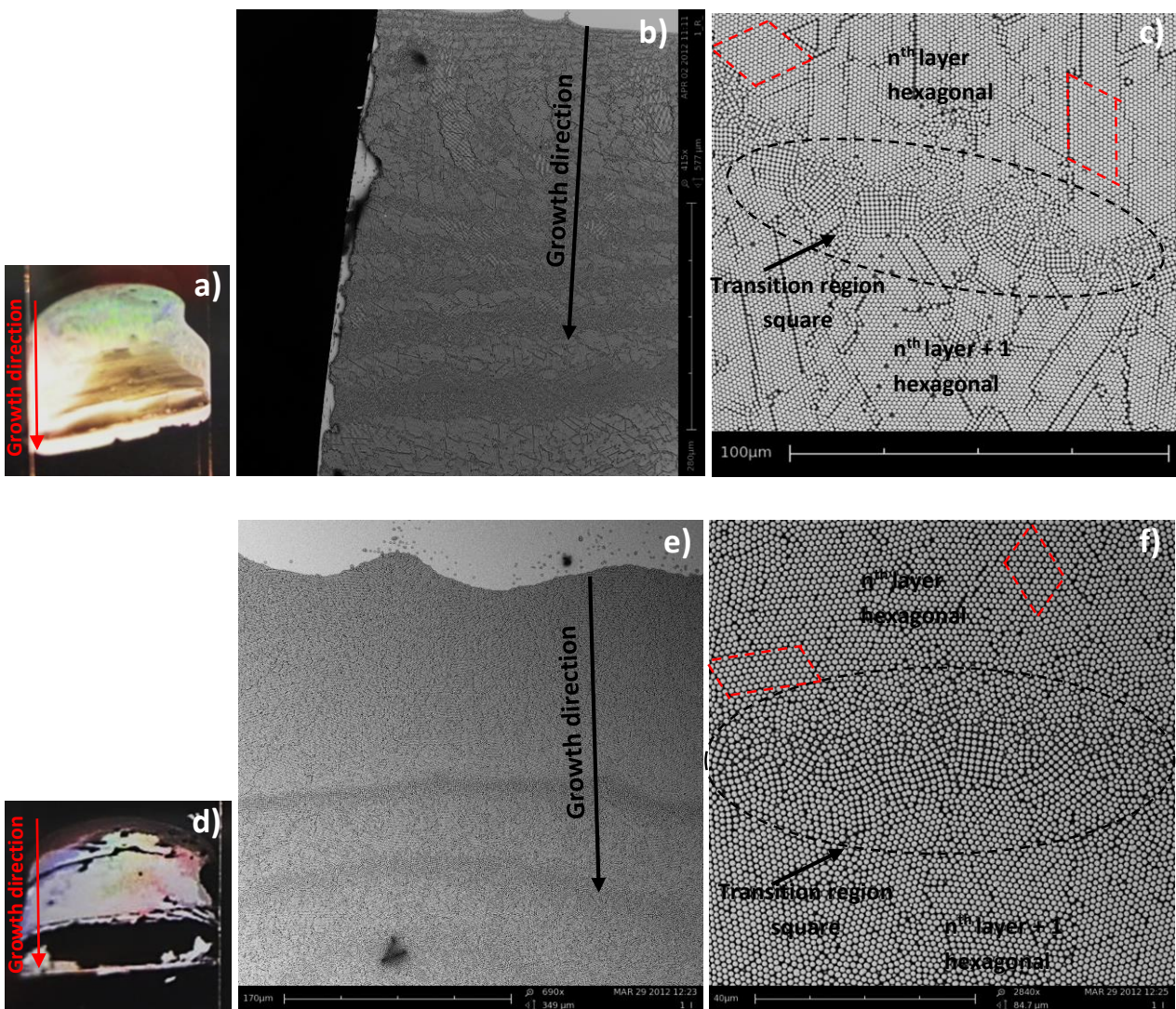


Figure 31: Results obtained from HD experiments with spheres(a-c polystyrene spheres, d-f silica spheres) in water with a slide angle of  $25 - 35^\circ$  a) Picture of a deposit of polystyrene spheres under white light illumination b) SEM image showing the formation of a multilayered structure, 8 layers, starting at the growth start at the top of the image c) SEM image showing the transition from  $n$  to  $n+1$  layers, where clearly square order can be observed at the transition region and hexagonal order in the layers d) Picture of a deposit of silica spheres under white light illumination d) SEM image showing the formation of a multilayered structure, starting at the formation of a monolayer  $350 \mu\text{m}$  at the growth start at the top of the image f) SEM image showing a transition region form  $n$  to  $n+1$  layers where square order can be observed at the transition region and hexagonal order in the layers.

A deposit of silica spheres under white light illumination obtained from a HD experiment in water with a slide angle of 25-35° is shown in figure 31d. Strong Bragg reflections are observed under white light illumination. The area of the substrate covered by silica spheres is smaller compared to the area covered by polystyrene spheres (fig 31a), which is probably caused by the difference in concentration used in the experiments. In figure 31e a SEM image of the growth start is shown, where a fluctuating contact line is observed at the growth start. At the growth start a monolayer is formed, followed by the formation of a second layer on top of the monolayer ~350 μm from the growth start. A third layer is formed ~500 μm from the growth start. The area covered by the monolayer at the growth start is larger compared to the polystyrene sample, which is probably caused by the difference in concentration. In the SEM image of figure 31f a transition region from n to n+1 layers is visible. It can be seen that hexagonal ordered domains of 5 x 10 PS are formed. However, at the transition region from n to n + 1 layers square-like order is observed. Comparison of the size of the ordered domains found in multilayers for polystyrene spheres and silica spheres shows larger domains are formed with polystyrene spheres. The orientation of the domains is different. The size of the ordered domains formed in HD experiments is also larger compared to the domains formed in DD experiments. The most successful HD experiments with colloidal spheres were performed in water using KOH-etched plain substrate with a slide angle of 25 - 35°. The area of the substrate covered with colloids is increased with concentration, whereas the area covered by the monolayer is thought to decrease with concentration. HD experiments with cubes were performed under these conditions.

### 3.3.3. Flow-controlled vertical deposition

Only a few test experiments with the FCVD method were performed. For these tests polystyrene spheres were used. The inset in figure 32a shows a picture of a deposit obtained from a FCVD experiment at 45°C and a surface dropping velocity of 1 mm/h under white light illumination. A large part of the substrate, ~2 cm<sup>2</sup>, is covered with lines of deposit showing strong Bragg reflections. The deposit is thin and areas without particles are observed as well.

In the SEM image shown in figure 32a a structure of polystyrene spheres formed at the growth start can be seen. The black dotted line at the top of the image indicates the shape and position of the contact line at the growth start. This contact line is more straight compared to the contact lines formed in DD and HD experiments (fig 31b and 31c). At the growth start only a short monolayer is formed followed by the formation of a multilayered structure ~5 μm from the growth start. At the bottom of the image an area without particles is observed. Mainly hexagonal order is observed in the structure, as can be seen in figure 32b. Enclosed by the black dashed line a transition region from n to n+1 layers is observed. Here, it can be observed in detail how the structure develops in this transition region. The red arrow indicates the position where the hexagonal order develops to square order. An open structure is observed, which develops to a square arrangement. In the monolayer shown in figure 32c it can be seen long-range ordered domains of ~ 10 x 25 PS were formed. The size of the ordered domains obtained from FCVD experiments is largest compared to the domains formed with the DD and HD method. The orientation of the domains is similar as well, which is not observed in deposits obtained with the DD and HD method. A possible explanation for these differences is the shape of the contact line at the growth start, since with the DD and HD method a fluctuating, curved contact line was formed resulting in differently oriented cubes at the growth start, whereas with the FCVD method a straight growth start is induced.

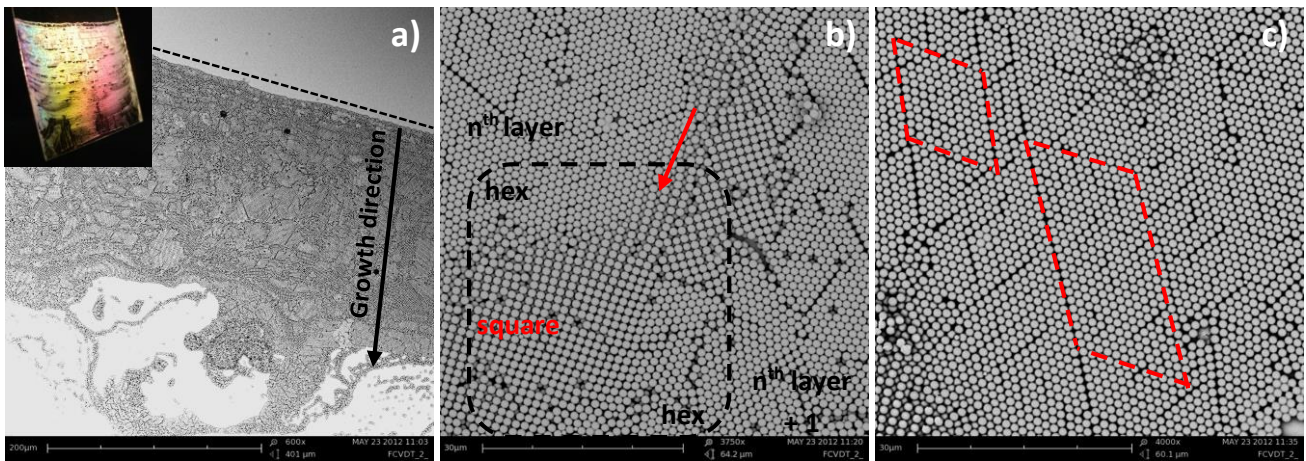


Figure 32: Results obtained from a FCVD experiment with polystyrene spheres in water at 45 °C with a surface dropping velocity of 1 mm/h a) SEM image of a structure formed from the growth start at the top of the image. The inset shows a picture of the deposit under white light illumination showing strong Bragg reflections b) SEM image showing a transition region from mono- to bilayer. Hexagonal order is observed in the layers, whereas square-like order is observed in the transition region. The red arrow indicates the position where the hexagonal order starts to develop to square order c) SEM image of a monolayer showing large ordered domains were formed of similar orientation.

### 3.3.4. Conclusion

In CA experiments with the DD, HD and FCVD method with polystyrene and silica spheres structures with ordered domains are formed. In general the area of the substrate covered by particles is smallest with the DD method and largest with the FCVD method. All deposits show Bragg reflections under white light illumination, indicating ordered domains are formed.

With all methods a monolayer is formed at the growth start followed by the formation of a multilayered structure. The order of the spheres found in the structures is mainly hexagonal. Only at transition regions square-like order is observed. The size of the ordered domains of polystyrene spheres is larger than the domains formed by silica spheres. This is assumed to be caused by the difference in PD between the two colloidal systems. The size of the ordered domains is dependent on the method used as well. With the FCVD method the largest ordered domains are formed. Also, only with this method ordered domains of similar orientation are observed. This is assumed to be caused by the shape of the contact line at the growth start.

The experimental conditions as found best for colloidal spheres, experiments performed in water at concentrations of approximately 0.4 %V, will be used in CA experiments with hollow silica cubes.

## 3.4. Results & Discussion: Cubes

CA experiments with micron-sized hollow silica cubes(5\_S2\_H) with  $m = 3.6$  are performed with the DD, HD and FCVD method. In this section the results obtained from these experiments will be presented. First, the results obtained with the DD method will be discussed, followed by the results obtained with the HD method and the FCVD method. Finally, results obtained from CA experiments with patterned substrates will be presented and discussed.

### 3.4.1. Drying droplet

In DD experiments the behaviour of hollow silica cubes in dispersion was studied in real-time with IM. Multiple experiments were performed at 0.4 %V in water, where typically a 25  $\mu\text{L}$  dispersion droplet was placed on a KOH-etched plain substrate and studied with M using a 100x oil lens. IM images of such an experiment are shown in figure 33. In figure 33a single cubes are observed indicating no strong attractive inter-particle interactions are present. Also, no attraction between the cubes and the substrate was observed, which was expected since both the silica particles and the KOH-etched substrate were negatively charged. A strong particle flux from the bulk to the meniscus at the edges of the droplet was observed. At the edges of the droplet the meniscus was pinned by colloids and a nucleus of cubes was formed within seconds. In figure 33b the formation of an ordered monolayer of cubes at the growth start can be observed. In figure 34a an IM image of the edge of a droplet is shown where the formation of a multilayered structure is observed. It can be seen that the pinned cubes at the growth start form an ordered monolayer and a second layer is formed on top of the monolayer  $\sim 8 \mu\text{m}$  from the growth start, followed by the formation of a third layer  $\sim 16 \mu\text{m}$  from the growth start. This resulted in the formation of a multilayered structure of 10 – 12 layers. Formation of the structure was mainly studied by focusing at the bottom layer of the structure, since here the highest resolution was obtained. It was observed that colloidal structures covering an area of a few 100  $\mu\text{m}$  from the growth start were formed. Figure 34b shows and IM image of the growth front approximately 100  $\mu\text{m}$  from the growth start.

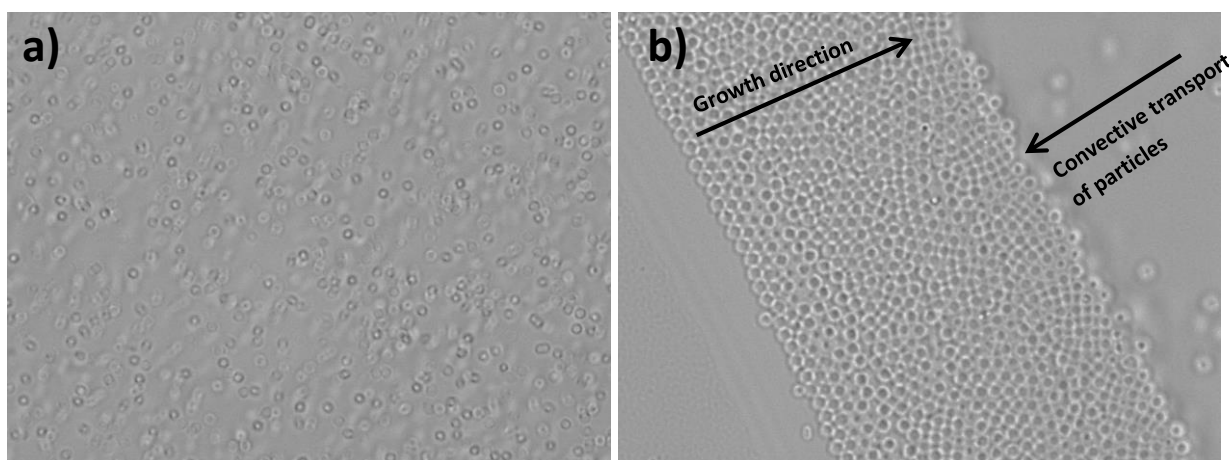


Figure 33: IM images of a DD experiment with hollow silica cubes(5\_S2\_H) in water a) The bulk at the center of a 0.4 %V dispersion droplet, showing single particles b) The edge of a 0.2 %V dispersion droplet, where a monolayered nucleus of cubes is formed at the growth start. On the right it can be seen single particles are convectively transported toward this nucleus.

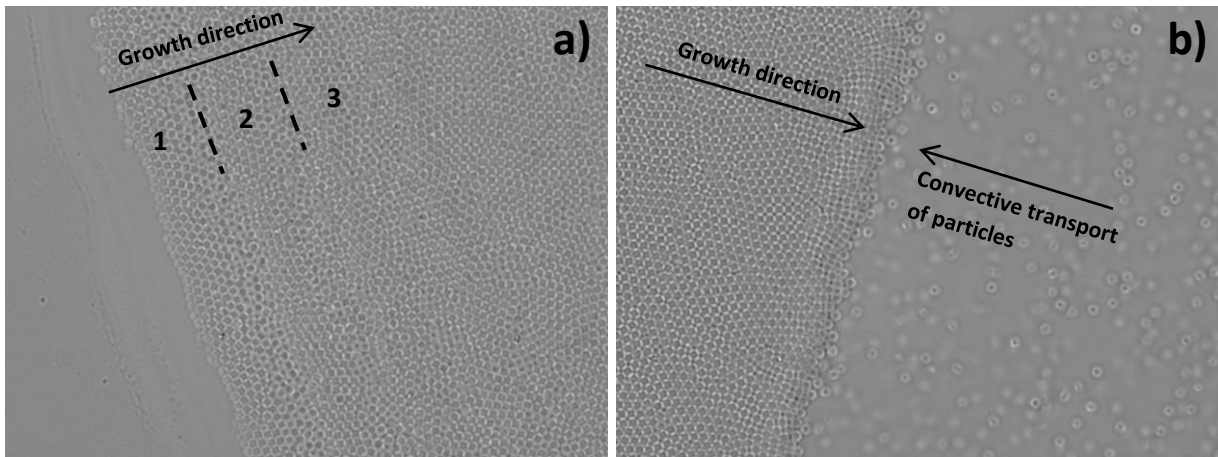


Figure 34: IM images of a 0.4 %V dispersion droplet of hollow silica cubes(5\_S2\_H) in water a) Edge of the droplet, showing the growth start and the formation of a multilayered structure b) Growth front  $\sim 100 \mu\text{m}$  from the growth start, showing order in the bottom layer is remained and the structure is still growing

In figure 35 IM images of the bottom layer of a structure a few 100  $\mu\text{m}$  from the growth start are shown. Here, it can be observed that in the bottom layer still ordered domains of cubes are formed. Both in figure 35a and 35b large ordered domains can be recognized. The orientation of these domains, indicated by the arrows was different. This was presumably caused by the fluctuating contact line at the meniscus at the edges of the droplet. By following the growth process of the crystal structures over time we observed that the structure is dynamic during growth. The structure could be observed to expand and compress continuously. This indicates changes in particle density and is most likely related to the reorientation and relocation of the cubes in the structure. As a result the particle density in the structure increases and a highly close packed structure is obtained.

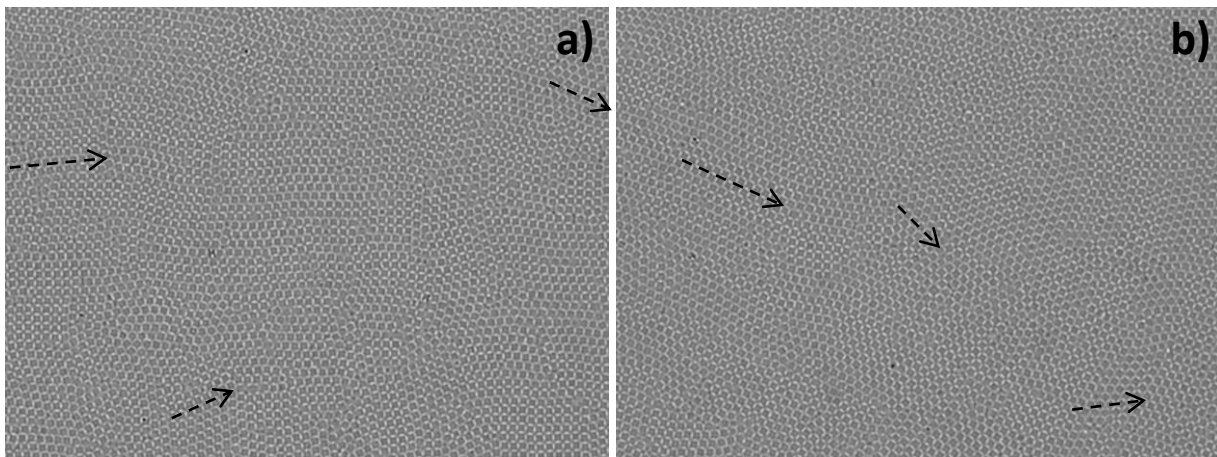
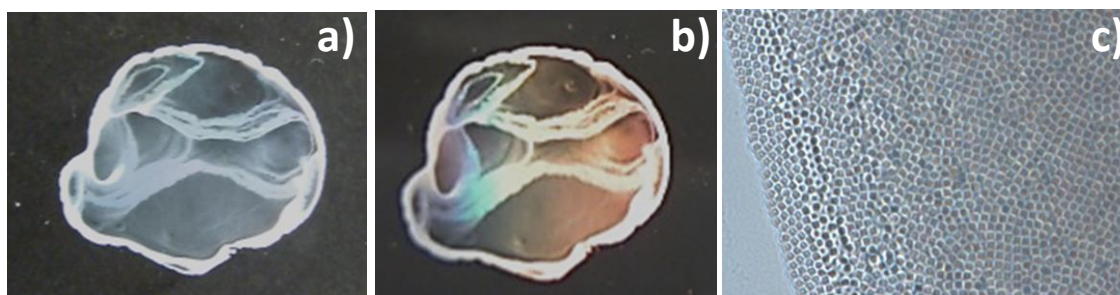


Figure 35: IM images of the bottom layer of a structure of cubes formed  $\sim 100 \mu\text{m}$  from the growth start in a DD experiment of a 0.4 %V dispersion droplet(5\_S2\_H). Both images show ordered domains are formed with different orientation indicated by the arrows.



**Figure 36: Results obtained from a DD experiment with a 0.4 %V dispersion droplet(5\_S2\_H) after solvent evaporation a) Picture of a ring-like deposit b) Deposit under white light illumination showing Bragg reflections c) IM image of the growth start after solvent evaporation**

A typical example of a deposit obtained from a DD experiment after solvent evaporation is shown in figure 36a. A ring-like deposit is observed showing bright colours under white light illumination (figure 36b). These Bragg reflections indicate ordered domains of cubes are formed during the experiment. The shape of the deposit was different in every experiment, since very little experimental parameters are controlled with the DD method. Evaporation of the solvent from the cavity of the cubes caused the cubes to shrink in size. In figure 36c an IM image of the growth start after solvent evaporation is shown. It can be seen that the cubes still form ordered domains and it is assumed the orientation of the cubes was not changed upon drying.

With SEM the structures formed by the cubes were studied in more detail. Figure 37a shows a SEM image of a structure formed at the outer ring of the deposit. At a distance of  $\sim 100 \mu\text{m}$  from the growth start a multilayered structure is observed of  $\sim 15$  layers, as can be seen by the inset of area 2 in the image. Here, it is observed that in the top layer of this structure no order was observed. An SEM image of the edge of a structure is shown in figure 37b. The formation of a monolayer is observed at the growth start, which is observed with IM as well (figure 37b). Two different orientations of cubes at the growth start are observed, with their sides parallel to the contact line (indicated by the blue arrow) or with their edge pointed to the contact line (indicated by the yellow arrow). The orientation of these cubes influenced the orientation of the neighbouring cubes. Approximately  $8 \mu\text{m}$  from the growth start a second layer is formed on top of the monolayer and a third layer is formed  $\sim 16 \mu\text{m}$  from the growth start.

In the upper layers small ordered domains are observed, as can be seen in figure 37c. Here, it seems the cubes order in square-like,  $\Lambda_0$ -like or  $\Lambda_1$ -like arrangements. The size of the domains is typically  $5 \times 5$  PS. The large cracks indicated by the red arrows are typical for multilayered structures. It is observed that the cubes on each side of the cracks fit together like puzzle pieces. It is therefore assumed that the cracks are formed by drying effects, after formation of the structure.

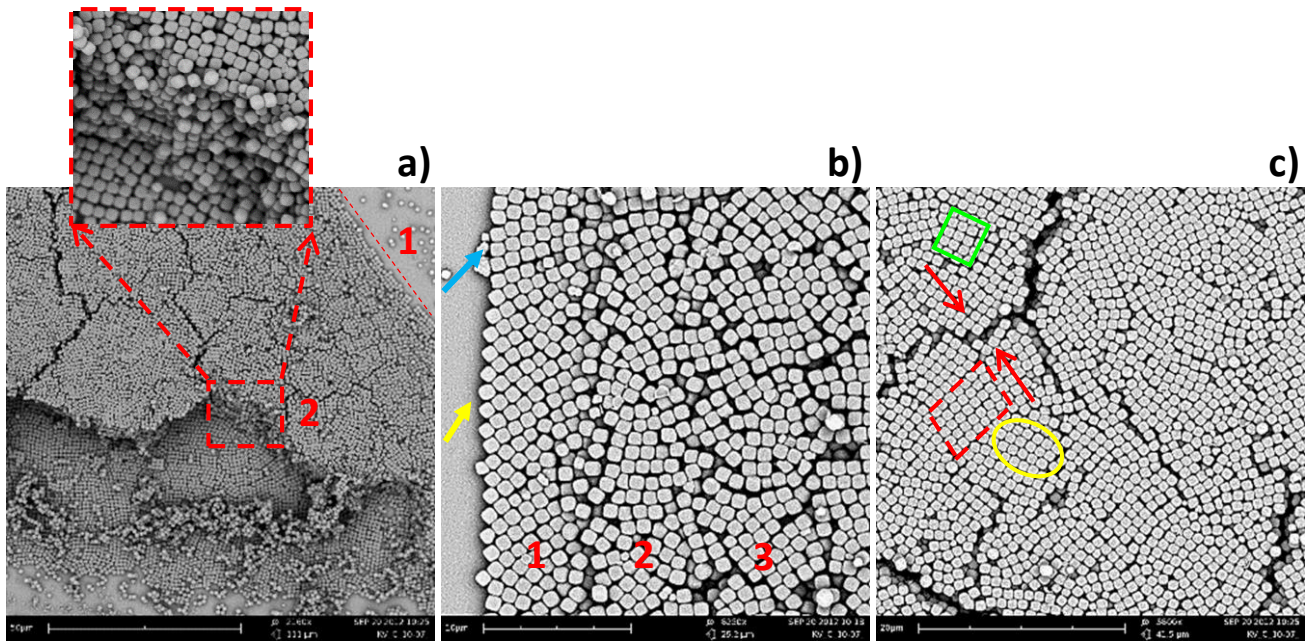


Figure 37: SEM images of a deposit of hollow silica cubes(5\_S2\_H) obtained from a DD experiment at 0.4 %V in water a) Overview of a multilayered structure formed over a short distance in the outer ring b) Growth start at the edge of the droplet, where the first pinned cubes align with either their sides(blue arrow) or their edges(yellow arrow) to the contact line. The formation of a trilayered structure is observed c) Toplayer of a multilayered structure, showing small domains with square-like(green square),  $\Lambda_0$ -like(yellow oval) and  $\Lambda_1$ -like order is formed. The red arrows indicate that the cubes on each side of the crack fit together like puzzle pieces

## Conclusion

With DD experiments the behaviour of the cubes in dispersion and the CA process is studied in real-time. With IM the formation of large ordered structures of a few 100  $\mu\text{m}$  is observed. During structure formation the cubes are able to reorient and relocate their orientation and position resulting in the formation of ordered close-packed structures. With SEM is observed that the orientation of the particles at the growth start is different and determinant for the orientation of the neighbouring cubes. It is also shown that a multilayered structure is formed over a short distance, presumably caused by a high contact angle at the meniscus, which is typical for DD experiments. Small ordered domains are observed in the upper layers, where the cubes seem to arrange in a square-like,  $\Lambda_0$ -like or  $\Lambda_1$ -like arrangement.

While the DD method is ideal to study dynamics and structure formation during CA, this method is not suited to form large ordered structures. To form large ordered structures a lower contact angle is required and experimental conditions need to be controlled to obtain reproducible results.

### 3.4.2. Horizontal deposition

To obtain a large deposit with ordered structures of micron-sized hollow silica cubes(5\_S2\_H) the HD method is used. Experiments were performed at different concentrations in water. For these experiments the conditions as found best for colloidal spheres; a KOH-etched substrate, a slide angle of 25 – 35° and a sample volume of 100  $\mu\text{L}$ , are used.

In figure 38 a picture of a typical cube deposit obtained from a HD experiment performed at 0.4 %V is shown. The different characteristics of the deposit are indicated by the numbers 0 – 6 and are discussed here. A curved growth start is observed at the top of the image(fig 38.1), which is characteristic for all deposits obtained from HD experiments. The curved growth start is presumably formed since with the HD setup the solvent is evaporated in many directions. At the growth start a thin deposit is obtained, where strong Bragg reflections are observed under white light illumination(fig 38.2). A few particles are found above the growth start as well(38.0), which was caused by an experimental error when the sample was injected between the two slides with a pipet. A small touch of the pipet against the horizontal slide when the sample is injected in the corner can change the shape of the meniscus and therefore the contact line at the growth front.

After the thin region an area with a thicker deposit(fig 38.3) is observed. The formation of this area indicates that there was an increase in the contact angle at the meniscus and an increase in particle concentration at this position. Close to the contact point of the two slides(fig 38.5) some 'empty' areas and small areas covered with cubes are observed on the substrate(fig 38.4). Below the contact point some particles are found as well(fig 38.6), which can only be caused by leakage of the sample at the contact point. This influenced the fluid flow inside the sample, explaining the formation of small areas of cubes and empty regions close to the contact point.

In general the thickness of the deposit and thus the amount of cubes increased with particle concentration. The size of the area of the substrate covered with cubes is found to depend on concentration as well. In figure 39 pictures of deposits obtained from HD experiments at 0.1, 0.2, 0.4, 0.5 and 1.2 %V are shown. All deposits show strong Bragg reflections under white light illumination, as can be seen in figure 39A – 39E, indicating ordered domains of cubes are formed in all experiments. In figure 39a a picture of a deposit formed at 0.1 %V is shown. Here, it can be seen that only a small part of the substrate is covered with cubes. At the growth start at the top of the image a small region

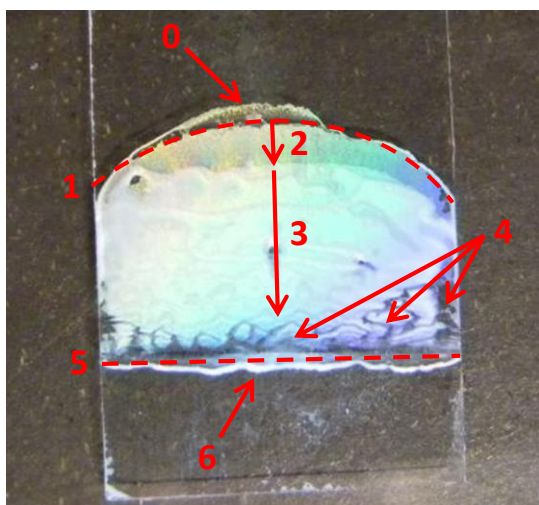
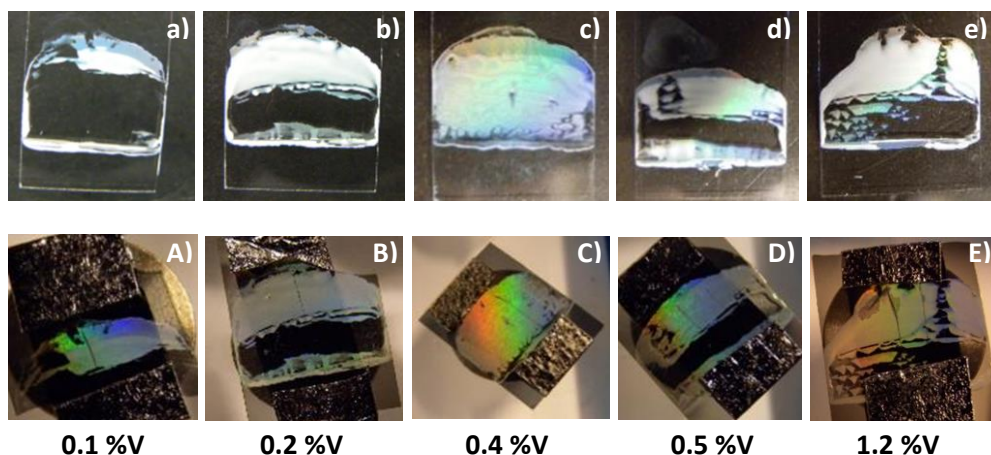


Figure 38: Typical deposit under white light illumination obtained from a HD experiment with hollow silica cubes(5\_S2\_H) at 0.4 %V in water 0) Small area of deposited cubes above the contact line 1) The dashed line indicates the position and shape of the contact line at the growth start 2) A thin deposit formed at the growth start showing strong Bragg reflections 3) A thick white deposit with weak Bragg reflections 4) Small areas of cubes and empty regions 5) Point where the two slides are in contact 6) Cube deposit below the contact point



**Figure 39:** Pictures of deposits under white light illumination obtained from HD experiments with hollow silica cubes(5\_S2\_H) in water at a) 0.1 %V b) 0.2 %V c) 0.4 %V d) 0.5 %V e) 1.2%V. Images A - E are pictures of the deposits shown in a – e respectively, coated with 6-8 nm platina for SEM imaging

with thin deposit is formed followed by a small region of a thick deposit. Below this the substrate is uncovered until the contact point. This large ‘gap’ was formed since all particles were already transported to the growth front at this low concentration at the beginning of the experiment. Therefore, no particles were available when the meniscus arrived at the ‘gap’. A picture of a deposit obtained at 0.2 %V is shown in figure 39b. Here, a larger area of the substrate is covered with cubes. However, a gap between the thick deposit region and the contact point is observed for this sample as well. At 0.4 %V the substrate is almost completely covered with a cube deposit of  $\sim 0.8 \text{ cm}^2$ . In figure 39c it can be seen that this deposit was thin and strong Bragg reflections are observed.

At higher concentrations, 0.5 %V and 1.2 %V, only a small area at the growth start is covered with a thin deposit. Instead, a large area with a thick deposit is formed, followed by a ‘gap’ without particles, as can be seen in figure 39d and 39e for 0.5 %V and 1.2 %V, respectively. At high concentration many particles are transported to the growth front, resulting in the accumulation of particles at the growth front. Therefore, many particles are deposited at the growth front resulting in the formation of a thick deposit. Since a large part of the substrates is uncovered, it is assumed that all particles were already transported to the growth front before all solvent was evaporated. Therefore, no particles were available when the meniscus arrived at the ‘gap’. Note that the shape of the deposits was difficult to reproduce, since not all experimental parameters in HD experiments could be controlled.

To study the structures formed by the cubes, the deposits were imaged with SEM. In all deposits a monolayer is formed at the growth start. Three typical SEM images of the growth start are shown in figure 40. In figure 40a it can be seen that initially a fluctuating contact line was formed, indicated by the dark line at the top of the image, when the meniscus was pinned on the substrate. Below this line a white area is observed with a monolayer of cubes covered with precipitated silica. The ordering of the cubes in this monolayer is visible at the bottom of the image where no precipitated silica is present. Silica was often found to infiltrate the monolayers at the growth start. In figure 40b a monolayer of cubes can be recognized with on the left cubes without the infiltration of precipitated silica and on the right a monolayer with infiltrated silica. It is observed that in both regions ordered domains of cubes were formed. This indicates that the silica was deposited after structure formation of the cubes in the monolayer therefore not influencing the ordering of the cubes. In figure 40c a SEM image of a monolayer of cubes formed at the growth start without infiltration of silica is shown.

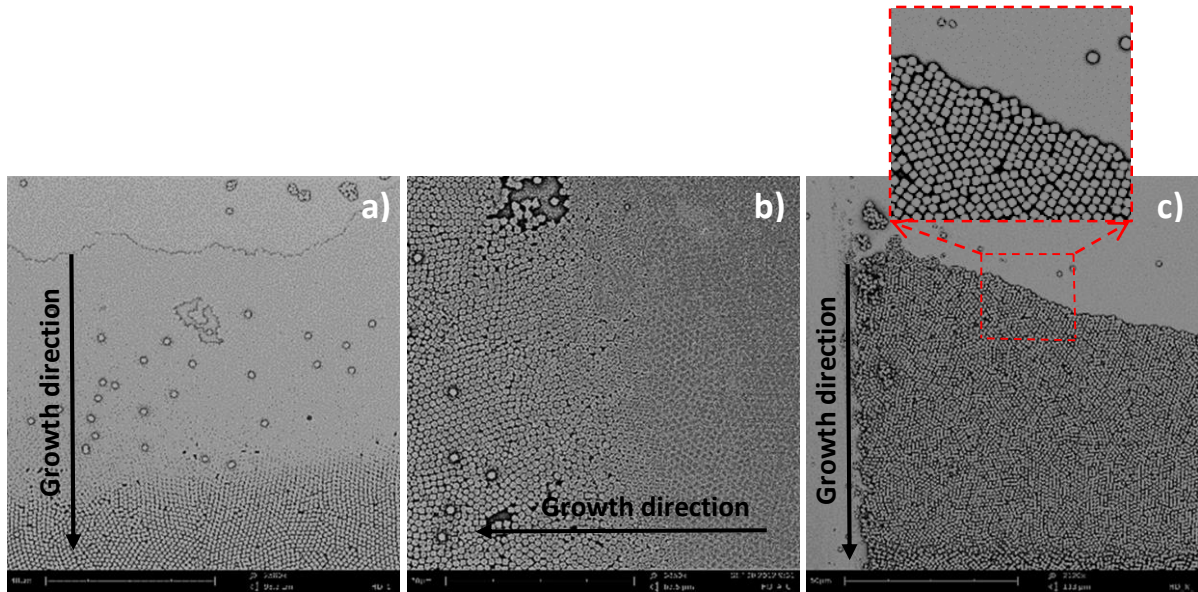


Figure 40: SEM images of the growth start of a structure of cubes formed in a HD experiment with hollow silica cubes(5\_S2\_H) in water at 0.4 %V a) A monolayer of cubes is observed with infiltration of silica at the growth b) A monolayer of cubes with ordered domains even when silica has infiltrated the layer(right side of the image) c) Monolayer of cubes formed at the growth start where the orientation of the cubes at the contact line is shown in the inset

Although this was unusual it is useful, since the orientation of the cubes pinned at the initial contact line can be observed. It can be seen that the cubes at the growth start have different orientations and the orientation of the neighbouring cubes is influenced by the orientation of these cubes. The difference in orientation of the cubes at the growth start induced the formation of different orientated ordered domains, as can be seen in the inset of figure 40c. In all deposits single cubes on top of the structure as well as vacancies were observed. It is assumed that these single cubes were part of the structure, but due to preparation of the sample for SEM imaging, where the substrate had to be cut with a diamant pen, the structure was slightly distorted and some cubes were removed from the structure.

In figure 41 SEM images of monolayers of cubes formed in a HD experiment at 0.1 %V are shown. In figure 41a a large ordered domain of  $\sim 25 \times 25$  PS is observed. The inset is an illustration of the  $\Lambda_1$  arrangement and the ordering of the cubes in the image seems to be similar to this  $\Lambda_1$  arrangement. Small domains with different orientation are observed as well, as can be seen in figure 41b and c. The differences in orientation of the domains is thought to be caused by the fluctuating contact line at the growth start. In figure 41b arrangements similar to both  $\Lambda_0$  and  $\Lambda_1$  are observed, as is indicated by the yellow en red dashed lines, respectively. In figure 41c ordered domains with predominantly an arrangement close to  $\Lambda_0$  is observed. Close inspection of the images reveals that defects in the structure, caused by vacancies or particles with a size largely deviating from the average size, reduce the size of the domains.

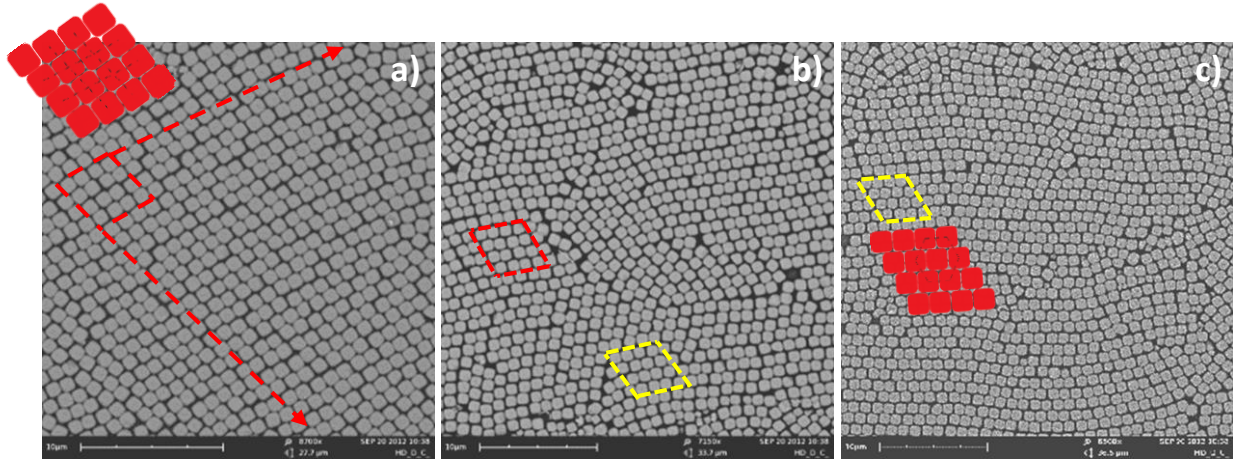


Figure 41: SEM images of monolayers of hollow silica cubes(5\_S2\_H) obtained from a HD experiment at 0.1 %V in water a) Large ordered domain where the cubes seem to arrange on a  $\Lambda_1$ -lattice, indicated by the red dashes lines b) Small ordered domains arrangements similar to the  $\Lambda_1$  and  $\Lambda_0$  lattices c) Ordered domains of cubes with predominantly arrangements similar to the  $\Lambda_0$ -lattice, indicated by the yellow dashed lines

Multilayered structures are observed at 0.1 %V as well. In bi- and trilayers the observed order of the monolayer is found to persist throughout the layers, as can be seen in figure 42a. Here, it can be seen that small domains of  $\Lambda_0$ (yellow lines) and  $\Lambda_1$ (red lines) arrangements are formed. At the transition regions from mono- to bilayer and bi- to trilayer different arrangements are found compared to the arrangements found in the individual layers. At transition regions square-like arrangements is observed, which was also observed for spheres by Meng *et al.* At some positions in the deposit small multilayered areas are observed, as is shown in figure 42b a SEM where a multilayered structure of 6 layers is shown. Here, it is also observed that a large monolayer covering at least 400  $\mu\text{m}$  is formed at the growth start before the second layer is formed.

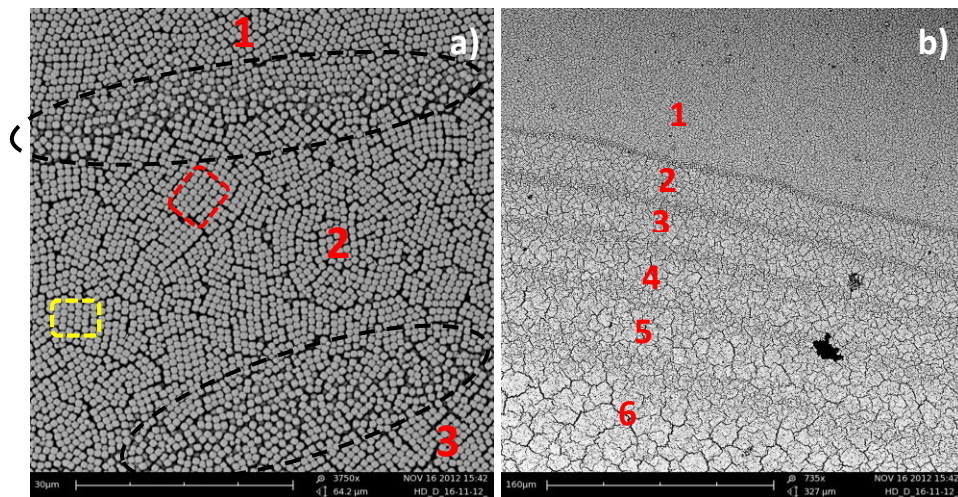
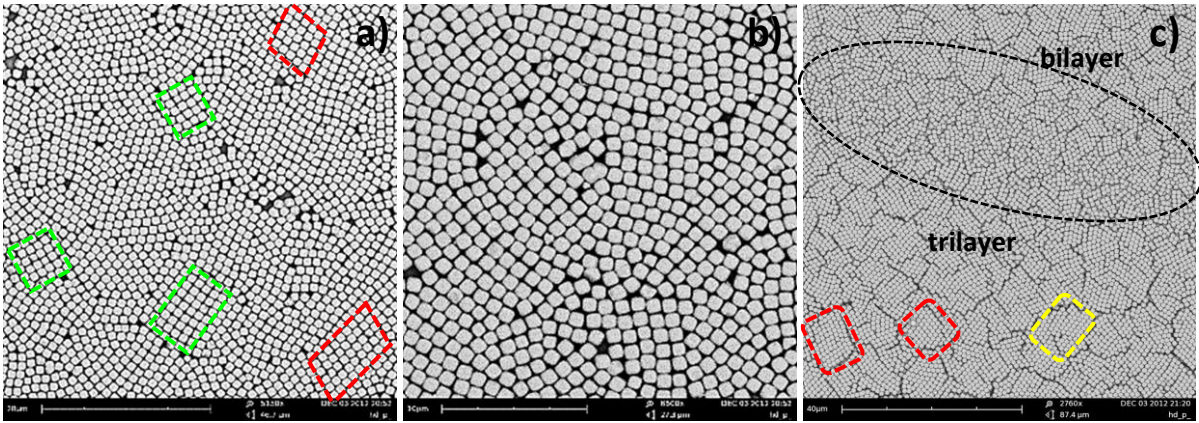


Figure 42: SEM images of multilayers of hollow silica cubes(5\_S2\_H) formed in HD experiment a 0.1%V in water a) Transition regions from mono- to bilayer at the top of the image and bi- to trilayer at the bottom of the image, indicated by the black dashed oval. At the transition region square order is observed and in the bilayer  $\Lambda_0$ -like(yellow) and  $\Lambda_1$ -like(red) arrangements are observed c) Multilayered structure of cubes of 6 layers.



**Figure 43: SEM images of monolayers of hollow silica cubes(5\_S2\_H) formed in an HD experiment at 0.4 %V in water a) Small ordered domains of different orientation with square-like (green dashes) and  $\Lambda_1$ -like(red dashes) arrangements b) Monolayer with many defects c) Transition region(black oval) from a bi- to trilayer. In the trilayer ordered domains with  $\Lambda_1$ -like(red dashes) and  $\Lambda_0$ -like(yellow dashes) are observed**

SEM images of structures of cubes formed in an experiment at 0.4%V are shown in figure 43. In figure 43a a monolayer formed at the growth start is shown. Here, small ordered domains, typically 5 x 10 PS, with different orientation are observed. The ordering of the cubes in these domains is mainly square-like(green dashes) and  $\Lambda_1$ -like(red dashes). In figure 43b it can be seen that many defects were present in the structure, decreasing the size of the ordered domains. In the deposit at max 4 layers are observed. In figure 43c it is observed that order persists through the layers. Ordered domains with arrangements close to the  $\Lambda_1$ -lattice(red dashes) and the  $\Lambda_0$ -lattice(yellow dashes) are observed.

Multilayered structures are mainly observed in deposits obtained from HD experiments performed at concentrations > 0.4 %V. In figure 44 SEM images of a structure of cubes formed in a HD experiment at 0.5 %V are shown. In the image shown in figure 44a the formation of a multilayered structure of 7 layers is observed. A scratch in the deposit revealed the bottom and top layer of the structure(fig 44b). In both layers ordered domains are observed, which indicates order persists through the layers meaning the cubes order in 3D. In the toplayer of a multilayered structure, shown in figure 44c, ordered domains of typically 5 x 10 PS are observed with different orientation. The ordering of the cubes in these domains can be square-like,  $\Lambda_0$ -like or  $\Lambda_0$ -like, as can be seen by close inspection of the images in figure 44b and 44c. The cracks observed in the multilayered structure are assumed to be formed after structure formation, since the cubes on each side of the crack fit together like puzzle pieces(fig 44c).

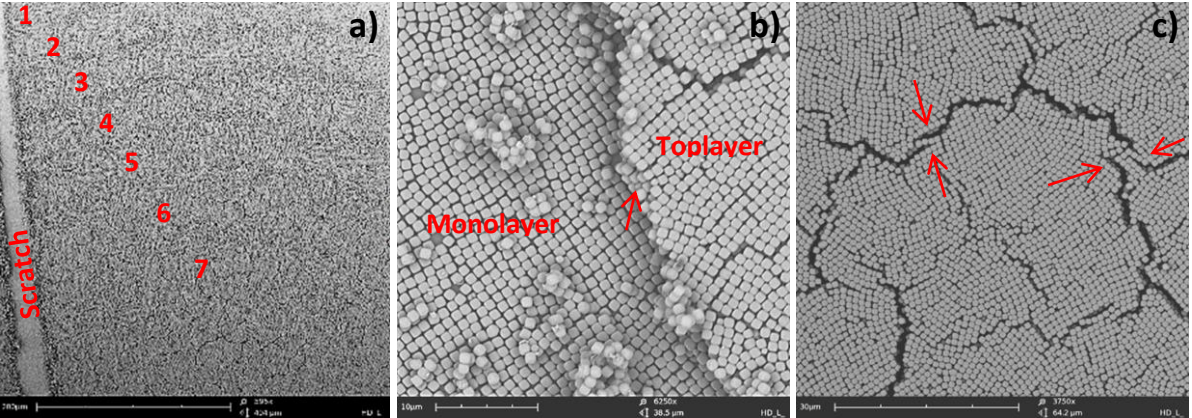


**Figure 44: SEM images of a cube(5\_S2\_H) deposit obtained from a HD experiment at 0.5 %V in water a) Overview of the formation of a multilayered structure of 7 layers b) Bottom and toplayer of a multilayered structure where both ordered domains are observed c) Toplayer of a multilayered structure with ordered domains of different orientation**

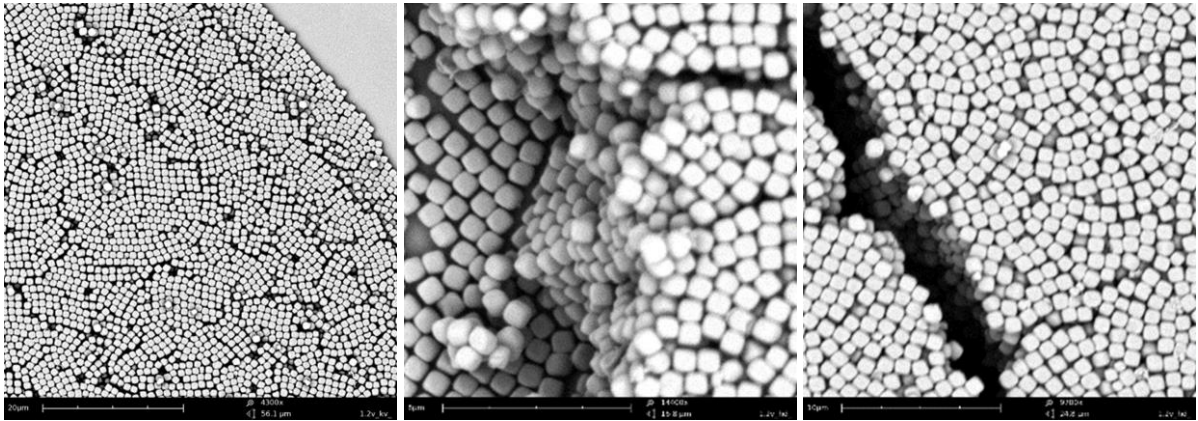


**Figure 45: SEM images of a deposit of hollow silica cubes(5\_S2\_H) obtained from an HD experiment at 1.2 %V in water a) Growth start showing the formation of a multilayered structure of 4 layers b) Exposure of the stacking in a multilayered structure, where a maximum of 10 layers is recognized c) Toplayer of a multilayered structure showing no ordered domains are formed**

At 1.2 %V, a multilayered structures was already formed shortly after the growth start, as can be seen in figure 45a. Here, the formation of a short monolayer is observed since the formation of a second layer is already observed at of  $\sim 5 \mu\text{m}$  from the growth start. Every of  $\sim 5 \mu\text{m}$  a new layer is formed on top of the previous one untill 4 layers are obtained. Figure 45b shows very thick structures are formed as well. Here, the stacking of the multilayered structure is exposed and 10 layers are recognized. The toplayer, shown in figure 45c, shows disordered structures are formed in these thick structures. This indicates that at 1.2 %V the multilayered structure is formed over a short distance and time span, similar to thick ring-like deposits obtained from DD experiments.

## Conclusion

The results show that a large part of the substrate is covered with a cube deposit in HD experiments. All deposits obtained showed strong Bragg reflections under white light illumination. From the results presented in this section it can be concluded ordered domains of hollow silica cubes can be formed using the HD method. The range of the order in the domains can be large in monolayers,  $25 \times 25$  PS, but decreases in the upper layers. The domains have different orientations which can be understood by the different orientation of the cubes at the growth start due to the fluctuating contact line. It seems the cubes order in arrangements similar to the  $\Lambda_0$  and  $\Lambda_1$  lattices predicted in simulations for superball-shaped particles. Square order is observed as well, mainly at the transition regions from  $n$  to  $n+1$  layers.

### 3.4.3. Flow-controlled vertical deposition

With the FCVD method experimental conditions such as; sample temperature, volume fraction and surface dropping velocity are controlled. Therefore, it is expected that results obtained with this method are easier to reproduce than results obtained with the DD or HD method. With the DD and HD method small ordered domains were formed with different orientations, since heat was transferred in many directions resulting in a curved contact line. With the FCVD method heat transfer of the dispersion with the surroundings can only occur in one direction. Therefore, it is expected that the contact line at the growth start will be straight resulting in a structure with larger ordered domains of similar orientation.

Pictures of two deposits obtained from FCVD experiments with hollow silica cubes in water at 45 °C with a surface dropping velocity of 1 mm/h are shown in figure 46. The characteristic regions observed in the deposit are designated by the numbers 0 – 6. In the left picture a deposit obtained from a FCVD experiment performed at 1 %V is shown. It can be seen that the contact line at the growth start (fig 46.1) was straight in the middle of the substrate and slightly curved at the edges. The numbers 1.1 and 1.2 designate the formation of a thin line deposit in horizontal direction, which are attempts of forming a new growth start. After the real growth start at the top of the image an 'empty' region is observed (fig 46.2). At 1 %V a uniform cube deposit of ~1 cm in length is formed after the empty region (fig 46.3). Here, strong Bragg reflections are observed under white light illumination, indicating the ordered domains are formed. At low concentration region 3 was not found, instead the empty region immediately developed to an area with alternating covered and uncovered regions (fig 46.4), as can be seen in the right picture of figure 46. In region 4 only a few particles were pinned on the substrate forming a small nucleus for further growth of the structure. From these few pinned particles an array was grown in the direction of the moving meniscus, resulting in elongated shaped deposits, 5. At the bottom of the substrate a thick white deposit was formed (fig 46.6). This indicates the concentration used for the experiment was sufficient, but the elevated temperature used in the experiment was only enough to oppose sedimentation for a certain amount of time.

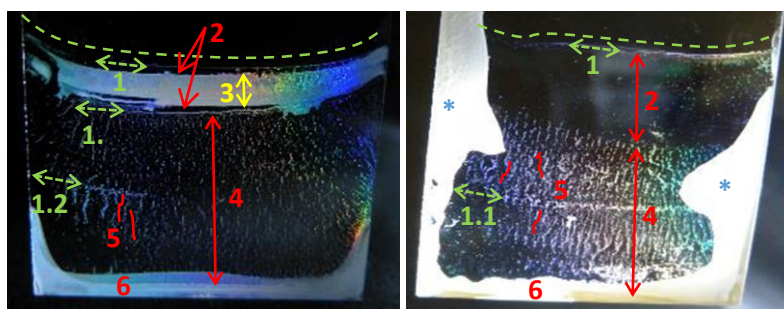
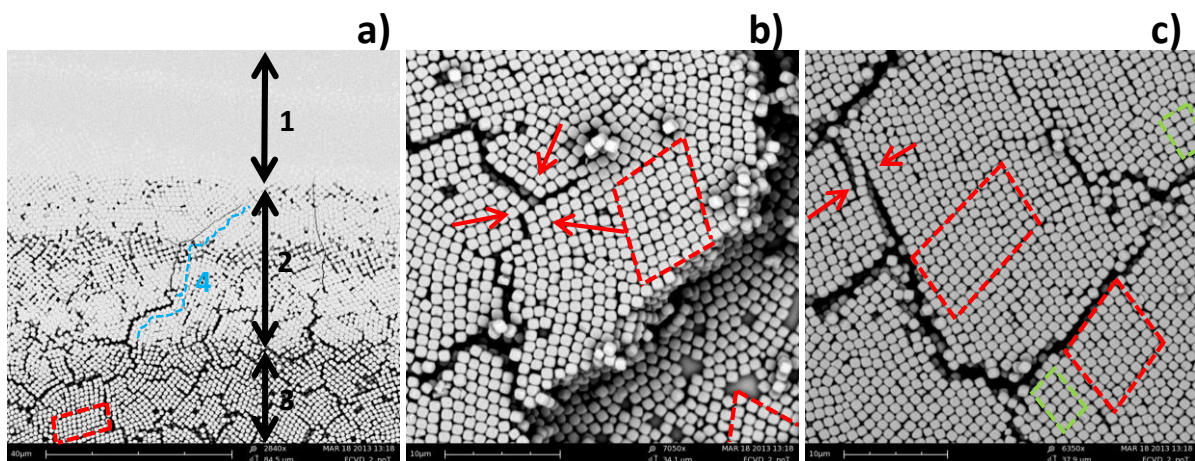


Figure 46: Pictures of deposits of hollow silica cubes(5\_S2\_H) under white light illumination obtained from FCVD experiments in water at 45 °C and a surface dropping velocity of 1 mm/h. With on the left a deposit formed at 1 %V and on the right a deposit formed at 0.5 %V. The shape of the contact line at the growth start is illustrated by the dashed green line. 1) Position of the contact line 1.1&1.2) Thin horizontal lines of deposit 2) Areas without deposit 3) Uniform deposit of cubes showing strong Bragg reflections 4) Region with covered and uncovered areas 5) Illustration of the elongated shaped deposits 6) Thick deposit \*) The white area's in the right image are discussed in the next paragraph

SEM images of region 3 are shown in figure 47 and the characteristic regions are designated with the numbers 1 - 4. In figure 47a the formation of a structure at the growth start is shown. At the growth start at the top of the image a monolayer of cubes is formed with silica infiltration (fig 47.1). Part of the silica shell of the cubes was dissolved in water and precipitated at the growth start. In region 2 some silica still infiltrated in the layers, but still the formation of ordered domains of cubes is observed. This order is remained in region 3 where no precipitated silica is observed. It is therefore assumed that the silica precipitated on the cubes after formation of the structure. The ordering of the cubes in the domains was found to be close to the  $\Lambda_1$ -arrangement. In figure 47b the stacking of a multilayered structure is visible and 7 layers individual layers can be recognized. Both in the bottom and the toplayer of the structure ordered domains are observed. In these domains the cubes are observed to arrange on a  $\Lambda_1$ -like lattice, as is indicated by the green dashed lines. This indicates that the order persists through the layers and the cubes order in 3D. In figure 47c a SEM image of the toplayer of a multilayered structure is shown. Here, long-ranged ordered domains of typically 10 x 25 PS in size are formed.  $\Lambda_1$ -like and square-like arrangements are observed as indicated by the green dashed lines and blue lines, respectively. The ordered domains have similar orientation, presumably induced by the relatively straight contact line at the growth start. The red arrows around the cracks illustrate how the pieces of structure fit together like puzzle pieces. This indicates that the cracks are formed after formation of the structure.



**Figure 47:** SEM images of a deposit of hollow silica cubes(5\_S2\_H) obtained from a FCVD experiment at 1 %V in water at 45 °C and a surface dropping velocity of 1 mm/h a) Multilayered structure with 1) A monolayer of cubes at the growth start completely covered by silica 2) Area where the cubes in the silica can be recognized showing ordered arrangements are formed 3) An area with ordered domains of cubes 4) A crack in the structure b) Stacking in a multilayered structure of 7 layers, showing  $\Lambda_1$ -like ordered domains (green dashed lines) are formed in both the bottom and the toplayer c) Toplayer of a multilayered structure showing large ordered domains are formed. Ordered domains with an  $\Lambda_1$ -like arrangement (red dashed lines) and a square-like arrangement (green dashed lines) are observed. The red arrows indicate that the cubes around cracks fit together like puzzle pieces

## Convective assembly between plates

Besides FCVD experiments with a single plain glass substrate, experiments are performed with two substrates as well. Here, the substrates are placed parallel to each other in the dispersion with an interspace of  $\sim 30\ \mu\text{m}$ . During a FCVD experiment the dispersion is sucked between the two slides due to capillary forces filling the space between the substrates. Evaporation of the solvent started at the bottom of the two plates, as can be seen in figure 48a. Here, the cubes are located at the edges of the two plates, forming a wet white deposit. In time the solvent was evaporated from the top as well (fig 48b), resulting in a flux of particles to the middle of the two slides since they are pushed from the top and the bottom. The wet structures showed very strong Bragg reflections under white light illumination. In figure 48c the dry deposit is shown where Bragg reflections were observed as well although less strong compared to the wet deposit. This loss in strength of the Bragg reflections can be caused by the formation of cracks in the crystalline structure due to drying effects. Most particles have accumulated at the middle of the slide forming a dense deposit.

To study the structures formed by the cubes in the deposit the two substrates were detached after drying and both substrates were imaged with SEM. In figure 49 SEM images of the deposit obtained from a FCVD experiment with 1 %V hollow silica cubes(5\_S2\_H) in water at 45 °C and a surface dropping velocity of 1 mm/h are shown. In figure 49a the stacking of a multilayered structure is visible. At the top of the image a structure of 9 layers is observed, indicated by the green arrow. The monolayer visible in this image is the bottom layer of the multilayered structure and parts of the bi- and trilayer are exposed as well. Ordered domains of cubes are observed in all layers. This clearly indicates that order was preserved throughout the layers. In the monolayer ordered domains of typically  $30 \times 30$  PS were found. Some domains are designated by the red dashed lines and it can be seen that the domains have similar orientation. By eye, it seems that the cubes in these domains are ordered on a  $\Lambda_1$ -lattice. In figure 49b more layers of a multilayered structure are visible. This kind of view is useful since the ordering of the different layers can be observed and therefore it is possible to determine whether the cubes order in 3D. In this image mainly domains with  $\Lambda_1$ -like order are observed (red dashes), but some small  $\Lambda_0$ -like (yellow dashes) and square-like (green dashes) ordering is observed as well.

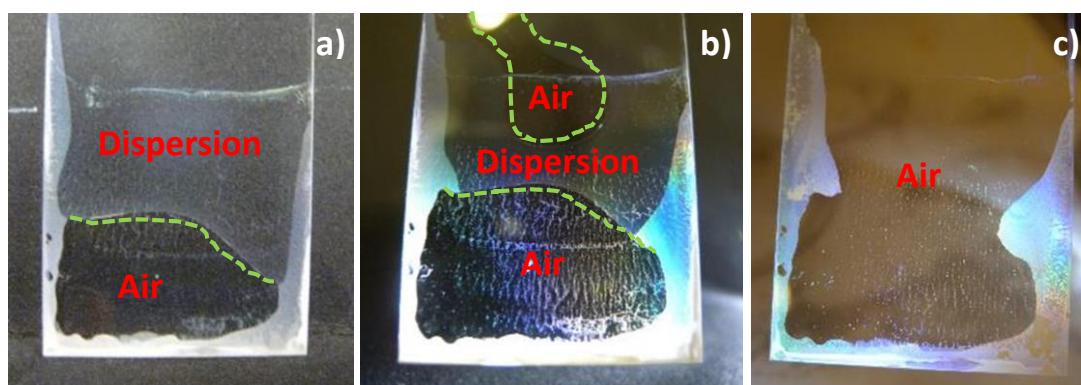


Figure 48: Images of two attached slides with dispersion of hollow silica cubes(5\_S2\_H) sucked between the slides during evaporation of the solvent a) The solvent has evaporated from the bottom and particles have accumulated at the edges of the substrates b) Due to solvent evaporation from the top and bottom (seen by the air bubbles) the particles are transported and a more dense region of particles is formed in the middle, showing strong Bragg reflections under white light illumination c) Deposit after solvent evaporation showing strong Bragg reflections under white light illumination

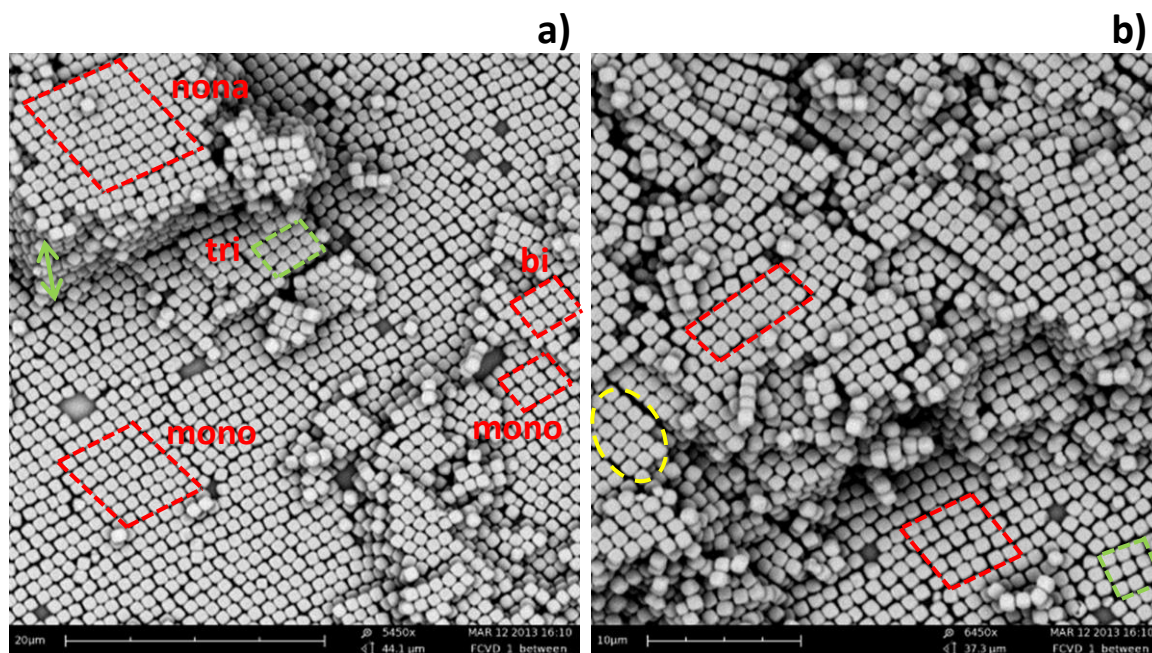


Figure 49: SEM images of a structure of hollow silica cubes formed between two plates in a FCVD experiment at 1 %V in water(45 °C, surface dropping velocity of 1 mm/h) a) Different layers of a multilayered structure are visible. At the green arrow 9 layers are recognized. Ordered domains are recognized as is indicated by the dashed red lines b) Exposure of different layers in a multilayered structure. Ordered domains with  $\Lambda_1$ -like (red dashes),  $\Lambda_0$ -like (yellow dashes) and square-like (green dashes) arrangements of cubes are observed

## Conclusion

With the FCVD method ordered domains of hollow silica cubes are formed. Observations of SEM images indicate ordered domains can be formed with the FCVD method. Experiments performed at a concentration of 1 %V, 45 °C and a surface dropping velocity of 1 mm/h resulted in the formation of a deposit showing strong Bragg reflections at the growth start. In this deposit ordered domains are observed with infiltrated silica at the growth start. Observation of this growth start showed the structure formed by the cubes was not influenced by the precipitated silica, indicating the structure was formed before the silica was precipitated.

SEM images of multilayered structures revealed long-range ordered domains are formed with similar orientation. In the domains the cubes seem to order on  $\Lambda_1$ ,  $\Lambda_0$  and square lattices. In the bottom and top layer of multilayered structures ordered domains with similar arrangement are observed. By using a two-plate substrate, the stacking of the layers and the order of the individual layer is studied in more detail. In this experiment large ordered domains are formed with similar orientation. Different ordering of the cubes is observed in the domains with predominantly a tendency to order on a  $\Lambda_1$ -lattice. The order is observed to persist throughout the layers.

## 3.5. Results & Discussion: Fluorescent cubes

SEM analyses of cube structures formed in CA experiments show that the silica cubes have a tendency to order in 3D. With optical microscopy and electron microscopy it is difficult to study structures formed in 3D in detail. Therefore, confocal microscopy can be used to image and study the stacking in a multilayered structure and the order of the cubes in the separate layers. To image the structures of cubes with confocal microscopy Rhodamine B is incorporated in the silica shell of the hollow silica cubes, resulting in fluorescent hollow silica cubes(HC\_R\_fIH). Results obtained from CA experiments with fluorescent cubes will be described in this section.

### 3.5.1. Drying droplet

DD experiments with fluorescent silica cubes are performed to study the behaviour of these cubes in dispersion with IM. In figure 50a a SEM image is shown where the edge of a droplet is visible. Here, it can be observed that some cubes are pinned on the substrate, but no ordered monolayer is formed. The cubes formed an open structure indicating that the capillary forces at the growth front were too weak to form a dense close-packed structure of cubes. With IM it was observed that only a few cubes were transported to the edges of the droplet and many cubes attached to the substrate on their way to the growth front. This can be seen in figure 50a where the cubes pinned at the edge are in the same focus as the single cubes on the right of the image. This indicates that there was a strong attraction between the fluorescent cubes and the substrate. It was often observed that cubes that did arrive at the growth front formed large dynamic clusters, as is designated by the red dashed oval in figure 50a, which indicates strong attractive inter-particle forces were present as well. In figure 50b an IM image of the center of the droplet is shown. Although single cubes are observed, many cubes are in focus and therefore attached to the substrate. This explains why there was only a weak particle flux observed to the growth front at the edges of the droplet.

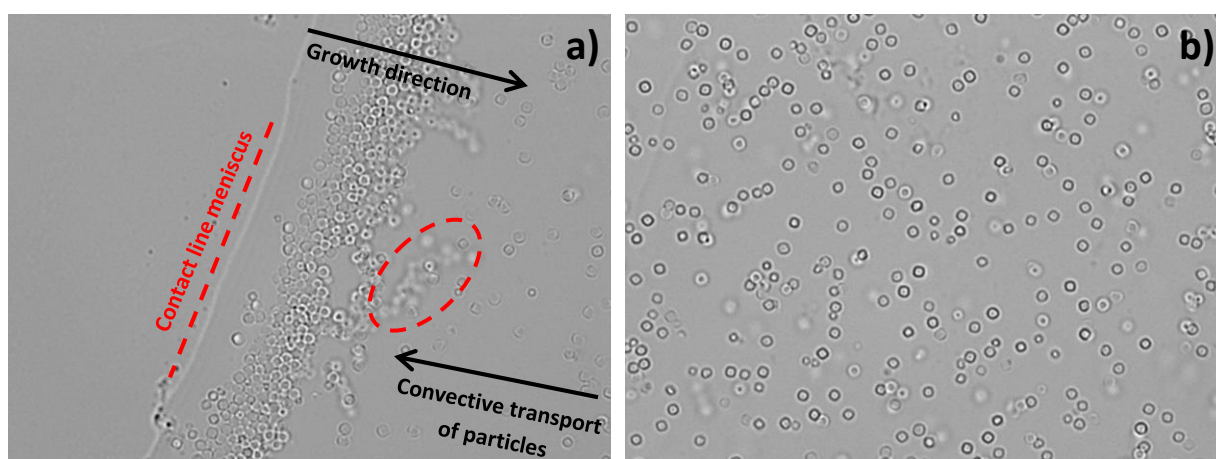


Figure 50: IM images of a DD experiment with fluorescent hollow silica cubes(HC\_R\_fIH) at 0.4 %V in water a) Growth front at the edge of the droplet. A few pinned cubes are observed forming an open structure. The single particles on the right of the image that are in focus are stuck on the substrate. The particles that do move are out of focus and assembly in clusters as indicated by the red dashed oval b) Center of the droplet where single particles are observed. Most particles are attached to the substrate and therefore immobile.

### 3.5.2. Horizontal deposition

HD experiments are performed with fluorescent silica cubes as well. A typical deposit obtained from a HD experiment at 1 %V is shown in figure 51b. Similar to experiments with non-fluorescent hollow silica cubes a curved growth start is formed, indicated by the black dashed line. At the growth start alternating regions covered and uncovered with cubes are found. This is followed by the formation of a thick pink deposit, which almost completely covers the substrate. The deposit shows no Bragg reflections under white light illumination, indicating disordered structures are formed.

Further investigation with SEM revealed that the cubes were randomly ordered in both the mono- and multilayered regions. In figure 51a a SEM image of the deposit close to the growth start is shown. Here, an open structure of clusters of cubes is observed. In the thicker part of the deposit an open structure of cubes is observed as well, as can be seen in figure 51c. The structures formed by these fluorescent cubes are very different from the structures of non-fluorescent cubes obtained from HD experiments, where ordered densely packed structures are formed. This indicates that other interaction forces are present in the HD experiments with the fluorescent cubes. The fact that the particles don't form close-packed structures indicates that immersion capillary forces at the meniscus are too weak to push the particles together. The presence of clusters of cubes indicate that strong attractive inter-particle forces are present as well.

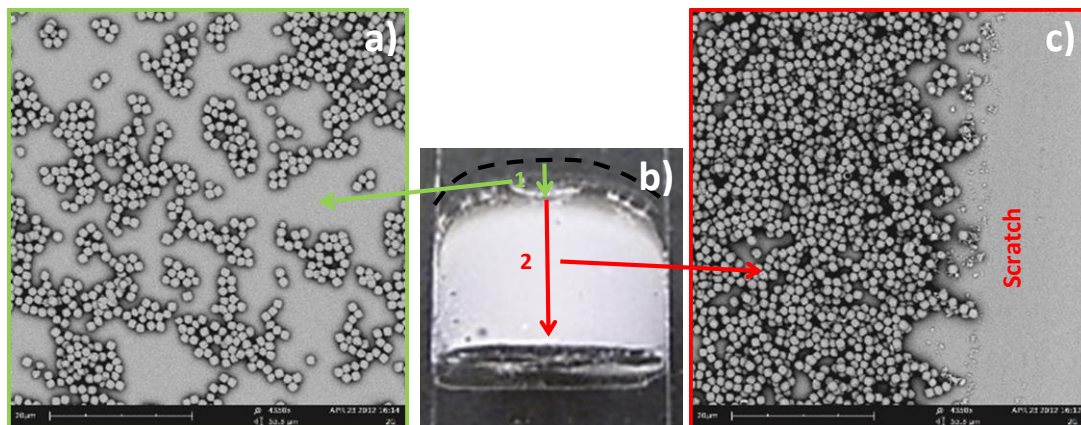


Figure 51: Images of a deposit of fluorescent silica cubes(HC\_R\_fIH) obtained from a HD experiment at 1 %V in water a) SEM image of clusters of cubes formed close to the growth start b) Picture of the deposit 1. At the growth start uncovered and covered areas are observed 2. A thick pink deposit c) In the thick pink deposit random open structures are formed by the fluorescent cubes

### 3.5.3. Vertical deposition

Vertical deposition experiments at elevated temperatures are performed as well. A picture of the deposit obtained from this experiment where 10 mL 1.3 %V dispersion in water was heated to 46 - 48 °C using an oilbath for 48 hours is shown in figure 52a. The substrate is completely covered by a thick pink deposit and three regions with different characteristics are recognized. Under white light illumination no Bragg reflections are observed.

Region 1 includes the growth start at the top of the deposit. A SEM image of the growth start is shown in figure 52b where an area with light grey and dark grey cubes is recognized separated by a clear border. Close inspection reveals that the light grey cubes are covered with precipitated silica, whereas the dark grey cubes are not. The infiltration of silica was observed at every position in the rest of the deposit. It is therefore assumed that the cubes without precipitated silica are attached to the substrate above the contact line at the growth start when the substrate was placed in the dispersion by hand. A SEM image of the middle area of the deposit, region 2, is shown in figure 52c. Here, a lot of infiltrated silica is observed and the cubes form disordered structures. No ordered domains of cubes are observed in the middle region. In region 3, at the bottom of the substrate, thick multilayered structure of cubes are observed, as can be seen in figure 52d. Multilayered structures of up to 20 layers are formed and no order of the cubes is observed. Many broken and 'squeezed' cubes are observed, caused by the long exposure time of the cubes to water at elevated temperatures.

In none of the CA experiments with fluorescent cubes ordered domains of cubes were formed. Cubes attach to the substrate and the formation of clusters is observed as well. This indicates attractive interaction forces are present between the substrate and the cubes and between the cubes themselves. Although two silica coating steps are performed during the synthesis of the fluorescent cubes, the behaviour of the cubes implies that other components than silica are present at their surface. Since the second coating step was performed immediately after the first coating step it is very likely that some unreacted dye molecules were still present in the solution during the second coating step, thus ending up at the surface. Since Rhodamine B is positively charged, the surface charge of the cubes becomes neutral or positive. This will cause attraction between the cubes and the slightly negatively charged substrate, which was observed in DD experiments. This also explains the formation of open disordered structures.

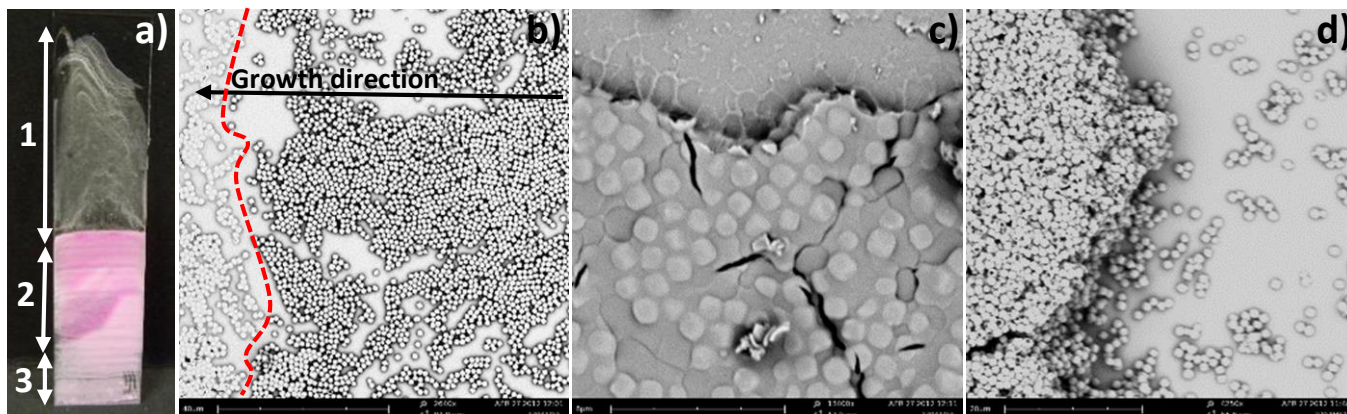


Figure 52: Results obtained from a VD experiment at 46 – 48 °C in water with fluorescent hollow silica cubes(HC\_R\_fIH) a) Picture of the deposit b) SEM image of region 1 of the deposit. At the growth start two areas are observed of cubes with and without precipitated silica c) Typical SEM image of region 2, where fluorescent silica cubes are embedded in a silica matrix d) SEM image of the bottom of the substrate in region 3. A thick multilayered structure is observed and the presence of many broken and ‘squeezed’ cubes is observed

### *Conclusion*

In CA experiments with fluorescent hollow silica cubes open disordered structures are formed. The results obtained in CA experiments with fluorescent cubes are clearly different from the results of non-fluorescent cubes, where dense ordered structures are formed. It is assumed that Rhodamine B molecules at the surface of the fluorescent cubes changed the surface charge and therefore the interactions with other cubes and the solvent. To perform successful experiments with fluorescent cubes a new batch of fluorescent silica cubes should be synthesized, where dye molecules will not be present at the surface of the cubes.

## 3.6. Results & Discussion: Controlling Crystal Growth

Substrates with straighteners of several materials are used to induce a straight growth start. The results of CA experiments with these substrates will be presented and discussed in this section. This is followed by the presentation of results obtained from CA experiments with substrates with saw-patterned polymer lines. These substrates are used to study whether a  $\Lambda_1$  arrangement could be induced.

### 3.6.1 Straightener try-outs

This study shows that in CA experiments with the DD and HD method a curved growth start is formed. Due to the curvature of the growth start cubes are pinned on the substrate with different orientation. Since these cubes determine the orientation of the neighbouring cubes, ordered domains of different orientation are formed. With the FCVD method the contact line at the meniscus is less curved, resulting in a straighter growth start. Therefore, large domains of similar orientation are formed with this method. To induce a straight growth start with similar oriented cubes, CA experiments are performed using substrates with macroscopic straighteners. Human hairs, a marker line made with different markers and a line barrier of Tippex or tape are used as straighteners. Figure 53a shows a HD setup used for an experiment with fluorescent hollow silica cubes in water. Here, a human hair was used to induce a straight growth start. The cubes deposited on one side of the hair and the meniscus was clearly pinned by the hair resulting in a straighter growth start. Unfortunately, a thick deposit is observed at the growth start, indicating that the hair was too thick to induce the formation of a monolayer at the growth start. From optical microscopy images of hairs it is determined that the hairs had diameter of  $\sim 100 \mu\text{m}$ , which is 100 times the size of the cubes. It is therefore thought that thinner straighteners are required to induce the formation of monolayers at the growth start.

A deposit obtained when a waterproof marker was used as straightener is shown in figure 53b. Here, strong Bragg reflections are observed under white light illumination. By eye it can be seen that the marker influenced the shape of the contact line at the meniscus resulting in a straighter growth start. A SEM image of the growth start is shown in figure 53c. Here, it can be seen that pieces of the markerline detached from the substrate and therefore no straight growth start was obtained.

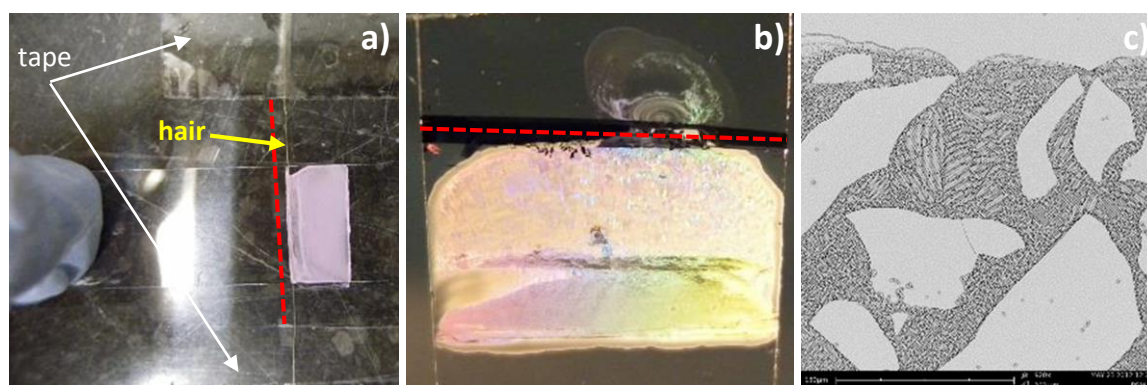


**Figure 53: Results obtained from HD experiments with straighteners attached to the substrate to form a straight contact line at the meniscus a) A HD setup with a human hair attached to the bottom substrate by tape. A pink deposit of fluorescent hollow silica cubes(HC\_R\_fIH) is formed on the right side of the hair indicating the meniscus was pinned at the hair. A thick deposit is observed at the growth start b) Deposit of polystyrene spheres obtained from a HD experiment in water under white light illumination. Strong Bragg reflections are observed. A black waterproof marker line is observed at the growth start c) A SEM image of the growth start of the deposit shown in figure 53b where it is observed that part of the marker line was detached from the substrate during the experiment**

In other experiments with simple materials, such as Tippex or tape, no straight monolayered growth start was induced either. These results indicate that more accurate lines are required to straighten the contact line at the meniscus.

### 3.6.2. Polymer coated templates

To gain control over the structures formed by colloids templates can be used. Ng *et al.* showed that the amount of grain boundaries and defects in a structure of colloidal spheres formed by CA were reduced when templates with straight polymer lines were used.<sup>84</sup> The spheres were observed to align resulting in a straight growth start. To study whether a straight growth start can be induced silica wafers with straight hydrophobic SU-8 polymer lines, similar to the patterned substrates used by Ng *et al.*, are used in CA experiments with hollow silica cubes. The height of the polymer lines,  $\sim 500$  nm, is smaller than the size of the cubes,  $\sim 1$   $\mu\text{m}$ , to induce the formation of monolayers at the growth start. The results obtained with the templates will be discussed in this section.

#### *Tuning hydrophobicity*

To study the behaviour of hollow silica cubes on the templates in real time DD experiments are performed. Since the SU-8 polymer is hydrophobic the contact angle of water with the polymer is high,  $72^\circ$ . During a DD experiment the contact line was observed to shift toward the center of the droplet along with a dynamic ordered structure of cubes formed close to the contact line. This indicates that the contact angle was too high for the cubes to pin the meniscus on the substrate. A typical cube deposit obtained with the untreated template is shown in figure 54a. Thick lines of deposit can be seen parallel to the polymer lines, indicating the cubes were eventually influenced by the lines.

To induce meniscus pinning, the hydrophobicity of the polymer lines was decreased using UV/Ozone. A treatment of two minutes was enough to decrease the contact angle of water with the polymer to  $62^\circ$ . However, this effect is not permanent and an increase in contact angle is already observed within hours. Since it was not possible to use the templates in CA experiments within a few hours after the UV/Ozone treatment, another method had to be used to make the templates less hydrophobic.

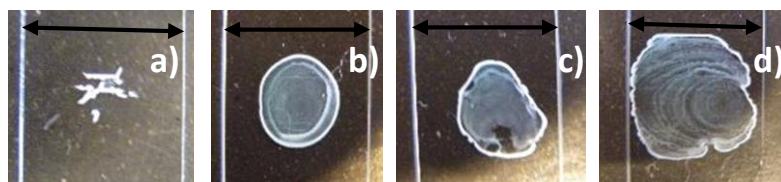


**Figure 54:** Pictures of deposits of hollow silica cubes(5\_S2\_H) on substrates patterned with straight polymer lines obtained from DD experiments at 0.4 %V in water. The black two-sided arrow indicated the width of the substrate which is the same for each experiment, 1 cm a) Deposit formed at the center of the substrate indicating the meniscus was not pinned at the edges of the droplet b) A ring-like deposit with a thick outer ring formed on a substrate pretreated for 6 s with the glow discharger c) A ring-like deposit formed on a substrate pretreated for 15 s with the glow discharger d) A ring-like deposit covering a large area of a substrate pretreated for 30 s with the glow discharger

With a Glow Discharger the hydrophobicity of substrates can be reduced as well. In figure 54b – 54d pictures of cube deposits obtained on templates pretreated with the Glow Discharger are shown. The duration of the glow discharge treatment is increased from 6 to 15 to 30 seconds (fig 54b – 54d). It can be seen that by increasing exposure time the spreading of the droplet increases as well, which indicates that the template becomes more hydrophilic.

It is determined that the best results, e.g. a ring-like deposit where the meniscus is pinned at the edges and cubes align to the polymer lines, are obtained when the templates are first flushed with ethanol followed by a glow discharge treatment of 15 s. This pretreatment is therefore performed for all templates used in CA experiments with cubes.

## *Straight polymer lines*

### Macroscopic observations

A typical deposit of cubes obtained from a DD experiment with 0.4 %V hollow silica cubes(5\_S2\_H) in water on a template with straight polymer lines is shown in figure 55a. Here, strong Bragg reflections are observed under white light illumination, indicating the formation of ordered domains. A ring-like deposit is formed and the position of the polymer lines is recognized (red dashed lines). Close inspection of the outer ring shows that the shape of the deposit is changed at the position of the polymer lines. A deposit obtained from a HD experiment with hollow silica cubes on a template is shown in figure 55b. The Bragg reflections indicate ordered structures of cubes are formed. At the growth start a straight line of particles is formed, indicated by the green arrow, followed by a large area without deposited particles. Then a region with large thick islands of particles is formed.

Figure 55c shows a picture of a deposit obtained from a FCVD experiment (1 %V(5\_S2\_H), 45°C, 1 mm/h, water). Lines of deposit are observed spaced with the exact distance of the polymer lines (red dashed lines), indicating that the deposit formation is indeed influenced by these polymer lines. As well as with the DD and the HD method, strong Bragg reflections are observed under white light illumination.

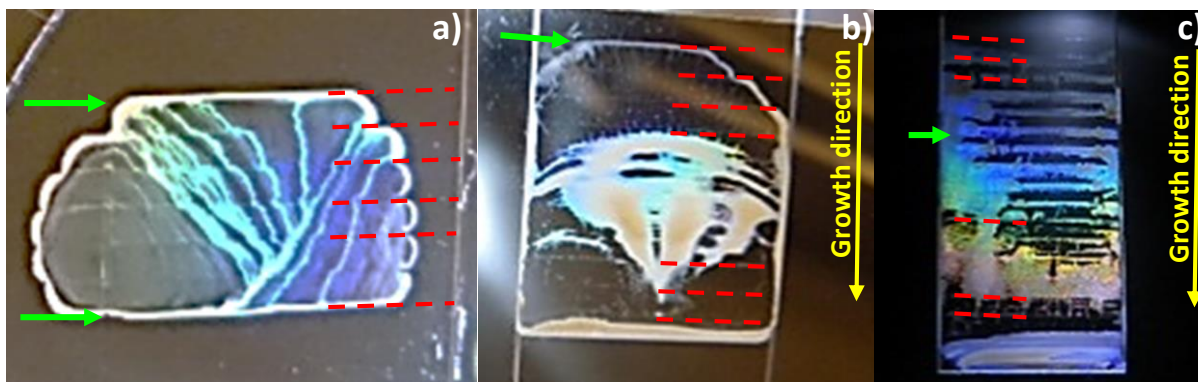


Figure 55: Pictures of deposits of hollow silica cubes(5\_S2\_H) under white light illumination on patterned substrates with straight polymer lines obtained in CA experiments in water. The red dashed lines indicate positions of some of the polymer lines on the substrates. The distance between two lines is 1 mm a) Ring-like deposit obtained from a DD experiment at 0.4 %V under white light illumination, exposing Bragg reflections. The shape of the outer ring clearly indicates the presence and influence of the polymer lines, indicated by the green arrows b) Deposit obtained from a HD experiment. The green arrow indicates the position of the growth start, where a small straight line of deposit at a polymer line is observed. This is followed by an almost empty space of 3 mm, whereafter a cone-shaped deposit is formed showing Bragg reflections c) Deposit obtained from a FCVD experiment at 1%V, 45 °C and 1 mm/h. Line-shaped deposits are observed at every polymer line showing strong Bragg reflections

## Microscopic observations

### *Drying droplet*

SEM images of a deposit of hollow silica cubes(5\_S2\_H) obtained from a DD experiment at 0.4 %V in water are shown in figure 56. In figure 56a and 56b cubes are observed to be located both on top of the polymer lines as on the glass substrate. Next to the polymer line a single row of cubes is observed to be aligned. In figure 56c an ordered monolayer is observed on top and next to the polymer line. It is very likely that part of the structure was moved by the meniscus in the growth direction and deposited on the polymer since the line functionalizes as a bump. At all positions ordered domains of cubes were observed, although many defects were present as well. In figure 56d the orientation of the aligned cubes is visible and it can be seen that cubes are aligned with their face side parallel to the polymer line. The orientation of the neighbouring cubes is clearly influenced by this alignment and an ordered monolayer is formed, as is indicated by the yellow dashes. The cubes seem to form both  $\Lambda_1$ -like and  $\Lambda_0$ -like structures.

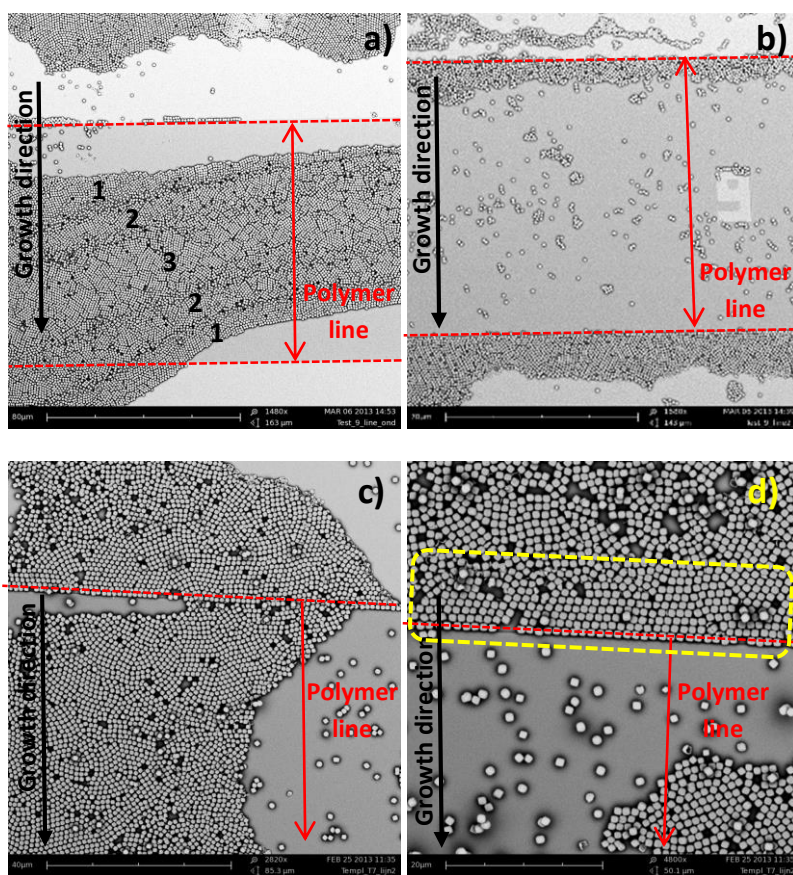


Figure 56: SEM images of deposits of hollow silica cubes(5\_S2\_H) on a patterned substrate with straight polymer lines obtained from DD experiments at 0.4 %V in water a) Typical multi-layered structure formed on top of the polymer line. Next to the polymer line a single row of aligned cubes is observed b) At the top particles have deposited on top of the polymer line and at the bottom cubes have deposited next to the line c) Ordered monolayer are formed on top of the polymer line as well as aligned at the polymer line d) Cubes oriented with their face side parallel to the line. The orientation of the neighbouring particles is influenced by these cubes

### Horizontal deposition

SEM images of a deposit of hollow silica cubes(5\_S2\_H) on a patterned substrate with straight polymer lines formed in a HD experiment are shown in figure 57. A typical view of the deposit is shown in figure 57a, where a cube deposit is formed on top of the polymer as well as next to the polymer line. It can be seen that the shape of the deposit is different close to the edges of the polymer line, indicating the meniscus shape was influenced by the height differences on the template. At the bottom of the image a single row of aligned cubes, stroked by yellow dashes, is observed. Ordered monolayers on top of and next to the polymer line can be observed in figure 57b. In figure 57c the orientation of aligned cubes is visible and it can be seen that the cubes are oriented with their face side parallel to the line. The formation of large multilayered structures is observed as well, as can be seen in figure 57d. Here, the multilayered structure is formed on the substrate and not on the polymer line. In figure 57e it is visible that the structure is detached from the polymer line. Here, the orientation of the cubes in the first layer of this structure is random, suggesting that these cubes were not aligned when the multilayered structure was formed. Multilayered structures of cubes obtained from HD experiments are often detached but located close to polymer lines, whereas monolayers are often aligned. This indicates that the meniscus shape and the contact angle are different when mono- or multilayers are formed.

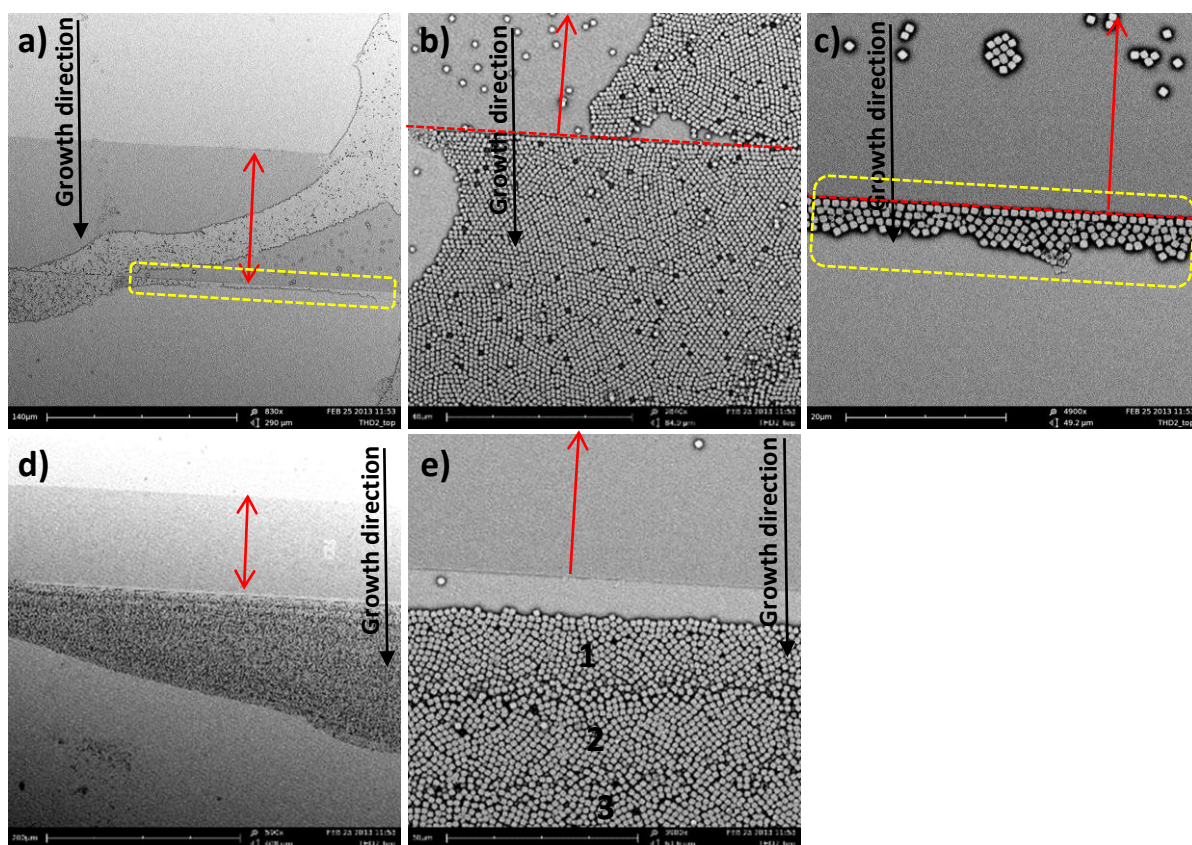


Figure 57: SEM images of a deposit of hollow silica cubes(5\_S2\_H) on a patterned substrate with straight polymer lines obtained from a HD experiment at 0.4 %V in water. The red arrows designate the position of the polymer lines a) Typical deposit, where part of the cubes have deposited on top of the polymer line and part on the substrate. The yellow dashed show some cubes are aligned b) Ordered monolayers formed on top of the polymer and on the substrate c) Cubes aligned with their face side parallel to the line d) Formation of a multilayer detached from the polymer line e) Three layers of a multilayered structure detached from the line

### Flow controlled vertical deposition

Figure 58 shows SEM images of cube deposits obtained with a FCVD experiment. In figure 58a it can be seen that a large area is covered with precipitated silica, influencing the alignment of the cubes. In deposits obtained from FCVD experiments dissolved silica was often observed to disturb the alignment of the cubes. In figure 58b it can be seen that multilayered structures are formed, where the monolayer is sometimes attached to the polymer line, which is not observed with the DD and HD method. A thin line of precipitated silica or a single row of cubes is observed close to the line edge. The multilayers consist of large ordered structures of cubes with similar orientation, as can be seen in figure 58c where the toplayer of a multilayered structure is shown. This shows that a straight growth start clearly induces the formation of large ordered structures of similar orientation. The aligned cubes in the monolayer of the multilayered structures are not always oriented with their face side completely parallel to the line, as can be seen in figure 58d and 58e. Here, again a single row of cubes is formed on top of the polymer indicating that the height of the polymer is not uniform, presumably caused by an error in the fabrication of the templates.

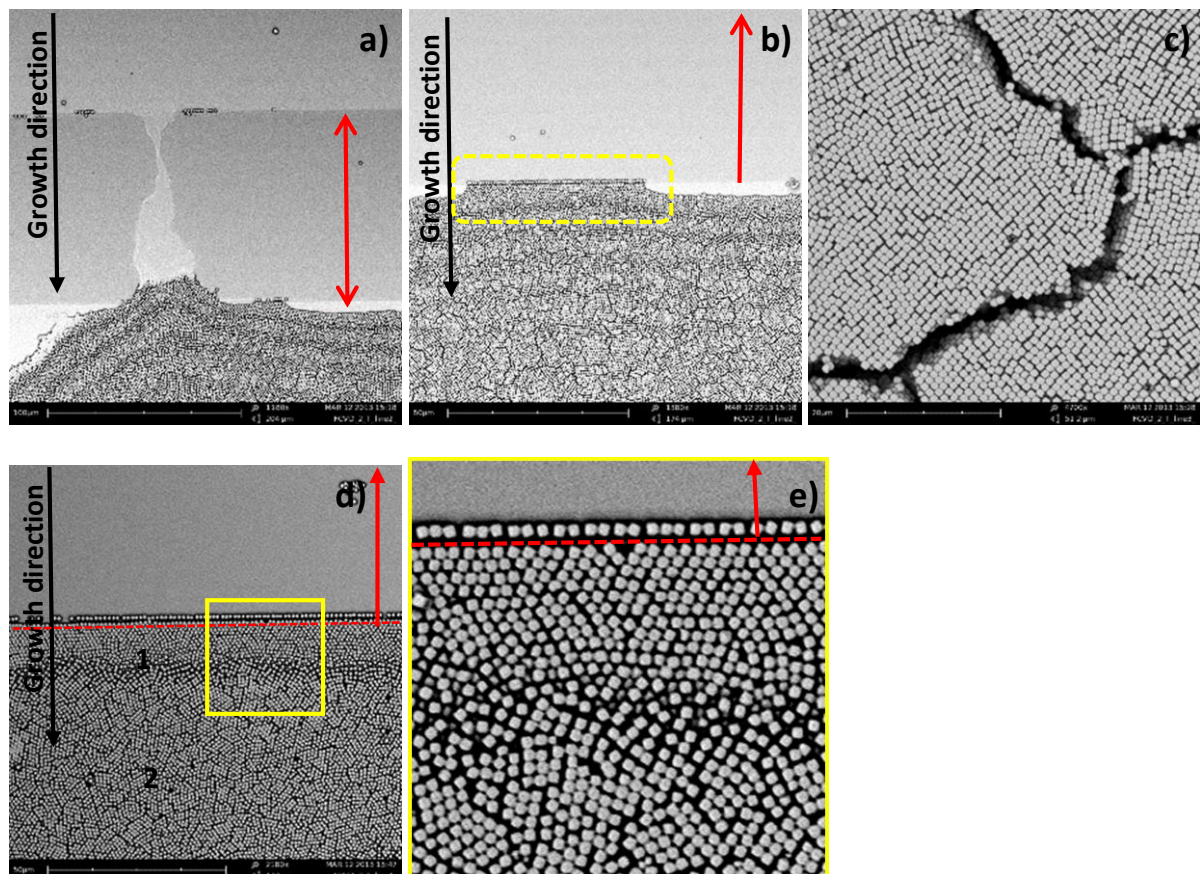


Figure 58: SEM images of a deposit of hollow silica cubes(5\_S2\_H) on a substrate patterned with straight polymer lines obtained from a FCVD experiment at 1 %V in water at 45 °C and a surface dropping velocity of 1 mm/h a) Overview of the formation of a multilayered structure at the growth start b) Formation of a multilayered structure with part of the monolayer attached to the polymer line c) Toplayer of a multilayered structure where large ordered domains of similar orientation are observed d) Formation of a multilayered structure with the monolayer attached to the polymer line. The edge of the polymer line is indicated by the red dashed line e) Enlargement of the area enclosed by the yellow square in figure 58d. The cubes in the monolayer at the polymer line have different orientation and a single row of cubes with similar orientation of observed on top of the polymer

### Patterned polymer lines

A few CA experiments with hollow silica cubes(5\_S2\_H) are performed on substrates with saw-patterned polymer lines. The saw pattern was initially fabricated to induce the formation of a  $\Lambda_1$  arrangement. Saw patterns of different dimensions are fabricated and in figure 59a it is shown that the patterns with dimensions  $< 1 \mu\text{m}$  are not fabricated accurately due to the limited resolution of optical lithography. Although a better result is obtained for dimensions  $> 1 \mu\text{m}$  the edges of the saw stay rounded instead of sharp, as can be seen in figure 59b.

Despite the failure of the fabrication, interesting results are obtained with saw patterns larger than  $1 \mu\text{m}$ . In figure 59c a SEM image is shown of cubes on a saw-patterned substrate obtained from a DD experiment performed at  $0.4 \text{ \%V}$  in water. It can be seen that the cubes are influenced by the pattern since they deposited in triangle shapes. The orientation of the cubes at the polymer line is observed to influence the orientation of the neighbouring cubes as well. This indicates that with the right dimensions of the saw pattern a  $\Lambda_1$ -like structure could be induced.

Experiments with the arches pattern and the tooth pattern are not performed yet. But since promising results are obtained with the straight lines and saw pattern, the other two patterns are interesting for future studies as well. With the tooth pattern  $\Lambda_0$ -like arrangements could be induced and with the arches pattern the role curvature at the growth start can be studied.

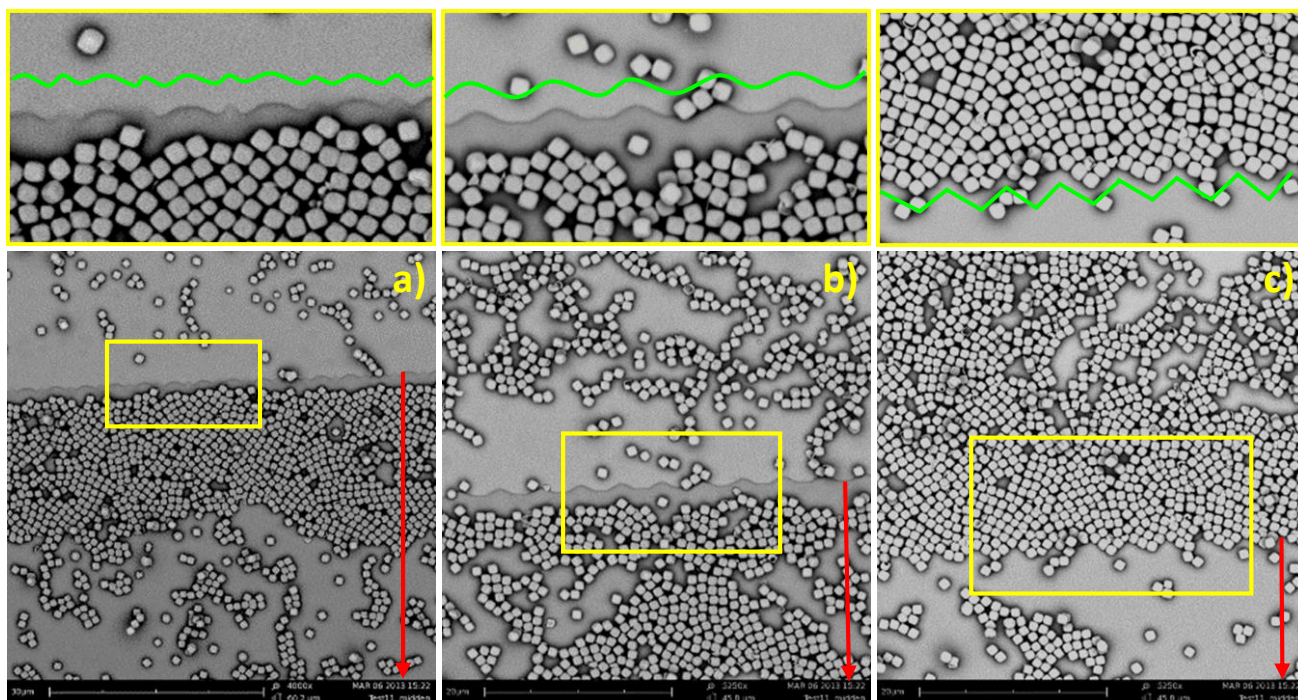


Figure 59: SEM images of a deposit of hollow silica cubes(5\_S2\_H) on a substrate with saw-patterned lines obtained from a DD experiment at  $0.4 \text{ \%V}$  in water. The red arrows indicate the position of the polymer. The areas enclosed by the yellow rectangular boxes are displayed above the images a) Observation of the saw pattern at the lines indicate the pattern was not fabricated very well b) A saw-patterned line showing curves instead of sharp triangles were fabricated c) Alignment of cubes at the lines, showing the orientation of the cubes at the lines and the neighbouring cubes was influenced

## *Conclusion*

To induce a straight growth start in CA experiments accurate straighteners are required. Try outs with macroscopic polymer lines showed that lines of smaller height compared to the particles are required to induce the formation of monolayers. Templates with straight polymer lines of  $\sim 500 \mu\text{m}$  in height are used in CA experiments using the DD, HD and FCVD method. It is observed that with all three methods hollow silica cubes of  $\sim 1 \mu\text{m}$  can be aligned. Cubes in monolayered structures are observed to often align with their face side parallel to the polymer, inducing a straight growth start. The influence of a straight growth start was especially visible from results obtained with FCVD experiments, where large ordered multilayered domains of similar orientation are observed to form on the templates. With saw-patterned substrates the orientation and position of the cubes could be influenced as well. It can be concluded that with templates the alignment of the cubes and therefore the formation of the structure can be influenced and controlled.

## 4. Crystal Structure Analyses

### 4.1. Theory & Background

To analyze crystal structures of colloids order parameters can be used. In this section the radial distribution function,  $g(r)$ , will be defined, which is used to determine the positional and translational order in a colloidal crystal. In 2D structures of superball-shaped particles the particles are expected to arrange on a  $\Lambda_0$  or  $\Lambda_1$  lattice. Therefore, both lattices will be defined in detail for a proper analysis of the cube structures obtained from CA experiments.

#### 4.1.1. Radial distribution function, $g(r)$

To determine the positional and translational order of particles in a crystal plane the radial distribution function, also referred to as the pair correlation function,  $g(r)$ , can be determined by using the coordinates of the center of the particles. The radial distribution function describes the possibility to find a neighbouring particle at a particular distance from the center particle. In this study only the two-dimensional radial distribution function, describing translational order in a crystal plane, is used. The radial distribution function is defined as

$$g(r) = \rho^{-2} \left( \sum_i \sum_{j \neq i} \delta(\vec{r}_i) \delta(\vec{r}_j - \vec{r}_i) \right)$$

where  $\rho$  is the average density of particles in the plane,  $r_i$  is the center particle and  $r_j$  the most probable location for surrounding particles of  $r_i$ . The summations run over all values of  $j$  and  $i$ , meaning all particles in the plane are examined.

#### 4.1.2. $\Lambda_0$ and $\Lambda_1$ Classification

The MPD of superball-shaped particles in 2D is obtained with  $\Lambda_0$  and  $\Lambda_1$  arrangements.<sup>39</sup> To determine whether these arrangements are formed and to distinguish between them the lattices have to be defined in great detail. This is done using the lattice vectors of both lattices, described in section 3.1.3. In figure 60 an illustration of cubes on a  $\Lambda_0$  and  $\Lambda_1$  lattice is shown. Here, it is illustrated that within a distance of 2.1 times the particle size(PS) from the center particle, indicated by the green circle, the amount of nearest neighbours(NN) is different for the  $\Lambda_0$  and  $\Lambda_1$  lattice. For the  $\Lambda_0$ -lattice 6 NN are recognized with two NN(dark blue) located at  $45^\circ$  with respect to the diagonal orientation(DO) of the center particle(green). The position of the other four NN(light blue) depends on the  $m$ -value of the cubes. The lattice vectors of the  $\Lambda_0$  lattice determine that for cubes with  $m = 3.6$  these four NN are positioned at  $\pm 17^\circ$  from the DO of the center particle.

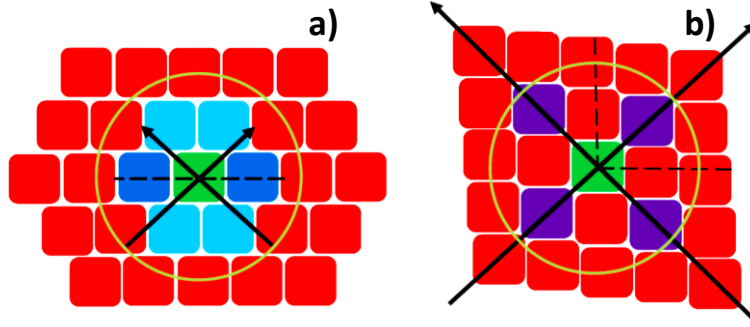


**Figure 60: Illustration of superball-shaped particles arranged on different lattices. The arrows indicate the diagonal orientation of the center cube(green) and the green circle indicated the cutoff distance from the origin of the center particle where NN are examined with IDL a) Cubes on a  $\Lambda_0$ -lattice, where 6 NN are examined with 2 NN located at  $45^\circ$ (dark blue) and 4 NN at  $\pm 17^\circ$ (light blue) from the diagonal orientation of the center particle(for  $m = 3.6$ ) b) Cubes on a  $\Lambda_1$ -lattice where 8 NN are examined with 4 NN in line with the diagonal orientation of the center particles and 4 NN at  $40 - 50^\circ$ (red) of the diagonal orientation of the center particle**

In figure 60b, an illustration of cubes on a  $\Lambda_1$ -lattice is shown. Here, 8 NN are recognized within the green circle. Four NN(purple) are observed in line with the DO of the center particle(green), as is indicated by the black arrow. The other four NN are located at  $40 - 50^\circ$  from the DO of the center particle, which is the angle between the black arrow and the black dashed line. This shows that for cubes with  $m = 3.6$  a clear distinction can be made in the analyses between  $\Lambda_0$  and  $\Lambda_1$  arrangements.

## 4.2. Experimental

SEM images of 2D structures of cubes obtained from CA experiments are quantitatively and qualitatively analyzed. In this section it will be described how the analyses are performed. First, it will be described how the coordinates and orientation of the cubes is determined with a particle tracking procedure in iTEM. This is followed by a description of the procedure used for the structure analyses using Interactive Data Language(IDL).

### 4.2.1. Particle tracking

To distinguish between the  $\Lambda_0$  and  $\Lambda_1$  arrangement in a structure analyses it is required to determine the position and orientation of the cubes. Therefore, the positional coordinates and orientation of all individual cubes in SEM images were determined by particle tracking using iTEM. To obtain the correct values the scale bar and thresholds were manually set and the image was binarized. Since some cubes could not be recognized as single particles the binarized image was smoothed by erosion once or twice(depending on the quality of the image) before the coordinates were determined. The orientation of the cubes was determined by detecting the longest axis of the cube, which is one of the diagonals of the square visible in microscopy images, with respect to the horizontal x-axis. To view the orientation of the cubes, the cubes were labelled with a colour. In figure 61 is shown that the cubes could be labelled with 6 different colours. Each colour represents a particular orientation. An example of an analyses with iTEM where the orientation of the cubes is assigned with a colour label is shown in figure 61. Here, it can be seen that domains of cubes with similar orientation can easily be recognized.

 (°)	Color	 (°)
0 - 15	Red	90 - 105
15 - 30	Magenta	105 - 120
30 - 45	Blue	120 - 135
45 - 60	Cyan	135 - 150
60 - 75	Green	150 - 165
75 - 90	Yellow	165 - 180

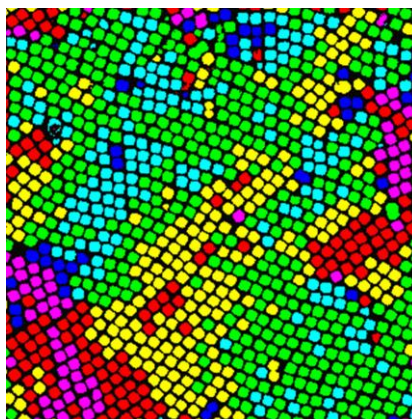


Figure 61: Colourlabels used in iTEM analyses to view the orientation of the cubes in a SEM image. On the right a typical image is shown where the orientation of the cubes observed in a SEM image is assigned with different colours

## 4.2.2. Structure analyses

The coordinates determined by particle tracking were used to determine  $g(r)$  using purposely written Interactive Data Language (IDL) algorithms. Using the information from the  $g(r)$  for a NN cut off distance of 2.0 or 2.1 times the average particle size and the particle coordinates + orientation, the local particle environments can be classified using an additional IDL algorithm. Here, a particle is characterized as  $\Lambda_0$  when 2 particles are found at  $15^\circ$  from the DO of the center cube and at least 3 particles at  $17^\circ$ . The amount of NN positioned in line with the DO of the center cube should be less than 3. A particle is characterized  $\Lambda_1$  when 3 or more NN are positioned in line with the DO of the center cube. A square structure is identified when the  $\Lambda_1$  criteria are met and three or more NN are found at  $45^\circ$  of the DO of the center cube.

In the IDL analysis of the structure, the cubes can be assigned with five different labels:  $\Lambda_1$ ,  $\Lambda_1$ -like,  $\Lambda_0$ ,  $\Lambda_0$ -like and square. The specific requirements for each label are summarized in table 12. Each label is represented by a colour to obtain a clear overview of the arrangements found in a SEM image. The algorithm used for the analysis has included a deviation of  $3 - 15^\circ$  to compensate for small deviations due to polydispersity, drying effects and the detection sensitivity of the iTEM analysis.

Table 12: Settings used in IDL for the structure analyses of SEM images of cubes

Position of the NN Assignment	NN in line with the DO of the center cube ( $\pm 10^\circ$ )	NN at $45^\circ$ of the DO of the center cube ( $\pm 5-15^\circ$ )	NN at $17^\circ$ of the DO of the center cube ( $\pm 10^\circ$ )	NN at $45^\circ$ of the DO of the center cube ( $\pm 3^\circ$ )
$\Lambda_1$ -like	3			
$\Lambda_1$	$\geq 4$			
$\Lambda_0$ -like	$< 3$	2	3	
$\Lambda_0$	$< 3$	2	4	
Square	$\geq 3$			$\geq 3$

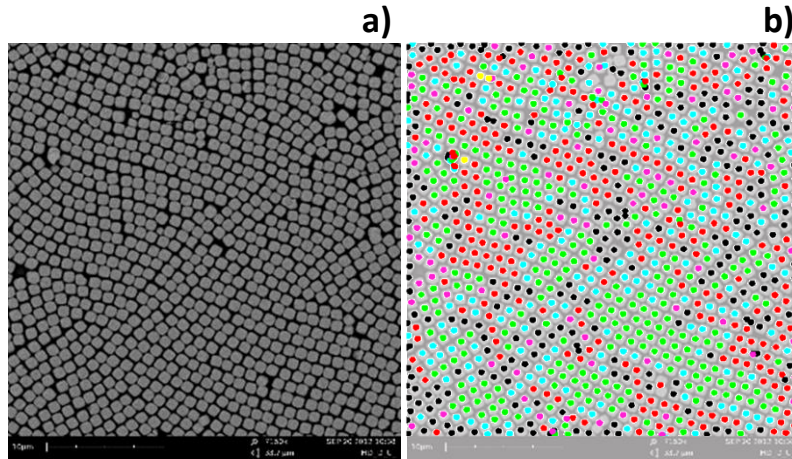


**Figure 62:** Example of an IDL analysis a) SEM image of a monolayer of hollow silica cubes obtained from a HD experiment b) Result of the IDL analysis of the SEM image showing the cubes are arranged on  $\Lambda_1$  and  $\Lambda_0$  lattices.

An example of a result of an IDL analysis is shown in figure 62. Here, a SEM image of a monolayer of cubes formed in a HD experiment, shown in figure 62a, is analyzed. The resulting image obtained from the structure analysis is shown in figure 62b. Here, every dot represents one cube and the colour of the dot represents the assigned structure label. It is observed that both the  $\Lambda_1$  and  $\Lambda_0$  lattices are formed (green and red dots) and domains of cubes with similar order are observed. The black dots indicate cubes that didn't fit any of the requirements for the five labels and are therefore not assigned.

## 4.3. Results & Discussion

In HD and FCVD experiments ordered monolayered and multilayered structures of colloidal cubes are formed. SEM images of 2D structures formed in CA experiments are analyzed in this study. With iTEM the orientation and the positional coordinates of the cubes are determined. Using the coordinates of the cubes a radial distribution function is constructed, which is followed by an analysis of the structure with IDL of mono- and multilayered structures.

### 4.3.1. Monolayers

Large ordered monolayers of cubes are mainly obtained from HD experiments. SEM images of these monolayers are analyzed. A typical SEM image of a monolayer is shown in figure 63a. Here, it can be observed by eye that ordered domains of cubes are formed. With iTEM the orientation and the coordinates of the cubes in this image are determined. In figure 63b the result of the iTEM analysis of the orientation of the cubes is shown. Here, domains of cubes labelled with the same colour can be observed, which means these cubes have similar orientation. Most cubes are labelled with a dark or light blue colour and in figure 63c it can be seen that these cubes all have an orientation of  $30 - 60^\circ$ . Using the positional coordinates the  $g(r)$  of the SEM image in figure 63a is determined as well.

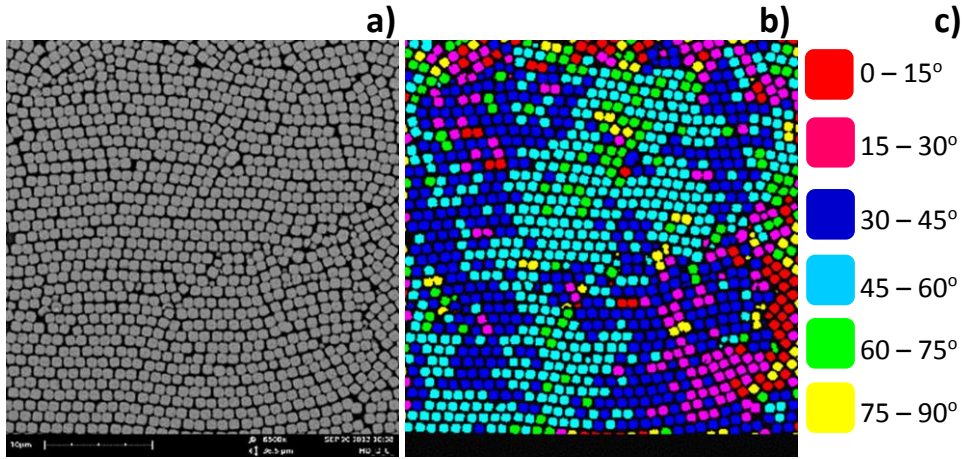


**Figure 63: iTEM analysis of a monolayer of cubes** a) Original SEM image of a monolayer of hollow silica cubes(5\_S2\_H) formed in a HD experiment(HD\_D\_13) at 0.2%V b) Result of the iTEM analysis of the SEM image. Cubes with similar orientation are labelled with the same colour, showing domains of cubes with similar orientation are formed c) The orientation of the cubes with respect to the horizontal axis belonging to the different colour labels.

The  $g(r)$  is shown in figure 64 where peaks are observed up to the 15<sup>th</sup> order. This indicates that a long-range ordered structure is formed. Peaks with a certain width are observed since polydispersity and crystal defects cause different unique spacings. The fact that the peaks are not symmetric indicates at the position of the broadened peaks some small peaks overlap at certain distances. The position of the peaks is determined by the arrangement of the particles.

Since superball-shaped particles are predicted to arrange on a  $\Lambda_0$  or  $\Lambda_1$ -lattice in 2D, the  $g(r)$  shown in figure 64 is compared to the theoretical  $g(r)$  for a perfect  $\Lambda_0$  or  $\Lambda_1$ -lattice. Since especially in the first four peaks of the experimental  $g(r)$  a fine structure is observed, only the first four peaks are compared to the theoretical  $g(r)$  for the  $\Lambda_0$  and  $\Lambda_1$ -lattice.

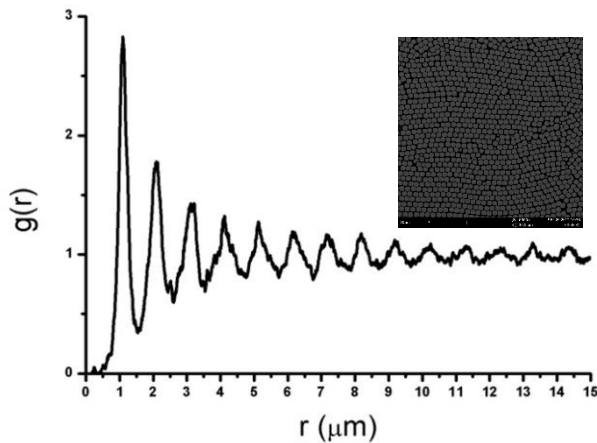


**Figure 64: Radial distribution function in a monolayer of cubes** determined by the analysis of the SEM image shown. The formation of more than 10 peaks is observed indicating long-range ordered domains are formed

In figure 65a, the experimental  $g(r)$  is shown up to a distance of 5  $\mu\text{m}$  from the origin. The red bars indicate the positions of neighbours found on a  $\Lambda_0$ -lattice. Comparison of the experimental  $g(r)$  with the theoretical  $g(r)$  for a  $\Lambda_0$ -lattice shows that the position of the first four peaks is similar. The intensity of the peaks is different especially for the third peak. The peak observed in theory at 4.9  $\mu\text{m}$  is not observed in the experimental  $g(r)$ . In figure 65b the experimental  $g(r)$  is compared to the theoretical  $g(r)$  (green bars) determined for a  $\Lambda_1$ -lattice. Here, the position of all four peaks is in agreement with the positions expected for the  $\Lambda_1$ -lattice. However, the fine structure and the intensity of the peaks is slightly different.

In CA experiments the MPD is not always obtained and since the difference in packing density of the  $\Lambda_0$  and  $\Lambda_1$  lattices is small, it is possible that a mixture of the two is formed. In figure 65c the experimental  $g(r)$  is compared to the theoretical  $g(r)$  for a 50:50 mixture of the  $\Lambda_0$  and  $\Lambda_1$  lattices. Here, it can be observed that the position of the first four peaks is in agreement. The fine-structure of the peaks is also more in agreement compared to the fine-structure expected for only the  $\Lambda_0$  or  $\Lambda_1$  lattice. This is a clear indication that the cubes order on both the  $\Lambda_0$  and  $\Lambda_1$  lattice.

To qualitative analyze the structures formed by the cubes the presence of the  $\Lambda_0$  and  $\Lambda_1$  arrangement in the monolayers was determined with IDL. The results of an IDL analysis of the SEM image shown in figure 63a is shown in figure 66. In the structure analysis the position and angle of the NN relative to the DO of the center cube were analyzed for all cubes in the image. By setting specific requirements for the  $\Lambda_0$  and  $\Lambda_1$  lattices it is determined what arrangement is formed by the cubes. Every cube is assigned with a label, which is indicated by a colour, shown in figure 66c. In figure 66b the colour label of every cube in the monolayer is shown and it can be seen that domains ( $\sim 5 \times 5$  PS) with  $\Lambda_1$  (green) and  $\Lambda_0$  (pink) ordered cubes are formed. This indicates that the cubes arrange on both the  $\Lambda_0$  and  $\Lambda_1$  lattice. Cubes with a  $\Lambda_0$ -like (pink) and  $\Lambda_1$ -like (blue) arrangement are located between the  $\Lambda_0$  and  $\Lambda_1$  ordered domains. Only a few cubes are arranged on a square lattice and some cubes are not assigned, which is mostly caused by the fact that not enough NN were recognized.

It is determined that in this SEM image 38% of the cubes is ordered in a  $\Lambda_0$ -arrangement and 39% in a  $\Lambda_1$ -arrangement. This confirms that the superball-shaped particles order on the  $\Lambda_0$  and  $\Lambda_1$  lattices, which was predicted by simulations of Jiao *et al.*<sup>39</sup> The alternating domains with  $\Lambda_0$  and  $\Lambda_1$  order, explains the long-range order found in the experimental  $g(r)$  that matched the theoretical  $g(r)$  of a 50:50 mixture of the  $\Lambda_0$  and  $\Lambda_1$  lattices.

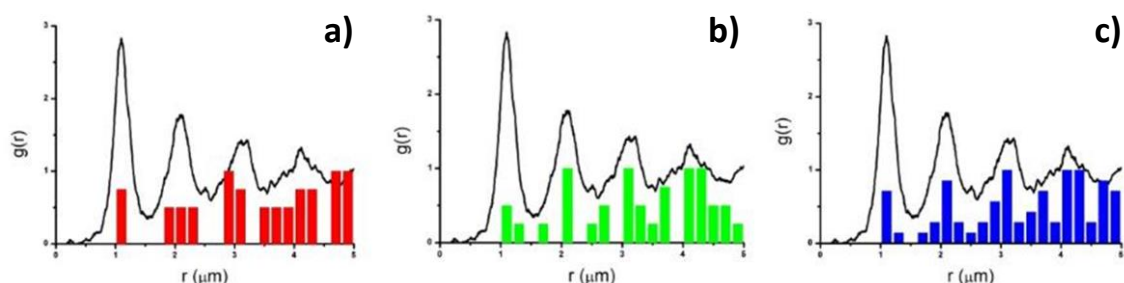


Figure 65: Comparison of the experimental  $g(r)$  shown in figure 64a to the theoretical positions of the NN on a) a  $\Lambda_0$  lattice b) a  $\Lambda_1$  lattice c) a 50:50 mixture of the  $\Lambda_0$  and  $\Lambda_1$  lattices

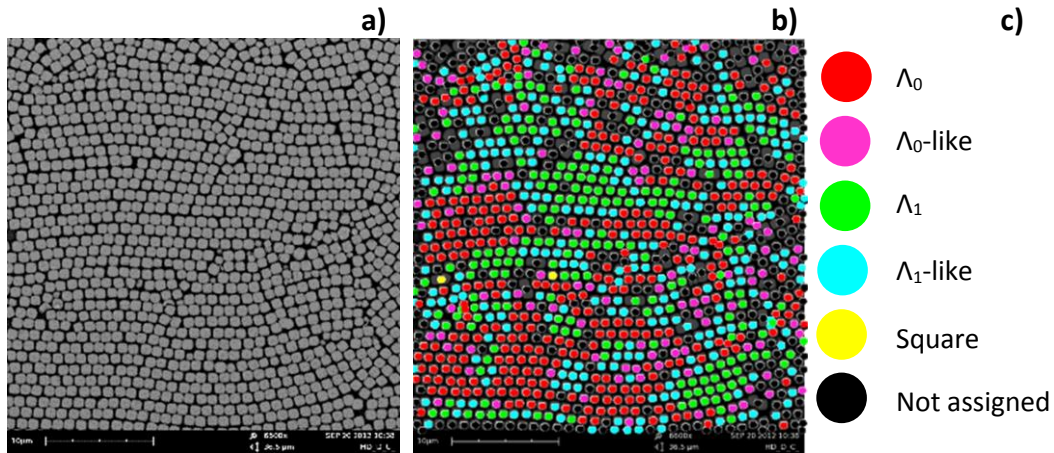


Figure 66: IDL analyses of a SEM image of a monolayer of hollow silica cubes(5\_S2\_H) formed in a HD experiment at 0.2 %V in water a) SEM image used in the analysis c) Resulting image from the IDL analysis. Cubes are observed to order on both  $\Lambda_0$  and  $\Lambda_1$  lattices forming small domains

Since the IDL analysis supports the explanation for the  $g(r)$  found for this image, only results of the IDL analyses will be presented and discussed for the other SEM images. Figure 67 shows the analysis of a SEM image taken at a different position in the same sample at a similar distance from the growth start. This SEM image is shown in figure 67a and by eye a large ordered domain of cubes can be observed. To qualitatively analyze the structure formed by the cubes the SEM image is analyzed with iTEM and IDL. The result of the iTEM analysis is shown in figure 58b. Here, the orientation of the cubes is visible and it is observed that most cubes have a similar orientation, since they are labelled with the same colour. The result of the IDL analysis is shown in figure 67c. Here, it can be seen that most cubes are arranged on a  $\Lambda_1$ -lattice, forming a large ordered domain of  $\sim 20 \times 20$  PS in size. It is also observed that in the ordered domain the cubes have a similar orientation(fig 67b and 67c).

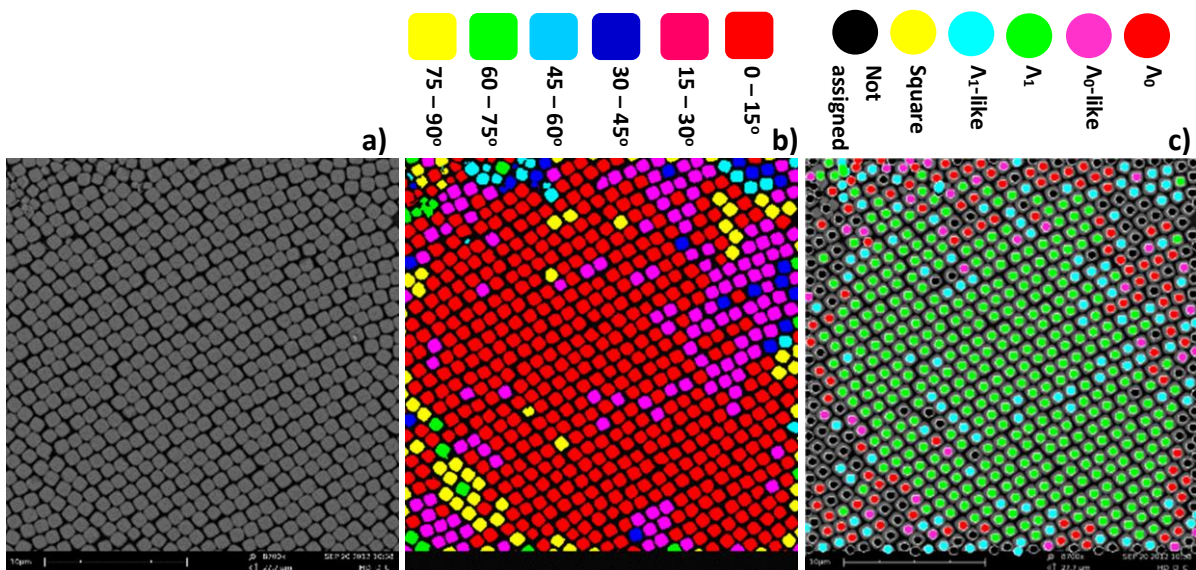


Figure 67: Analysis of a monolayer of hollow silica cubes(5\_S2\_H) formed in a HD experiment(HD\_D\_19) at 0.2 %V in water a) Original SEM image of the monolayer b) Orientation of the cubes determined with iTEM c) Structure analysis with IDL

The overall order of the cubes in this SEM image is 17%  $\Lambda_0$  and 68%  $\Lambda_1$ . The results of the analyses of the two SEM images discussed illustrate that a significant difference in order that can be found locally in monolayers. Therefore, a quantitative analysis is performed to determine the overall order of the cubes in the monolayers. In total 49633 particles from 25 SEM images of three different samples are analyzed. The results of these analyses are summarized in table 13. Here, it can be seen that over 2/3 of the cubes is assigned  $\Lambda_0$  or  $\Lambda_1$  in the analyses. It is also shown that 29.8 % of the cubes ( $m = 3.6$ ) is generally ordered on a  $\Lambda_0$  lattice and 41.5% on a  $\Lambda_1$  lattice in monolayers. This demonstrates that the cubes arrange on both  $\Lambda_0$  and  $\Lambda_1$  lattices in monolayers formed in HD experiments. It also shows that the  $\Lambda_1$  arrangement is dominant for these cubes in monolayers.

**Table 13: Results of IDL structure analyses of SEM images of monolayers obtained from HD experiments**

Parameter Sample	Conc (%V)	# SEM images	# Cubes	$\Lambda_0$ (%)	$\Lambda_0$ -like (%)	$\Lambda_0$ Total (%)	$\Lambda_1$ (%)	$\Lambda_1$ -like (%)	$\Lambda_1$ Total (%)	Square (%)	Not assigned (%)
HD_D	0.2	15	34095	22.2	8.7	30.9	21.9	20.8	42.7	0.4	26.1
HD_P	0.4	7	11605	16.0	9.8	25.8	17.4	21.4	38.8	0.5	35.0
HD_L	0.2	3	3933	23.3	9.5	32.8	18.2	21.8	40.0	0.2	27.0
<b>Average of all cubes</b>			49632	20.8	9.0	<b>29.8</b>	20.5	21.0	<b>41.5</b>	0.4	28.3

### 4.3.2. Multilayers

To determine whether  $\Lambda_0$  and  $\Lambda_1$  order persists in the layers in multilayered structures, the toplayer of multilayered cube structures is analyzed with iTEM and IDL as well. In figure 68a a SEM image of the toplayer of a multilayered structure of hollow silica cubes(5\_S2\_H) formed in a HD experiment at 0.2 %V in water is shown. Here, cracks in the structure and differences in height of the sediment are observed, which is typically found in multilayered structures. The height differences cause the cubes to be out of focus, which complicated the analyses. Therefore, in the iTEM analyses often not all cubes are recognized and assigned. Despite of these complications most cubes are analysed, as can be seen in figure 68b where the orientation of the cubes is determined. Here, cubes with very different orientation are observed. Also, no large domains of cubes with similar orientation are formed as is observed in monolayers, instead small domains are found.

A result of a structure analysis with IDL is shown in figure 68c. Here, small domains of cubes with  $\Lambda_0$  and  $\Lambda_1$  order are observed of typically 5 x 5 PS in size. Furthermore, many cubes that are positioned close to cracks are not assigned, since here too little NN are recognized within the cutoff distance of 2.0PS. Therefore, the structure analysis for these particles is incorrect. Since the cracks appear after the formation of the structure due to drying effects, the cubes close to the cracks are preferably taken into account in the analysis. Therefore, IDL analyses are performed with a cutoff distance of 2.1PS as well, as is shown in figure 68d. Already by eye it can be seen that less cubes are labelled with a black dot, indicating more cubes are analyzed. This is confirmed by the numbers shown in table 14. Here, it can be seen that ~10 % more cubes are analyzed when a cutoff distance of 2.1PS is used. The overall order of the cubes found with a cutoff distance of 2PS, was for 29.3 %  $\Lambda_0$  and for 35.6 %  $\Lambda_1$ . At a cutoff distance of 2.1PS, 33.6 % of the cubes arranged on a  $\Lambda_0$  lattice and 41.8 % on a  $\Lambda_1$  lattice.

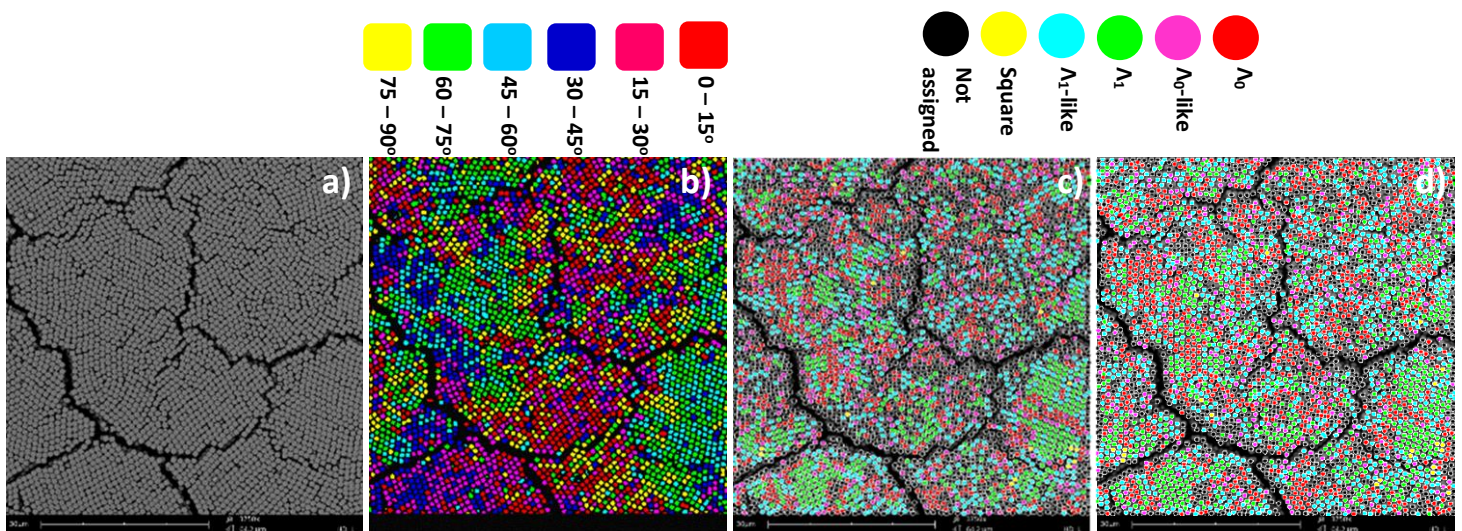


Figure 68: Analysis of the toplayer of a multilayered structure of hollow silica cubes(5\_S2\_H) formed in a HD experiment(L\_55) at 0.2 %V a) Original SEM image b) Orientation of the cubes determined with iTEM c) Structure analysis with IDL at a cutoff distance of 2PS d) Structure analysis with IDL at a cutoff distance of 2.1PS

**Table 14: Results of IDL structure analyses at different cutoff distances of one SEM image of multilayers obtained from a HD experiment**

Parameter Cutoff distance	$\Lambda_0$ (%)	$\Lambda_0$ -like (%)	$\Lambda_0$ Total (%)	$\Lambda_1$ (%)	$\Lambda_1$ -like (%)	$\Lambda_1$ Total (%)	Square (%)	Not assigned (%)
<b>2.0 PS</b>	19.6	9.7	<b>29.3</b>	14.7	20.9	<b>35.6</b>	0.4	<b>34.7</b>
<b>2.1 PS</b>	25.6	8.0	<b>33.6</b>	17.3	24.4	<b>41.8</b>	0.5	<b>24.1</b>

**Table 15: Average results obtained from IDL analyses of SEM images of structures of cubes formed in HD experiments**

Parameter Structure	Cutoff distance (PS)	# Samples	# SEM images	# Cubes	$\Lambda_0$ Total (%)	$\Lambda_1$ Total (%)	Not assigned (%)
<b>Monolayer</b>	2.0	3	25	49633	29.8	41.5	28.3
<b>Multilayer</b>	2.0	1	3	9926	22.6	34.8	38.3
<b>Multilayer</b>	2.1	1	3	9926	31.8	40.4	27.5

Since the analyses of these toplayers was difficult due to height differences in the multilayered structures only 9926 particles are analyzed obtained from 3 SEM images of the same sample. Although this is too little to perform a quantitative analysis the results are interesting. In table 15 the average results obtained from IDL analysis of monolayers and multilayers are summarized. First, it is observed that in both mono- and multilayers  $\Lambda_0$  and  $\Lambda_1$  order is observed, indicating that the order found in monolayers persists throughout the layers. Another interesting observation is that in both mono- and multilayers the  $\Lambda_1$  arrangement is dominant. This is supported by simulations that show that the MPD of superball-shaped particles with  $m = 3.6$  arranged on a  $\Lambda_1$  lattice is slightly compared the  $\Lambda_0$  lattice.<sup>39</sup> For multilayers almost 10% more cubes are analyzed when a cutoff distance of 2.1PS is used in the IDL analyses instead of 2PS. The average percentages of cubes arranged on a  $\Lambda_0$  or  $\Lambda_0$  lattice in multilayers is similar to the values found for monolayers when a cutoff distance of 2.1PS is used. It is therefore assumed that with the cutoff distance of 2.1PS more reliable results are obtained since cubes positioned close to cracks are included in the analysis.

With the FCVD method multilayered structures of cubes are formed as well. By eye it seems that ordered domains of larger size are formed with this method compared to the results obtained with the HD method. To analyze whether there is a difference in the size of the domains and the arrangements of the cubes, SEM images of toplayers of multilayered structures obtained from FCVD experiments are analyzed as well.

In figure 69a a SEM image of the toplayer of a multilayered structure of hollow silica cubes(5\_S2\_H) is shown. This structure is formed in an FCVD experiment at 1 %V(in water), 45°C and a surface dropping velocity of 1 mm/h. With iTEM the orientation of the cubes was determined and the result is shown in figure 69b. Here, cubes with a similar orientation can be observed.

Structure analyses with IDL are performed at two cutoff distances, 2PS and 2.1PS. Results of the analysis are shown in figure 69c and 69d, for 2PS and 2.1PS, respectively. In both images it is observed that cubes are arranged on both the  $\Lambda_0$  and  $\Lambda_1$  lattice. Although a similar orientation of the cubes was observed in the middle part of the image, as can be seen in figure 69b, the cubes are observed to arrange in small alternating  $\Lambda_0$  and  $\Lambda_1$  domains. This indicates that the cubes easily switch between  $\Lambda_1$

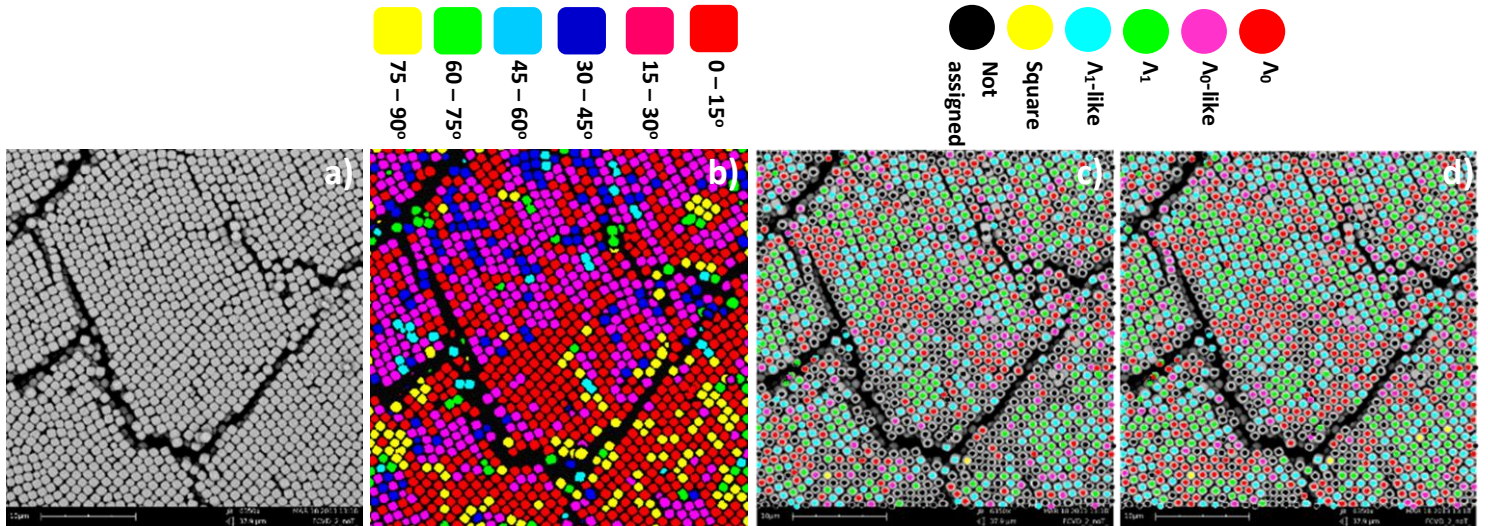


Figure 69: Analysis of the top layer of a multilayered structure of hollow silica cubes(5\_S2\_H) formed in a FCVD experiment(FCVD\_2\_noT\_46) at 1 %V, 45 °C and a surface dropping velocity of 1 mm/h a) Original SEM image b) Orientation of the cubes determined with iTEM c) Structure analysis with IDL at a cutoff distance 2PS d) Structure analysis with IDL at a cutoff distance 2.1PS

over  $\Lambda_0$  arrangements, which can be understood by the small difference in maximum packing density for both lattices.

Although this small difference in packing density, the  $\Lambda_1$  arrangement is dominant in the structure. This is observed by the overall order of the cubes which is 28.7 %  $\Lambda_0$  and 41.4 %  $\Lambda_1$  at a cutoff distance of 2PS and 35.3 %  $\Lambda_0$  and 46.7 %  $\Lambda_1$  at 2.1PS. Similar to the analyses of SEM images of multilayers formed in HD experiments more cubes are analyzed when a cutoff distance of 2.1PS is used, since the cubes positioned close to the cracks are more often taken into account.

In table 16 the average results obtained from IDL analyses of SEM images of multilayers formed in HD and FCVD experiments are summarized. It can be seen that with both methods the cubes arrange on a  $\Lambda_0$  and  $\Lambda_1$  lattice. The percentages of the cubes in a  $\Lambda_0$  and  $\Lambda_1$  arrangement are very similar and with both cases the  $\Lambda_1$  arrangement is dominant. Although too little cubes are analyzed to be conclusive, it can be indicated that with both the HD and FCVD method ordered domains of cubes with  $\Lambda_0$  and  $\Lambda_1$  arrangements are formed.

Table 16: Results obtained from structure analyses with IDL of SEM images of multilayers formed in HD and FCVD experiments. A cutoff distance of 2.1PS was used in the analyses

Method	Parameter	# Samples	# SEM images	# Cubes	$\Lambda_0$ Total (%)	$\Lambda_1$ Total (%)	Not assigned (%)
Method	HD	1	3	9926	31.8	40.4	27.5
	FCVD	1	4	8748	32.8	42.1	24.3

## *Conclusion*

These analyses show that ordered structures of micron-sized hollow silica cubes are formed in this study with the HD and the FCVD method. Domains of cubes with similar orientation are observed and in both mono- and multilayers  $\Lambda_0$  and  $\Lambda_1$  arrangements of cubes are observed. The  $\Lambda_1$  arrangement is observed to be dominant in both mono- and multilayers. These findings are in agreement with the simulations of 2D structures of superballs which showed that the MPD of the  $\Lambda_1$  lattice is slightly higher compared to the  $\Lambda_0$  lattice for superballs with  $m = 3.6$ .

The arrangements formed by the micron-sized cubes ( $m = 3.6$ ) are different from the arrangements observed for hollow silica cubes of with  $m = 2.9$ .<sup>44</sup> Here, mainly hexagonal-like structures were observed. This indicates that the  $m$ -value of the cubes is of major influence on the structures formed in CA experiments.

## 5. Conclusions

In this study hollow silica cubes of 1  $\mu\text{m}$  in size and a shell thickness of 48 nm are successfully synthesized. The shape of these cubes is approached by that of a superball using the deformation parameter  $m$  is used to determine the roundness of the edges. The micron-sized cubes have an  $m$ -value of 3.6.

Crystal structures of cubes are obtained from CA experiments using the drying(DD), horizontal deposition(HD) and flow-controlled vertical deposition(FCVD) method. All deposits show strong Bragg reflections under white light illumination indicating ordered structures are formed. With the drying droplet method the dynamics in the dispersion are studied using inverted microscopy. Here, a particle flux of single cubes from the bulk to the edges of the droplet is observed and due to immersion capillary forces at the edges ordered structures of hollow silica cubes of up to a few 100  $\mu\text{m}$  are formed resulting in ring-like deposits. With the HD and the FCVD method larger deposits are obtained and SEM images of the deposit showed ordered mono- and multilayered structures are formed. Both with the DD and the HD method a curved growth start is induced, whereas with the FCVD method the growth start is straighter. The surface charge of the cubes was observed to be of major influence in the CA process. Experiments with fluorescent hollow silica cubes with presumably a few dye-molecules at the surface of the cubes changed the interactions present in the system completely resulting in the formation of disordered structures.

Since a straight growth start is crucial for the formation of ordered domains of similar orientation CA experiments are performed with straighteners attached to the substrate. Cubes successfully aligned to straight polymer lines of 500 nm in height and it is observed that this influences the orientation of the neighbouring cubes. The use of patterned polymer show that the orientation of the cubes can be influenced at the growth start, allowing control over the structure formation. The structures formed are unfortunately too small to be analyzed.

With iTEM the position and orientation of cubes in SEM images is determined. This shows that with the FCVD method the largest ordered domains are formed of similar orientation. In structures formed with the DD and HD method smaller domains are observed and the domains have different orientation. Algorithms in IDL are used for quantitative analyses of the cube structures using the lattice vectors of the  $\Lambda_0$  and  $\Lambda_1$  lattice predicted for superballs. Monolayers and the toplayer of multilayered structures formed with all three CA methods are analyzed. The analyses show that the cubes arrange on both the  $\Lambda_0$  and  $\Lambda_1$  lattice in both mono- and multilayers. This suggests that the order in monolayers persists throughout the layers resulting in 3D ordered structures. A small preference for the  $\Lambda_1$  lattice over the  $\Lambda_0$  lattice is found. This is in agreement with calculations that show that the MPD of the  $\Lambda_1$  lattice is slightly higher compared to the  $\Lambda_0$  lattice for superballs with  $m = 3.6$ .



## 6. Outlook

The HD and FCVD methods can be further optimized by controlling more experimental parameters such as humidity, temperature and the airflow.

The multilayered structures formed in this study can be studied in more detail to determine whether and how the cubes order in 3D. Confocal microscopy could be used to study the 3D ordering of the cubes. To use this technique a new batch of fluorescent cubes should be synthesized without the presence of dye-molecules at the particle surface.

Experiments with substrates with polymer lines show that the orientation of the cubes at the growth start can be influenced. Further experiments are required to study whether certain arrangements of cubes can be induced by using patterned substrates. Substrates with tooth-patterned lines can be used to induce  $\Lambda_0$ -order and the saw-patterned lines to induce  $\Lambda_1$ -order. The arches-patterned lines could be used to study the effect of curvature at the growth start on the formation of the structure. The patterns on the substrates are fabricated with different dimensions, therefore cubes of different sizes can be used for these experiments.

In this study it is shown that cubes with an  $m$ -value of 3.6 arrange on a  $\Lambda_0$  and  $\Lambda_1$ -lattice. This is different from the predominantly hexagonal-like order observed for cubes of  $m = 2.9$ . Since the difference in MPD of the  $\Lambda_0$  and  $\Lambda_1$ -lattice increases with  $m$ , it is interesting to study whether  $\Lambda_1$  order is more dominant in structures formed by cubes with an  $m$ -value  $\gg 3.6$ .

# Acknowledgements

First of all, I would like to thank my daily supervisor Janne-Mieke Meijer for her enthusiasm, perseverance, patience and comments. I enjoyed working with you and you made me even more persistent to become a scientist! Thanks! I also want to thank Andrei Petukhov for his input and discussions, which greatly contributed to the results of my experimental work. Sonja Castillo is thanked for her help and knowledge on the cube syntheses and the discussions together with Albert Philipse about colloidal cubes in general. Of course I also thank the Crystal Club, other masterstudents and the many others working at the Van 't Hoff Laboratory. Thank you all for this great experience!

I think it's a privilege to learn new things every day from so many experienced scientists and I know there's still a lot to learn and to explore which makes me smile.

# Bibliography

---

- <sup>1</sup> Russel, W. B., *The Phase behaviour and Dynamics of Colloidal Dispersions*, Lecture Notes Debye professor 2000-2001, Princeton Materials Institute, Princeton University
- <sup>2</sup> Everett, D. H., *Basic principles of colloid science*, Royal Society of Chemistry, Cambridge, 1988
- <sup>3</sup> Pusey, P.N. and van Meegen, W., *Phase behavior of concentrated suspensions of nearly hard colloidal spheres*, Nature, **1986**, 320, 340-342
- <sup>4</sup> Pusey, P.N. et al., *Colloidal crystals, fluids and glasses*, Journal of Physics: Condensed Matter, **1990**, 2, SA373
- <sup>5</sup> Poon, W.C.K., *Colloids as Big Atoms*, Science, **2004**, 304, 830-831
- <sup>6</sup> Pusey, P.N. et al., *Phase behaviour and structure of colloidal suspensions*, Journal of Physics: Condensed Matter, **1994**, 6 A29
- <sup>7</sup> Cong, H. et al., *Current status and future developments in preparation and application of colloidal crystals*, Chemical Society Reviews, **2013**, 42, 7774-7800
- <sup>8</sup> Velev, O.D. and Lenhoff, A.M., *Colloidal crystals as templates for porous materials*, Current Opinion in Colloid & Interface Science, **1990**, 5(1-2), 56-63
- <sup>9</sup> Joannopoulos, J.D., *Photonic crystals: Putting a new twist on light*, Nature, **1997**, 386(6621), 143-149
- <sup>10</sup> Ishii, M. et al., *Large-Domain Colloidal Crystal Films Fabricated Using a Fluidic Cell*, Langmuir, **2005**, 21, 5367-5371
- <sup>11</sup> Inanc, I. and Watson, G.H., *Photonic Band Structure of fcc Colloidal Crystals*, Physical Review Letters, **1996**, 76(2), 315-318
- <sup>12</sup> Hynninen, A.P. et al., *Self-assembly route for photonic crystals with a bandgap in the visible region*, Nature Materials, **2007**, 6, 202-205
- <sup>13</sup> Hiemenz, P.C. and Rajagopalan, R., *Principles of colloid and surface chemistry*, Taylor & Francis, Boca Raton, **1997**
- <sup>14</sup> Sacanna, S. et al., *Engineering shape: the novel geometries of colloidal self-assembly*, Soft Matter, **2013**, 9, 8096-8106
- <sup>15</sup> Sacanna, S. et al., *Shaping colloids for self-assembly*, Nature Communications, **2013**, 4, 1688
- <sup>16</sup> Yethiray, A. and van Blaaderen, A., *A colloidal system with an interaction tunable from hard sphere to soft and dipolar*, Nature, **2003**, 421(6922), 513-518
- <sup>17</sup> Dolbnya, I.P. et al., *Coexistence of rhcp and fcc phases in hard-sphere colloidal crystals*, Europhysics Letters, **2005**, 72(6),
- <sup>18</sup> Glotzer, S.C. and Solomon, M.J., *Anisotropy of building blocks and their assembly into complex structures*, Nature Materials, **2007**, 6, 557-562
- <sup>19</sup> Damasceno, P.F. et al., *Predictive Self-Assembly of Polyhedra into Complex Structures*, Science, **2012**, 337, 453 - 457
- <sup>20</sup> Van der Kooij, F.M. et al., *Liquid crystal phase transitions in suspensions of polydisperse plate-like particles*, Nature, **2000**, 406, 868-871
- <sup>21</sup> Sacanna, S. and Pine, J.P., *Shape-anisotropic colloids: Building blocks for complex assemblies*, Current Opinion in Colloid & Interface Science, **2011**, 16, 96-105
- <sup>22</sup> Zhou, Z. and Zhao, X.S., *Flow-Controlled Vertical Deposition Method for the Fabrication of Photonic Crystals*, Langmuir, **2004**, 20, 1524-1526
- <sup>23</sup> Velev, O.D. and Kaler, E.W., *Structured Porous Materials via Colloidal Crystal Templating: From Inorganic Oxides to Metals*, Advanced Materials, **2000**, 12(7), 531-534
- <sup>24</sup> Denkov, N.D. et al., *Mechanism of Formation of Two-Dimensional Crystal from Latex Particles on Substrates*, Langmuir, **1992**, 8, 3183-3190
- <sup>25</sup> Deegan, R. et al., *Capillary flow as the cause of ring stains from dried liquid drops*, Nature **1997**, 389, 827-829
- <sup>26</sup> Denkov, N. et al., *2-Dimensional crystallization*, Nature, **1993**, 361(26)
- <sup>27</sup> Velev, O.D. et al., *Direct Measurement of Lateral Capillary Forces*, Langmuir, **1993**, 9, 3702-3709

- 
- <sup>28</sup> Norris, D.J. *et al.*, *Opaline Photonic Crystals: How does Self-Assembly Work?*, *Advanced Materials*, **2004**, 16(16), 1393-1399
- <sup>29</sup> Meng, L. *et al.*, *The Role of Thickness Transitions in Convective Assembly*, *Nanoletters*, **2006**, 6(10), 2249-2253
- <sup>30</sup> Cheng, Z. *et al.*, *Phase diagram of hard spheres*, *Materials and Design*, **2001**, 22, 529-534
- <sup>31</sup> Rossi, L. *et al.*, *Cubic crystals from cubic colloids*, *Soft Matter*, **2011**, 7, 4139-4142
- <sup>32</sup> Sugimoto, T. *et al.*, *Formation Mechanism of Monodisperse Pseudocubic  $\alpha$ -Fe<sub>2</sub>O<sub>3</sub> from Condensed Ferric Hydroxide Gel*, *Journal of Colloid and Interface Science*, **1993**, 159, 372-382
- <sup>33</sup> Pompe, C.E., *Catalytic degradation of organic molecules by colloidal hematite in a silica box via Fenton-like reaction*, Masterthesis, Chemistry department Utrecht University, **2013**
- <sup>34</sup> Hatton, B. *et al.*, *Assembly of large-area, highly ordered, crack-free inverse opal films*, *Proceedings of the National Academy of Sciences U.S.A.*, **2010**, 107(23), 10354-10359
- <sup>35</sup> Lee, S. *et al.*, *Degradation of Phenol with Fenton-like Treatment by Using Heterogeneous Catalyst (Modified Iron Oxide) and Hydrogen Peroxide*, *Bulletin of the Korean Chemical Society*, **2006**, 27(4), 489-494
- <sup>36</sup> Rossi, L., *PhD thesis: Colloidal Superballs*, Van 't Hoff Laboratory for Physical and Colloid Chemistry, Utrecht University, **2012**
- <sup>37</sup> Delaney, G.W. and Cleary, P.W., *The packing properties of superellipsoids*, *Europhysics Letters*, **2010**, 89, 34002
- <sup>38</sup> Avendano, C. and Escobedo, F.A., *Phase behavior of rounded hard-squares*, *Soft Matter*, **2012**, 8, 4675-4681
- <sup>39</sup> Jiao, Y. *et al.*, *Optimal Packings of Superdisks and the Role of Symmetry*, *Physical Review Letters*, **2008**, 100, 245504
- <sup>40</sup> Jiao, Y. *et al.*, *Optimal Packings of superballs*, *Physical Review E*, **2009**, 79, 041309
- <sup>41</sup> Batten, R.D. *et al.*, *Phase behavior of colloidal superballs: Shape interpolation from spheres to cubes*, *Physical Review*, **2010**, 81, 061105
- <sup>42</sup> Ni, R. *et al.*, *Phase diagram of colloidal hard superballs: from cubes via spheres to octahedra*, *Soft Matter*, **2012**, 8, 8826-8834
- <sup>43</sup> Marechal, M. *et al.*, *Freezing of parallel hard cubes with rounded edges*, *The Journal of Chemical Physics*, **2012**, 136, 144506
- <sup>44</sup> Meijer, J.M. *et al.*, *Self-Assembly of Colloidal Cubes via Vertical Deposition*, *Langmuir*, **2012**, 28, 7631-7638
- <sup>45</sup> Jenkins, J.S., *Continuous Convective-Sedimentation Assembly of Colloidal Microsphere Coatings for Biotechnology Applications*, *Coatings*, **2013**, 3, 26-48
- <sup>46</sup> Prevo, B.G. and Orlin, D.V., *Controlled, Rapid Deposition of Structured Coatings from Micro- and Nanoparticle Suspensions*, *Langmuir*, **2004**, 20, 2099-2107
- <sup>47</sup> Glotzer, S.C. and Solomon, M.J., *Anisotropy of building blocks and their assembly into complex structures*, *Nature Materials*, **2007**, 6, 557-562
- <sup>48</sup> Sugimoto, T., *Formation of Monodispersed Nano- and Micro-Particles Controlled in Size, Shape, and Internal Structure*, *Chemical Engineering & Technology*, **2003**, 26(3), 313-321
- <sup>49</sup> Pronk, S. and Frenkel, D., *Large effect of polydispersity on defect concentrations in colloidal crystals*, *Journal of Chemical Physics*, **2004**, 120(14), 6764
- <sup>50</sup> Schwertmann U. and Cornell R. M., *Iron Oxides in the Laboratory Preparation and Characterization*. Wiley-VCH, **2000**
- <sup>51</sup> Sacanna, S. *et al.*, *Magnetic Click Colloidal Assembly*, *Journal of the American Chemical Society*, **2012**, 134, 6112-6115
- <sup>52</sup> Hsu, W.P. *et al.*, *The Formation of Uniform Colloidal Particles of Magnesium Fluoride and Sodium Magnesium Fluoride*, *Journal of Colloid and Interface Science*, **1996**, 181, 142-148
- <sup>53</sup> Sevonkaev, I. *et al.*, *Formation and structure of cubic particles of sodium magnesium fluoride (neighborite)*, *Journal of Colloid and Interface Science*, **2008**, 317, 130-136

- 
- <sup>54</sup> Jerrim, B. J. and Velev, O. D., *Deposition of Coatings from Live Yeast Cells and Large Particles by "Convective-Sedimentation" Assembly*, *Langmuir*, **2009**, 25(10), 5692-5702
- <sup>55</sup> Giraldo, L.F. *et al.*, *Mesoporous Silica Applications*, *Macromolecular Symposia*, **2007**, 258, 129-141
- <sup>56</sup> Sugimoto T. *et al.*, *Characterization of Hematite Particles of Different Shapes*, *Journal of Colloid and Interface Science*, **1993**, 158, 420-428
- <sup>57</sup> Castillo, S., *Cubic hematite colloids with reproducible size and shape*, internal report Van 't Hoff Laboratory for Physical and Colloid Chemistry, Utrecht University, **2012**
- <sup>58</sup> Park, G.S. *et al.*, *Internal Structure Analysis of Monodispersed Pseudocubic Hematite Particles by Electron Microscopy*, *Journal of Colloid and Interface Science*, **1996**, 177, 198-207
- <sup>59</sup> Stöber W. *et al.*, *Controlled Growth of Monodisperse Silica Spheres in the Micron Size Range*, *Journal of Colloid and Interface Science*, **1968**, 26(1), 62-69
- <sup>60</sup> Hagemans, F., *Synthesis and Self-Assembly of Anisotropic Patchy Particles*, Masterthesis Van 't Hoff Laboratory for Physical and Colloid Chemistry, Utrecht University, **2013**
- <sup>61</sup> Born, P. *et al.*, *Crystallization Mechanisms in Convective Particle Assembly*, *Langmuir*, **2012**, 28(22), 8300 - 8308
- <sup>62</sup> Lin, Z., *Evaporative Self-Assembly of Ordered Complex Structures*, World Scientific Publishing Co. Pte. Ltd Singapore, 1<sup>st</sup> edition, **2012**
- <sup>63</sup> Majumder, M. *et al.*, *Overcoming the "Coffee-Stain" Effect by Compositional Marangoni-Flow-Assisted Drop-Drying*, *Journal of Physical Chemistry B*, **2012**, 116, 6536- 6542
- <sup>64</sup> Adachi, E., *Stripe Patterns Formed on a Glass Surface during Droplet Evaporation*, *Langmuir*, **1995**, 11, 1057 - 1060
- <sup>65</sup> Hu, H. and Larson, R.G., *Marangoni Effect Reverses Coffee-Ring Depositions*, *Journal of Physical Chemistry B Letters*, **2006**, 110, 7090 - 7094
- <sup>66</sup> Vlasov, Y.A. *et al.*, *On-chip natural assembly of silicon photonic bandgap crystals*, *Nature*, **2001**, 414, 289 - 293
- <sup>67</sup> Weon, B.M. and Je, J.H., *Capillary force repels coffee-ring effect*, *Physical Review E*, **2010**, 82, 015305
- <sup>68</sup> Takhistov, P. and Chang, H.C., *Complex Stain Morphologies*, *Industrial & Engineering Chemistry Research*, **2002**, 41, 6256 - 6269
- <sup>69</sup> Deegan, R.D. *et al.*, *Contact line deposits in an evaporating drop*, *Physical Review E*, **2000**, 62(1), 756 - 765
- <sup>70</sup> Truskett, V.N. *et al.*, *Influence of surfactants on an evaporating drop: Fluorescence images and particle deposition patterns*, *Langmuir*, **2003**, 19, 756 - 765
- <sup>71</sup> Still, T. *et al.*, *Surfactant-Induced Marangoni Eddies Alter the Coffee-Rings of Evaporating Colloidal Drops*, *Langmuir*, **2012**, 28, 4984 - 4988
- <sup>72</sup> Deegan, R.D., *Pattern formation in drying drops*, *Physical Review E*, **2000**, 61(1), 475 - 485
- <sup>73</sup> Yunker, P.J. *et al.*, *Suppression of the coffee-ring effect by shape-dependent capillary interactions*, *Nature Letter Research*, **2011**, 476, 308 - 3011
- <sup>74</sup> Born, P. *et al.*, *Role of the Meniscus Shape in Large-Area Convective Particle Assembly*, *Langmuir*, **2011**, 27, 8621 - 8633
- <sup>75</sup> Pusey, P.N. *et al.*, *Structure of Crystals of Hard Colloidal Spheres*, *Physical Review Letters*, **1989**, 62(25), 2753 - 2756
- <sup>76</sup> Vlasov, Y.A. *et al.*, *Manifestation of intrinsic defects in optical properties of self-organized opal photonic crystals*, *Physical Review E*, **2000**, 61(5), 5784 - 5793
- <sup>77</sup> Prevo, B.G. *et al.*, *Engineered deposition of coating from nano- and microparticles: A brief review of convective assembly at high volume fraction*, *Colloids and Surfaces A*, **2007**, 311(1-3), 2 - 10
- <sup>78</sup> Lee, A. *et al.*, *Colloidal Crystal Layers of Hexagonal Nanoplates by Convective Assembly*, *Langmuir*, **2006**, 22, 5217-5219
- <sup>79</sup> Hahn, C. and Cha-Hwan, O., *Characteristics of a Photonic Crystal Structure Made by Flow-controlled Vertical Deposition Method*, *Journal of the Korean Physical Society*, **2011**, 58(5), 1116-1119
- <sup>80</sup> Gasperino, D. *et al.*, *The role of fluid flow and convective steering during the assembly of colloidal crystals*, *Journal of Crystal Growth*, **2008**, 310, 131 - 139

- 
- <sup>81</sup> Wojciechowski, K.W. and Frenkel D., *Tetratic Phase in the Planar Hard Square System?*, Computational Methods in Science and Technology, **2004**, 10(2), 235-255
- <sup>82</sup> Zhao, K. *et al.*, *Entropic crystal-crystal transitions of Brownian squares*, PNAS, **2011**, 108(7), 2684-2687
- <sup>83</sup> Donev, A. *et al.*, *Neighbor list collision-driven molecular dynamics simulation for nonspherical hard particles. I. Algorithmic details*, Journal of Computational Physics, **2005**, 202(2), 737-764
- <sup>84</sup> Ng, E.C.H. *et al.*, *Controlling Inplane Orientation of a Monolayer Colloidal Crystal by Meniscus Pinning*, Langmuir, **2011**, 27, 2244 - 2249